

A ONE DIMENSIONAL MODEL FOR  
TRICKLE BED  
HYDRODESULFURIZATION

NURHIDAYAH BINTI MOHAMMAD

MASTER OF SCIENCE  
CHEMICAL ENGINEERING

UNIVERSITI TEKNOLOGI PETRONAS

AUGUST 2011

STATUS OF THESIS

Title of thesis

A ONE DIMENSIONAL MODEL FOR TRICKLE BED  
HYDRODESULFURIZATION

I NURHIDAYAH BINTI MOHAMMAD

hereby allow my thesis to be placed at the Information Resource Center (IRC) of Universiti Teknologi PETRONAS (UTP) with the following conditions:

1. The thesis becomes the property of UTP
2. The IRC of UTP may make copies of the thesis for academic purposes only
3. This thesis is classified as

Confidential

Non-confidential

If this thesis is confidential, please state the reason:

\_\_\_\_\_  
\_\_\_\_\_

The content of the thesis will remain confidential for \_\_\_\_\_ years.

Remarks on disclosure:

\_\_\_\_\_  
\_\_\_\_\_

Endorsed by

\_\_\_\_\_  
Signature of Author

\_\_\_\_\_  
Signature of Supervisor

Permanent address: No. 23, Lorong  
AU4/17C, Taman Sri Keramat  
Tengah, 54200 Kuala Lumpur

Name of Supervisor  
Prof. Dr. Duvvuri Subbarao

Date : 16 August 2011

Date : 16 August 2011



UNIVERSITI TEKNOLOGI PETRONAS  
A ONE DIMENSIONAL MODEL FOR TRICKLE BED  
HYDRODESULFURIZATION

by

NURHIDAYAH BINTI MOHAMMAD

The undersigned certify that they have read, and recommend to the Postgraduate Studies Programme for acceptance this thesis for the fulfillment of the requirements for the degree of Master of Science in Chemical Engineering.

Signature: \_\_\_\_\_

Main Supervisor: Prof. Dr. Duvvuri Subbarao

Signature: \_\_\_\_\_

Head of Department: Assoc. Prof. Dr. Shuhaimi Mahadzir

Date: 16 August 2011



A ONE DIMENSIONAL MODEL FOR TRICKLE BED  
HYDRODESULFURIZATION

by

NURHIDAYAH BINTI MOHAMMAD

A Thesis

Submitted to the Postgraduate Studies Programme

as a Requirement for the Degree of

MASTER OF SCIENCE

CHEMICAL ENGINEERING

UNIVERSITI TEKNOLOGI PETRONAS

BANDAR SRI ISKANDAR,

PERAK

AUGUST, 2011

## DECLARATION OF THESIS

Title of thesis

A ONE DIMENSIONAL MODEL FOR TRICKLE BED  
HYDRODESULFURIZATION

I NURHIDAYAH BINTI MOHAMMAD

hereby declare that the thesis is based on my original work except for quotations and citations which have been duly acknowledged. I also declare that it has not been previously or concurrently submitted for any other degree at UTP or other institutions.

Witnessed by

Signature of Author

Signature of Supervisor

Permanent address: No. 23, Lorong  
AU4/17C, Taman Sri Keramat  
Tengah, 54200 Kuala Lumpur

Name of Supervisor  
Prof. Dr. Duvvuri Subbarao

Date : 16 August 2011

Date : 16 August 2011

## ACKNOWLEDGEMENTS

First of all, I thank Almighty Allah, The Creator, for Mercy and Guidance in my whole life and giving me the ability to complete this research.

I would like to express my deepest sincere gratitude and deep appreciation to my supervisor, Prof. Dr. Duvvuri Subbarao for his patience, invaluable assistance and guidance, immense knowledge, continual encouragement, and valuable advices throughout this study. I greatly appreciate the time he spent for discussing the direction and progress work of this study.

My sincere thanks also go to my beloved family especially my parents, Mr Mohammad and Mrs. Faudziah for supporting me spiritually and patience over these years. I also would like to express my warm and sincere thanks to my dearest friends for their assistance, encouragement, comments and beautiful friendship.

Finally, I would like to thank to Universiti Teknologi PETRONAS for the financial support throughout the course of my study.

## ABSTRACT

The need for processing of heavy sour crudes is increasing as good quality crude oil reserves are depleting fast. Presence of sulfur in the crude oil can corrode the process equipment, poison the catalysts and can lead to environmental pollution. Trickle bed reactors are widely used for hydrodesulfurization by reacting sulfur in the crude with hydrogen. Optimal design of these units is possible through development of easy to use performance models for trickle bed reactors recognizing the multiphase nature of the reactor and nonlinearities in the parameters.

Liquid holdup in trickle bed reactors is an important hydrodynamic parameter which controls the liquid residence time in the bed and hence the degree of sulfur conversion. A new model to estimate liquid holdup in trickle beds is developed considering gas to flow around particles enveloped by trickling liquid. Ergun's equation for gas phase pressure drop is modified incorporating the effect of presence of liquid phase on gas phase voidage and tortuosity for gas flow. The model is compared with large experimental database available in the literature to evaluate the effect of parameters such as gas and liquid velocities, liquid properties, particle shape and size, operating temperature and pressure. The model equations compare reasonably well with the experimental observations.

A one-dimensional multiphase cells-in-series model is developed to predict the steady state behavior of trickle bed reactor applied to the hydrodesulfurization of vacuum gas oil (VGO). The reactor model is established through mass and enthalpy balances with reaction using carefully selected correlations and hydrodesulfurization reaction kinetics based on Langmuir-Hinshelwood mechanism from the literature. The model is validated with experimental data on hydrodesulfurization of VGO reported in the literature. The model is simulated to investigate the effect of various parameters to analyze ways and means to improve the sulfur reduction.

## ABSTRAK

Pemrosesan minyak dari 'sour crude' dilihat mampu untuk memenuhi permintaan kerana sumber minyak dari 'sweet crude' semakin mengalami penyusutan. Namun begitu, kandungan sulfur yang tinggi di dalam 'sour crude' akan mendatangkan kesan buruk kepada reaktor, mangkin dan mencemarkan alam sekitar. 'Trickle bed reactor' merupakan reaktor yang digunakan dalam proses hidrodeshulfurisasi dimana sulfur ditindakbalaskan dengan hidrogen bagi menghasilkan hidrogen sulfida. Rekabentuk secara optimum bagi reaktor tiga fasa ini dapat dilakukan melalui pembangunan model dengan mengenalpasti sifat dan keadaan reaktor serta ketidakseragaman parameter pada reaktor tersebut.

'Liquid holdup' merupakan parameter penting dalam menilai kecekapan reaktor kerana ia mengawal tempoh minyak berada di dalam reaktor dan seterusnya mempengaruhi kadar hidrodeshulfurisasi. Satu model baru telah dibangunkan bagi menganggarkan 'liquid holdup' di dalam reaktor. Persamaan Ergun telah diubahsuai dengan memasukkan kesan kehadiran fasa cecair terhadap aliran gas. Model ini menggunakan data-data eksperimen dari kajian terdahulu untuk melihat kesan beberapa pembolehubah seperti diameter partikel, suhu, tekanan, kelikatan cecair dan sebagainya terhadap 'liquid holdup'. Didapati bahawa nilai bagi 'liquid holdup' yang dianggarkan dari persamaan model memenuhi nilai dari data eksperimen.

Satu model reaktor baru telah dibangunkan (1-D cell in-series-model) bagi meramal keadaan di dalam 'trickle bed reactor'. Model ini dibangunkan melalui persamaan jisim dan tenaga, tindakbalas kimia, serta menggabungkan kolerasi hidrodinamika. Tindakbalas kimia bagi hidrodeshulfurisasi adalah berdasarkan mekanisma 'Langmuir-Hinshelwood'. Kesahihan model reaktor ini ditentukan melalui perbandingan dengan data eksperimen dari kajian terdahulu. Model ini disimulasi untuk menilai kesan beberapa parameter terhadap kadar hidrodeshulfurisasi dan seterusnya dapat diaplikasikan bagi meningkatkan kecekapan reaktor.

In compliance with the terms of the Copyright Act 1987 and the IP Policy of the university, the copyright of this thesis has been reassigned by the author to the legal entity of the university,

Institute of Technology PETRONAS Sdn Bhd.

Due acknowledgement shall always be made of the use of any material contained in, or derived from, this thesis.

© Nurhidayah binti Mohammad, 2011  
Institute of Technology PETRONAS Sdn Bhd  
All right reserved.

## TABLE OF CONTENTS

STATUS OF THESIS.....	i
APPROVAL PAGE.....	ii
TITLE PAGE.....	iii
DECLARATION.....	iv
ACKNOWLEDGEMENTS.....	v
ABSTRACT.....	vi
COPYRIGHT PAGE.....	viii
TABLE OF CONTENTS.....	ix
LIST OF TABLES.....	xiii
LIST OF FIGURES.....	xiv

### Chapter

1. INTRODUCTION.....	
1.1 Petroleum Industry.....	1
1.2 Hydrotreating Units.....	1
1.3 Research Background.....	3
1.4 Knowledge Gaps.....	4
1.5 Research Objectives and Scope.....	5
1.6 Thesis Outline.....	5
	6
2. LITERATURE REVIEW.....	
2.1 Sulfur Compounds in Petroleum Crude.....	7
2.2 Hydrodesulfurization Process.....	7
2.3 Hydrodesulfurization Catalysts.....	9
2.4 Trickle Bed Reactors.....	11
2.5 Reactor Hydrodynamics.....	13
2.5.1 Hydrodynamic Regimes.....	14
2.5.2 Pressure Drop in Packed Beds.....	15
2.5.2.1 Single Phase Pressure Drop.....	17

2.5.2.2	Pressure Drop for Two Phase Flow in Packed Beds.....	18
2.5.2.3	Pressure drop Correlations for Two Phase Flow in Packed Beds.....	19
2.5.3	Liquid Holdup.....	21
2.5.3.1	Liquid Holdup Correlations.....	23
2.5.4	Two Phase Flow Models.....	25
2.5.4.1	Relative Permeability Model.....	26
2.5.4.2	Slit model.....	27
2.5.4.3	Fluid-fluid Interaction Force Mode.....	29
2.5.4.4	Computational Fluid Dynamics Model.....	30
2.5.4.5	Comparisons of Two Phase Flows Models.....	31
2.6	Reaction Kinetics of Hydrodesulfurization.....	32
2.6.1	Representation of Sulfur Compounds .....	32
2.6.2	Reaction kinetics .....	33
2.7	Experimental Information on Reactor Performance.....	35
2.8	Hydrodesulfurization Reactor Models.....	36
2.9	Conclusions.....	38
	Notation.....	39
3.	MODEL FOR DYNAMIC LIQUID HOLDUP.....	43
3.1	Submerged Particle Model for Dynamic Liquid holdup.....	43
3.1.1	Evaluation of $C_{Dm}$ .....	45
3.1.2	Dynamic Liquid Holdup.....	46
3.1.3	Model for Pressure Drop in Trickle Bed Reactors.....	47
3.2	Results and Discussion.....	49
3.2.1	Submerged Particle Model Validation.....	51
3.2.1.1	Effect of Particle Diameter, Shape and Liquid Viscosity.....	51
3.2.1.2	Effect of Gas Velocity on Liquid Holdup.....	54
3.2.1.3	Effect of Temperature and Pressure on Liquid Holdup.....	56
3.2.1.4	Parity Plot.....	57
3.2.2	Validation of the Model for Gas Phase Pressure Drop.....	58
3.3	Tortuosity of Gas Flow Path.....	63
3.3.1	Pressure drop Model Validation (New Ergun Constants)..	64
3.3.1.1	Effect of Gas and Liquid Velocities on Pressure Drop.....	65
3.3.1.2	Effect of Pressure on Pressure Drop.....	67

3.3.1.3	Effect of Temperature on Pressure Drop.....	68
3.3.1.4	Effect of Particle Size on Pressure Drop.....	69
3.3.1.5	Parity Plot.....	70
3.4	Conclusion.....	72
	Notation.....	73
4.	MODEL FOR TRICKLE BED REACTOR .....	75
4.1	1-D Cells in Series .....	76
	Model.....	78
4.2	Model Governing Equations.....	78
4.2.1	Mass Balance Equations .....	78
4.2.1.1	Gas Phase.....	80
4.2.1.2	Gases in Liquid Phase.....	81
4.2.1.3	Sulfur in Liquid Phase.....	82
4.2.1.4	Reaction in Solid Phase.....	83
4.2.2	Energy Balance Equations.....	85
4.3	Reaction Kinetics .....	85
4.4	Estimation of Hydrodynamic and Physical Properties.....	86
4.4.1	Oil Density .....	86
4.4.2	Gas Solubility.....	87
4.4.3	Dynamic Liquid Viscosity.....	87
4.4.4	Diffusivity.....	88
4.4.5	Mass Transfer Coefficients.....	89
4.4.6	Heat Capacity.....	89
4.4.7	Wetting Efficiency.....	90
4.5	Solution Scheme for 1-D Reactor Model .....	92
4.6	Model Validation and Simulation Results.....	95
4.6.1	Results of the Simulation for the Pilot Plant.....	
4.6.2	Simulation Study to Explore the Performance of the Pilot Plant.....	100
	Plant.....	101
4.6.2.1	Effect of Reactor Length .....	101
4.6.2.2	Effect of Liquid Velocity .....	102
4.6.2.3	Effect of Feed Inlet Temperature .....	103
4.6.2.4	Effect of Reactor Pressure.....	104
4.7	Simulation of Hydrodesulfurization Commercial Unit.....	
4.7.1	Effect of Presence of Hydrogen Sulfide (H <sub>2</sub> S) in Feed Hydrogen.....	106
	Hydrogen.....	108
4.7.2	Effect of Feed Inlet Temperature.....	109
4.7.3	Effect of Reactor Pressure.....	110

4.7.4	Effect of Liquid Velocity.....	111
4.8	Conclusions.....	112
	Notation.....	115
5.	SUMMARY, CONCLUSIONS AND RECOMMENDATIONS .....	115
5.1	Summary.....	117
5.2	Conclusions.....	117
5.3	Recommendation.....	118
	REFERENCES.....	128
	APPENDICES.....	128
A	Submerged Particle Model Sample Calculation .....	133
B	Properties and Hydrodynamics for 1-D Cell-in-Series Model.....	143
C	Reactor Behavior (1-D Cell-in-Series Model).....	

## LIST OF TABLES

Table 2.1:	Sulfur compounds in petroleum.....	8
Table 2.2:	Some correlations for two phase flow in packed beds.....	20
Table 2.3:	Empirical correlations of liquid holdup.....	24
Table 2.4:	Various approaches for hydrodynamics modeling in trickle beds..	31
Table 2.5:	Mean absolute relative error for liquid holdup and pressure drop..	32
Table 2.6:	Selected kinetic models for hydrodesulfurization reaction.....	34
Table 2.7:	Experimental data on hydrodesulfurization performance.....	35
Table 3.1:	Details of operating conditions used for Submerged Particle Model validation.....	50
Table 3.2:	Details of operating conditions used for pressure drop model validation.....	59
Table 4.1:	Kinetics and thermodynamic data.....	86
Table 4.2:	Experimental data on hydrotreating of VGO on pilot plant scale...	93
Table 4.3:	Data on hydrotreating of VGO on commercial reactor.....	105
Table A.1:	Experimental data of Trivizadakis et al. [35].....	128
Table A.2:	Simulation results predicted by Submerged Particle Model for data of Trivizadakis et al. [35].....	132
Table B.1:	Input data for hydrodesulfurization reaction [36].....	133
Table C.1:	Simulation results of hydrodesulfurization of VGO on pilot plant scale estimated by 1-D cell-in series-model.....	150

## LIST OF FIGURES

Figure 1.1:	Global oil supply and demand from year 2005 up to 2016.....	1
Figure 1.2:	Total world oil reserves.....	2
Figure 1.3:	Malaysia’s oil production and consumption, 1990–2009.....	3
Figure 1.4:	Diesel regulatory timeline for the Asia-Pacific region.....	4
Figure 2.1:	Quenching alternatives for the industrial VGO hydrotreater.....	10
Figure 2.2:	Schematic representation of catalyst structure.....	11
Figure 2.3:	Particle shapes of industrial hydrotreating catalysts.....	12
Figure 2.4:	Schematic diagram of trickle bed reactor.....	14
Figure 2.5:	Schematic illustration of hydrodynamic regimes with respect to gas and liquid flowrates.....	16
Figure 2.6:	Schematic representative of slit based model.....	28
Figure 3.1:	Schematic representation of the concurrent gas-liquid downward flow through the void space of the packed bed.....	44
Figure 3.2:	Schematic representation of effective diameter particle, $d_p'$ .....	48
Figure 3.3:	Effect of particle size and liquid viscosity on liquid holdup.....	52
Figure 3.4:	Liquid holdup versus gas flux for various liquid mass velocities	53
Figure 3.5:	Influences of gas and liquid velocities on liquid holdup.....	54
Figure 3.6:	Effect of gas and liquid velocities on liquid holdup for porous packing.....	55
Figure 3.7:	Effect of temperature and pressure on liquid holdup.....	56
Figure 3.8:	Comparison of experimental data on liquid holdup with values predicted by Submerged Particle Model.....	57
Figure 3.9:	Effect of gas velocity on pressure drop.....	60
Figure 3.10:	Effect of liquid velocity on pressure drop.....	61

Figure 3.11	Comparison of experimental data on pressure drop with values predicted by modified Ergun's equation with standard Ergun's parameter ( $E_1=180$ , $E_2=1.80$ ).....	62
Figure 3.12	Effect of gas and liquid velocities on pressure drop.....	66
Figure 3.13	Effect of operating pressure on pressure drop .....	67
Figure 3.14:	Effect of temperature on pressure drop .....	68
Figure 3.15:	Pressure drop versus gas mass velocity for spherical and cylindrical extrudates.....	69
Figure 3.16:	Comparison of experimental data on pressure drop with values predicted by modified Ergun's equation with new Ergun parameter.....	70
Figure 3.17:	Comparison of experimental data on liquid holdup with values predicted by submerged particle model coupled with modified Ergun's equation and new Ergun parameters.....	71
Figure 4.1:	1-D Cells in Series Model.....	76
Figure 4.2:	Concentrations profile of reactants and product.....	77
Figure 4.3:	Mass balance for hydrogen in gas phase.....	79
Figure 4.4:	Mass balance for hydrogen sulfide in gas phase.....	79
Figure 4.5:	Mass balance for hydrogen in liquid phase.....	80
Figure 4.6:	Mass balance for hydrogen sulfide in liquid phase.....	81
Figure 4.7:	Mass balance for sulfur compound in liquid phase.....	81
Figure 4.8:	Mass balance in solid phase.....	82
Figure 4.9:	Heat transfer from solid phase to liquid phase.....	83
Figure 4.10:	Energy balance in liquid phase.....	84
Figure 4.11:	Energy balance in gas phase.....	84
Figure 4.12:	Computational flow sheet of the calculation procedure.....	94
Figure 4.13:	Hydrogen profiles along the reactor length in gas, liquid and solid phases.....	96
Figure 4.14:	Sulfur concentrations profile in liquid and solid phases.....	97
Figure 4.15:	Hydrogen sulfide profiles along the reactor length in gas, liquid and solid phases.....	99
Figure 4.16:	Bed temperature profile.....	100

Figure 4.17:	Effect of reactor length on product sulfur content.....	101
Figure 4.18:	Effect of liquid velocity on product sulfur content.....	102
Figure 4.19:	Effect of feed inlet temperature on product sulfur content.....	103
Figure 4.20:	Effect of operating pressure on product sulfur content.....	104
Figure 4.21:	Partial pressure profiles of hydrogen sulfide in gas phase for commercial reactor.....	106
Figure 4.22:	Concentration profile of hydrogen sulfide in liquid phase for commercial reactor.....	107
Figure 4.23:	Sulfur concentration profiles in liquid phase for commercial reactor with and without H <sub>2</sub> S content .....	108
Figure 4.24:	Effect of feed inlet temperature on product sulfur content.....	109
Figure 4.25:	Effect of reactor pressure on product sulfur content.....	110
Figure 4.26:	Effect of liquid velocity on product sulfur content.....	111

CHAPTER 1  
INTRODUCTION

**1.1 Petroleum Industry**

Petroleum industry is one of the largest and important industries with operations spread over every corner of the world. This industry covers petroleum products, natural gas and petrochemicals. It is continuously evolving to satisfy growing demand of fuel and petrochemical feedstock. Transportation fuels such as gasoline, diesel and jet fuel are the highest volume products from the petroleum industry [1]–[3]. Rapid growth of the petroleum industry is mostly credited to the availability of vast quantities of oil and gas as feedstock. According to the International Energy Agency (IEA), the oil demand is expected to surpass the oil supply by 2012 as shown in Figure 1.1 [4].

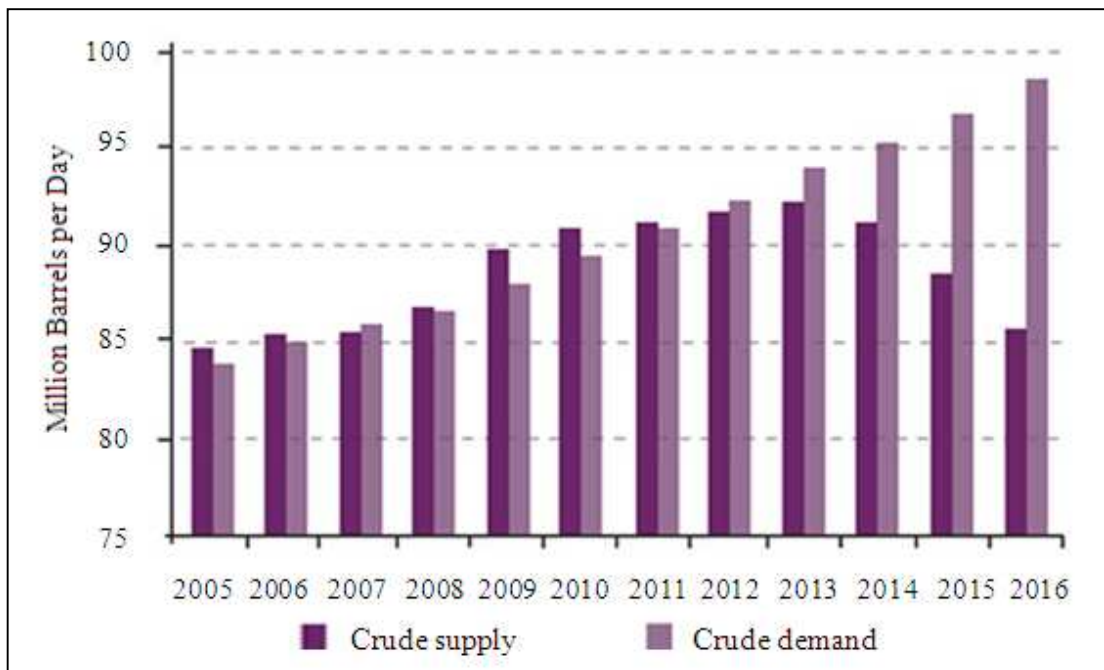


Figure 1.1: Global oil supply and demand from year 2005 up to 2016 [4]

Total world oil reserves indicate that the good quality conventional oil make up only 30% of oil resources while the rest - heavy oil, extra heavy oil and bitumen- are difficult to process (Figure 1.2). Known reserves of conventional good quality petroleum are getting depleted due to ever increasing consumption. To meet the future demands, it is necessary to use reserves such as extra heavy oil, shale, bitumen and oil sands.

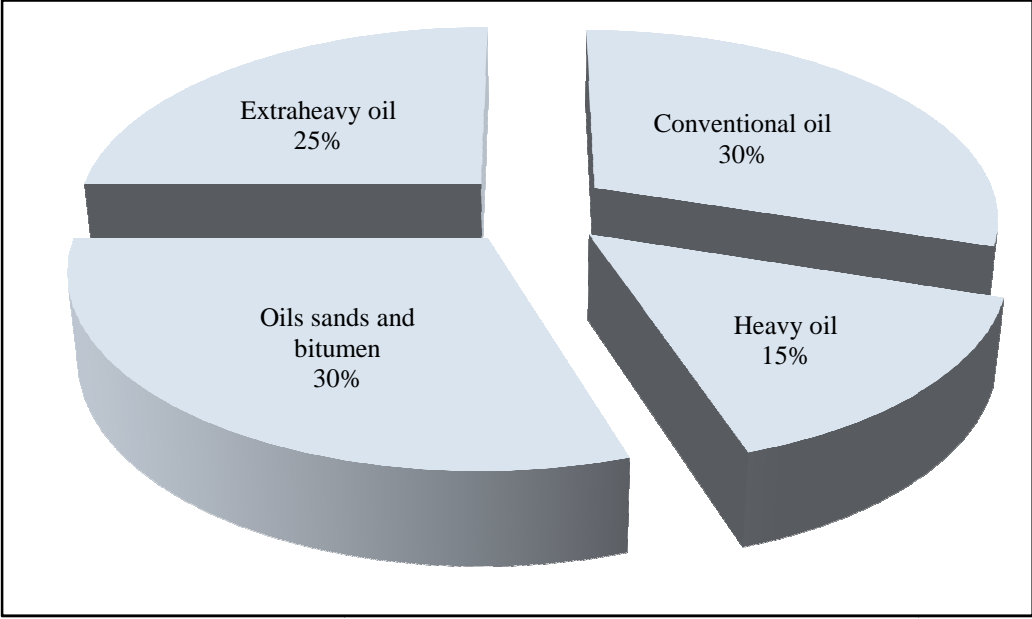


Figure 1.2: Total world oil reserves [5]

Malaysia has the third highest oil reserves in the Asia-Pacific region after China and India, and world’s tenth largest holder of natural gas reserves. It was reported that Malaysia holds proven oil reserves of 4 billion barrels as of January 2010 [6]. According to energy statistic from U.S government (Energy Information Administration, EIA), Malaysia’s oil production in 2009 was 693,000 barrels per day (bbl/d) while total oil consumption was 536,000 bbl/d as shown in Figure 1.3. Malaysia consumes the greater part of its production as consumption has been rising while production has been declining over the years. It is imperative that Malaysia needs to import crude oil in the years to come. Good quality oil is going to be more expensive than sour crudes. In the years to come, sour crudes need to be processed to meet the future demand while satisfying the environmental quality concerns.

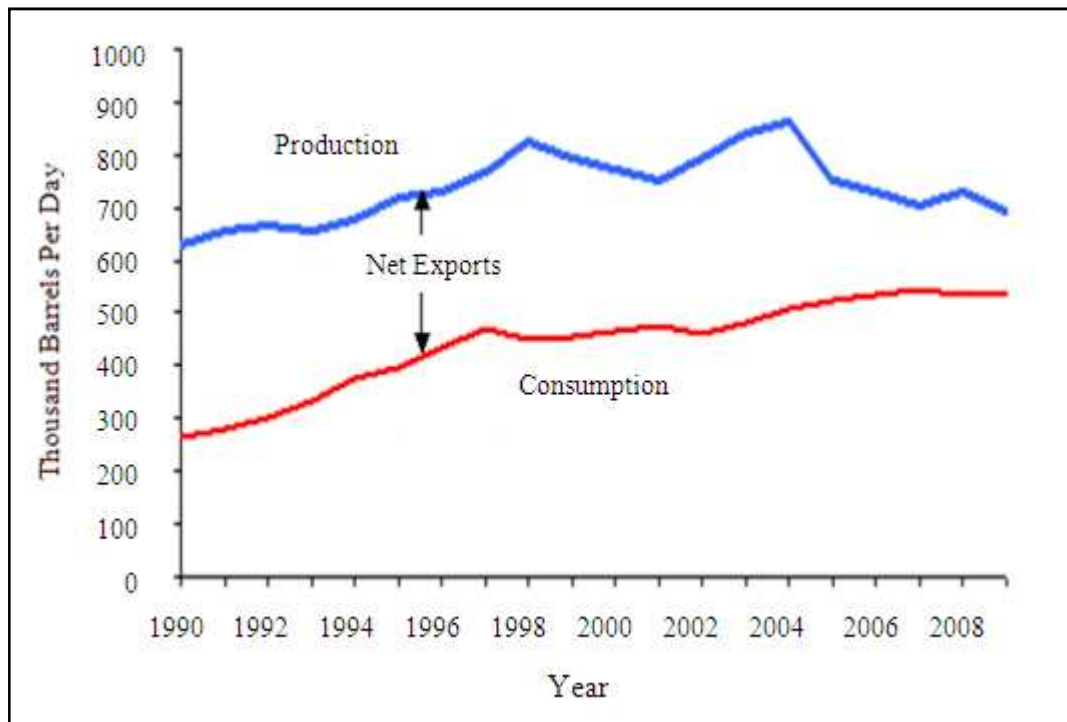


Figure 1.3: Malaysia's oil production and consumption, 1990–2009 [6]

## 1.2 Hydrotreating Units

The heavy oils contain higher volume of residue with boiling point higher than 525°C as well as more undesirable components such as sulfur, nitrogen, oxygen, halides and metals. Conventional refineries do remove the heteroatoms in hydrotreating units. Hydrotreating, which includes hydrocracking, hydrodesulfurization, hydrodeoxygenation, hydrodenitrogenation and hydrodemetallization, plays an important role in upgrading petroleum streams to meet the stringent quality requirements [1]–[3]. With the necessity of using heavier crudes while meeting the stringent quality restrictions on the products, future hydrotreating units need to be more efficient. Hydrodesulfurization is the focus of the present work.

### 1.3 Research Background

In the pursuit of cleaner environment, developed countries adopted stringent specifications on maximum allowable sulfur content in ultra low sulfur diesel (ULSD) (15 wppm in America and 10 wppm in Europe). Most other countries still have much higher sulfur content in their fuel at the moment. Figure 1.4 presents diesel regulatory timeline for the Asia-Pacific region.

	2005	2006	2007	2008	2009	2010	2010+
Japan	E4		10ppm S				
Hongkong	E4			10ppm S			
Singapore	E2	E4			10ppm S		
Australia	E2	E4			10ppm S		
New Zealand	E2	E4			10ppm S		
India	E3			E4		10ppm S	
Malaysia	E2					E4	
Thailand	E3					E4	
China	E2		E3			E4	
Indonesia	Country Specific		E2			E3	

Figure 1.4: Diesel regulatory timeline for the Asia-Pacific region. E2 standards at 500 ppm, E3 standards at 350 ppm, E4 standards at 50 ppm [7]

Hydrodesulfurization of heavier crudes is carried out by reacting sulfur in the crude with hydrogen gas in the presence of a porous catalyst in three phase trickle bed reactors. Performance of the trickle bed reactor is influenced by the liquid residence time in the reactor, efficiency of liquid solid contact and catalytic reaction kinetics. Liquid holdup is an important hydrodynamic parameter as it determines the liquid residence time as well as catalyst wetting efficiency. Modeling and simulation of the trickle bed reactor seems to be the best approach to evaluate the current technologies and to develop strategies to produce desired low level of sulfur efficiently.

## **1.4 Knowledge Gaps**

Trickle bed reactors have been the subject of many investigations, and several authors have summarized them in various reviews [8]–[15]. Hydrodynamic parameters such as liquid holdup and bed pressure drop received extensive attention. Several phenomenological models have been proposed so far, such as the permeability model of Saez and Carbonell [8], slit based model of Holub et al. [9], and fluid-fluid interaction force balance of Attou et al. [10]. Inconsistencies in these models were brought out by Carbonell [11]. A fresh look to develop a physically realistic model can be useful.

There were some attempts to develop performance models for hydrodesulfurization in trickle bed reactors based on continuum concepts (e.g. Bhaskar et al. [12], Rodriguez and Ancheyta [13] and Murali et al. [14]). However, the multiphase nature of the reactor and nonlinearities in the parameters make the models very complex and intractable for easy application. There is a need to develop a realistic easy to use model considering the multiphase nature of reactor applied to crude oil desulfurization.

## **1.5 Research Objectives and Scope**

The main objective of the present study is to develop a multiphase one dimensional cells-in-series model to describe the hydrodesulfurization (HDS) process in a trickle bed reactor to estimate the species concentration and temperature profile along the reactor. For efficient design of trickle bed reactor systems, model equations for liquid holdup and bed pressure drop are needed. Simulations using the model should be able to provide strategies for improved performance of HDS unit. The model would serve as a guide to understand the reactor behavior.

## **1.6 Thesis Outline**

A review of the literature on sulfur compounds in petroleum crudes, hydrodesulfurization process, hydrodesulfurization catalysts, trickle bed reactor, liquid holdup, pressure drop, and hydrodesulfurization reactor models is presented in Chapter 2. A new model to estimate liquid holdup and pressure drop in trickle bed reactors is developed and validated with literature data in Chapter 3. In chapter 4, a new model for describing hydrodesulfurization reaction in a trickle bed reactor is developed and validated. Chapter 4 also includes the trickle bed reactor model simulations to investigate options to improve the reactor performance to reduce sulfur content to the prescribed limits. Chapter 5 presents conclusions of the present work and recommendation for future work.

## CHAPTER 2

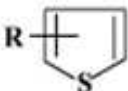
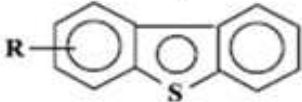
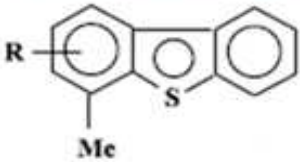
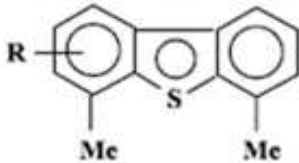
### LITERATURE REVIEW

Nature of sulfur compounds in petroleum crude is presented in section 2.1. Comprehensive descriptions of hydrodesulfurization (HDS) process to reduce sulfur content in crude oil are presented in section 2.2. Section 2.3 describes catalysts used for HDS reaction while section 2.4 describes reactors employed for HDS process. Hydrodynamics of trickle bed reactors is presented in section 2.5, with particular emphasis on liquid holdup and bed pressure drop. Relevant experimental information on reactor performance is given in section 2.6. Reviews on HDS reaction kinetic models as well as HDS reactor models are presented in section 2.7 and 2.8. Section 2.9 concludes the chapter.

#### **2.1 Sulfur Compounds in Petroleum Crude**

Sulfur in crude oil is present as compounds such as mercaptans, sulfides, disulfides, thiophenes etc. or as elemental sulfur. Sulfur content may vary from as little as 0.05 wt% to as high as 6 wt%. Most common sulfur contaminants are sulfides, disulfides, thiols (mercaptans) and its various thiophenic derivatives. The proportion and complexity of sulfur compounds generally increases with the boiling point of the distillate fraction [16]–[18]. Table 2.1 shows the distribution of sulfur compounds found in petroleum by boiling point.

Table 2.1: Sulfur compounds in petroleum [1]

Sulfur Compounds	Distillation Boiling Range
Mercaptanes <b>R-SH, R-S-S-R</b>	84°C
Thiophenes 	<218°C
Benzothiophenes 	220°C
Dibenzothiophenes 	334°C
4-methyldibenzothiophenes 	335-363°C
4,6-Dimethyldibenzothiophenes 	366°C

Presence of sulfur compounds in the petroleum streams is highly undesirable as they can cause corrosion of pipes, tanks and other process equipment. Moreover, they can deactivate some of the catalysts used in crude oil processing. Combustion of petroleum products containing sulfur compounds can release large quantities of sulfur dioxide into the atmosphere causing air pollution. Sulfur dioxide in the atmosphere can react with moisture in the air to pollute water streams through acid

rain. This can in turn affect agricultural land [1]–[2], [18]–[20]. Thus, reducing the sulfur content in the crude by treating with hydrogen in the presence of a suitable catalyst is essential.

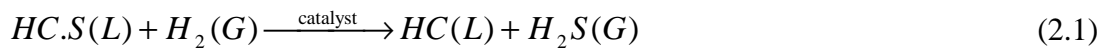
The reactivity of sulfur compounds varies depending on the electron density on the S atom. The higher the electron density on S atom and the weaker C-S bond, the higher the reactivity of sulfur compounds. Sulfur compounds in low boiling crude oil fractions are very reactive and can be removed easily from the crude oil in hydrotreating process. Sulfur contained in paraffins is easier to remove than naphthenes followed by aromatics. Sulfur in higher boiling crude oil fractions is included in ring compounds such as thiophenic rings, and they are much less reactive. The reactivity of sulfur compounds in high boiling crude oil decreases in the order thiophene > alkylated thiophene > benzothiophene > alkylated benzothiophene > dibenzothiophene. Many studies on hydrodesulfurization of sulfur compounds present in the gas oils mainly as dibenzothiophene and its alkyl derivatives have been reported in the literature [21]–[23].

## 2.2 Hydrodesulfurization Process

Sulfur content in the hydrocarbons can be reduced by reaction with hydrogen in a hydrodesulfurization (HDS) unit in presence of catalysts such as mixed sulfides of NiMo or CoMo supported on alumina. In the same reactor, other unwanted heteroatoms such as oxygen, nitrogen and metals may also be reduced. Depending on the operating conditions, there can be hydrocracking as well to produce lighter hydrocarbon. These processes are together referred to as hydrotreating processes [1], [2], [18], [19].

Hydrodesulfurization process for light feed (gas phase) is frequently performed in vapor phase fixed bed reactors. For heavier fractions, the reaction is commonly accomplished in trickle bed reactor. In this mode, gas (hydrogen) and liquid (oil) flow co-currently downward through a catalytic packed bed to undergo chemical reactions [19]–[20], [24]. Sulfur atoms attached to the hydrocarbon molecules in the liquid phase react with dissolved hydrogen on the surface of catalyst to form hydrogen sulfide.

The hydrodesulfurization reaction can be represented as follows



HDS reactors operate at elevated temperatures in the range of 300–450°C and elevated pressures, in the range of 0.7–15MPa. The operating conditions are a function of type of feed and the desired level of desulfurization in treated product [1], [3], [16]. All hydrotreating reactions are irreversible and exothermic in nature. Presence of higher levels of sulfur can lead to substantial increase in reactor temperature and it can be controlled by quenching with cooler hydrogen and liquid stream (Figure 2.1). Reviews on hydrogen and liquid quenching have been described by Alvarez and Ancheyta [24].

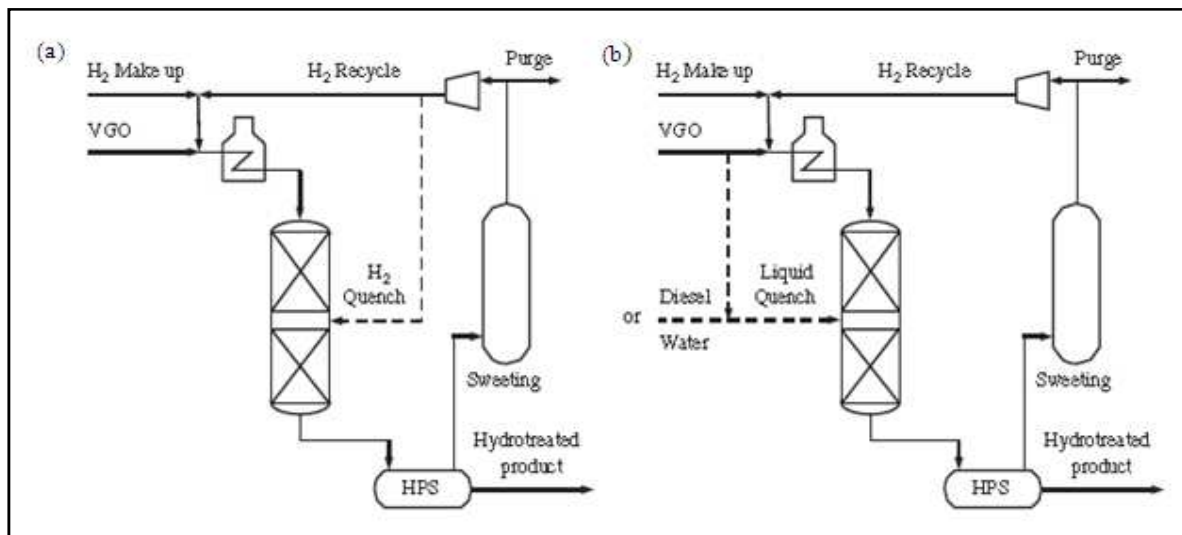


Figure 2.1: Quenching alternatives for the industrial VGO hydrotreater

(a) hydrogen quenching (b) liquid quenching [24]

Many past studies have reported that increasing reactor temperature would enhance hydrodesulfurization reaction rate [14], [25]–[27]. However, it should be noted that high temperature also may cause excessive hydrocracking of the feed which in turn reducing desirable product yield. Also, it can lead to coke formation and shorten catalyst cycle life [1], [18], [28].

Hydrogen partial pressure is an important variable to manipulate to achieve satisfactory performance. It is affected by reactor pressure and hydrogen purity in the feed gas. Increasing reactor pressure leads to an increase in hydrogen partial

pressure, thus improves the solubility of hydrogen gas and the driving force for gas-liquid mass transfer. An increase in hydrogen purity would decrease the hydrogen sulfide partial pressure and thus reduces the hydrogen sulfide inhibition effect. Operation at high hydrogen partial pressure not only favors the HDS reaction rate, but also can diminish the coke deposits on the catalysts and hence increases the catalysts life. Hydrogen requirements for the hydrodesulfurization process depend upon the degree of desired sulfur removal [16], [18], [28].

### 2.3 Hydrodesulfurization Catalysts

Mixed metal sulfides of molybdenum promoted by cobalt or nickel and supported on a high surface area of  $\gamma$ -alumina,  $\text{Al}_2\text{O}_3$  are used as the catalyst for hydrodesulfurization reaction. Nickel-molybdenum catalyst is often chosen when higher activity is required [29]–[31]. The high surface area in a porous catalyst particle is essentially due to pore size. Based on pore size, catalysts can be identified as

1. Microporous catalysts (pore diameter  $\leq 2$  nm),
2. Mesoporous catalysts (pore diameter 2–50 nm) and
3. Macroporous catalysts (pore diameter  $\geq 50$  nm).

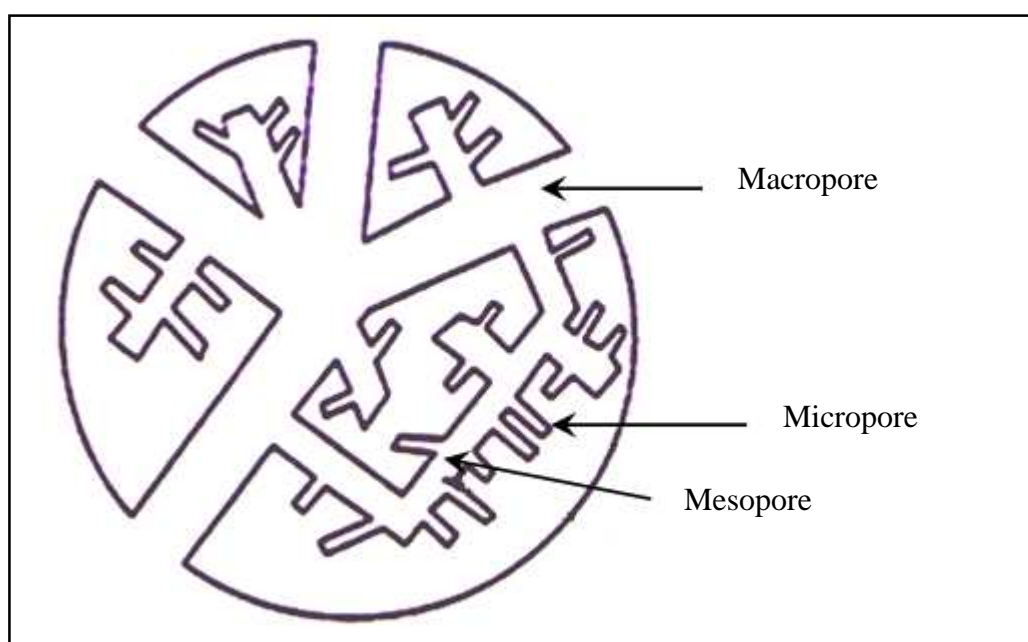


Figure 2.2: Schematic representation of catalyst structure [30]

Effective utilization of catalyst is determined by the pore diffusion of reactants into and products out of the pores. The larger the diameter of the catalyst particle, the lower the effectiveness factor. However, the use of smaller particles increases bed pressure drop. So it is necessary to find the optimal size of catalyst particle [32]–[35].

Bed voidage is around 0.4 for spherical and near spherical particles, and bed pressure drop is high with such a low bed voidage. To reduce bed pressure drop, there were many attempts to increase bed voidage by creating particle of different shapes such as big particles with multi holes (like Raschig rings) and small diameter multi lobe extrudates. Extrudate particles of sizes with diameter of 0.13-0.3 cm are the preferred catalyst type for HDS process [29], [31]–[34]. Typical particle shapes of industrial hydrotreating catalysts are shown in Figure 2.3.

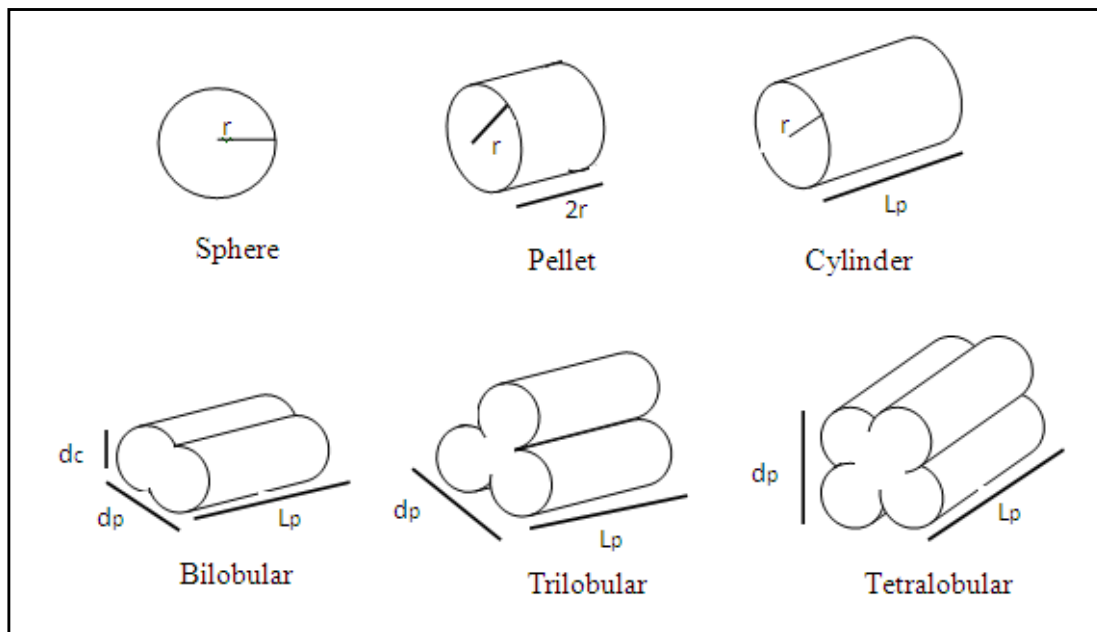


Figure 2.3: Particle shapes of industrial hydrotreating catalysts [33]

Various investigations on the effect of particles shape and size on HDS catalyst behavior have been reported in the literature [31]–[35]. De Bruijn et al. [31] studied the influences of non-cylindrical shape of extrudates on the HDS of oil fractions. They found that non-cylindrical extrudates provides a higher catalyst activity compared to the cylindrical extrudates. Cooper et al. [33] emphasized that particle

size, shape, pore size and catalyst loading should be taken into account for reliable design of hydrotreating catalysts.

## 2.4 Trickle Bed Reactors

Trickle bed reactors are the most frequently used reactors for hydrodesulfurization of oil fractions. In trickle bed reactors, gas and liquid reactant flow concurrently downwards over a fixed bed of catalyst particles (Figure 2.4). There is no flooding limitation due to the concurrent downflow and hence velocities can be high. This improves gas-liquid mass transfer. Also, the gas-liquid flow approaches plug flow characteristics and can provide better conversions [15], [36].

However, gas-liquid reactions such as hydrogenations and oxidations often suffer from the low solubility of the gas phase reactant in the liquid phase. Therefore, elevated pressures are required to increase the solubility of gas reactants in the liquid phase which in turn can increase the conversion rate. Also, it was reported that high pressure enables to slow down the catalyst deactivation [37]–[38]. In most industrial applications, trickle bed reactors operate adiabatically at high temperatures (350°C to 425°C) and high pressures (up to 30 MPa). Industrial reactors can reach up to 3 m in diameter and up to 30 m in height. Fluid phase maldistribution can be a problem in trickle bed reactors which may give rise to hot spots, catalyst sintering and poor performance [15], [20], [37].

Due to higher hydrogen sulfide concentration in the reactor outlet, conversion of sulfur compounds in the exit region can be restricted by product ( $H_2S$ ) inhibition. A few investigators proposed that countercurrent operation can be helpful (e.g. Mederos and Ancheyta [36], Cheng et al. [39], and van Hasselt et al. [40]). However, countercurrent operation restricts the operating flexibility due to flooding.

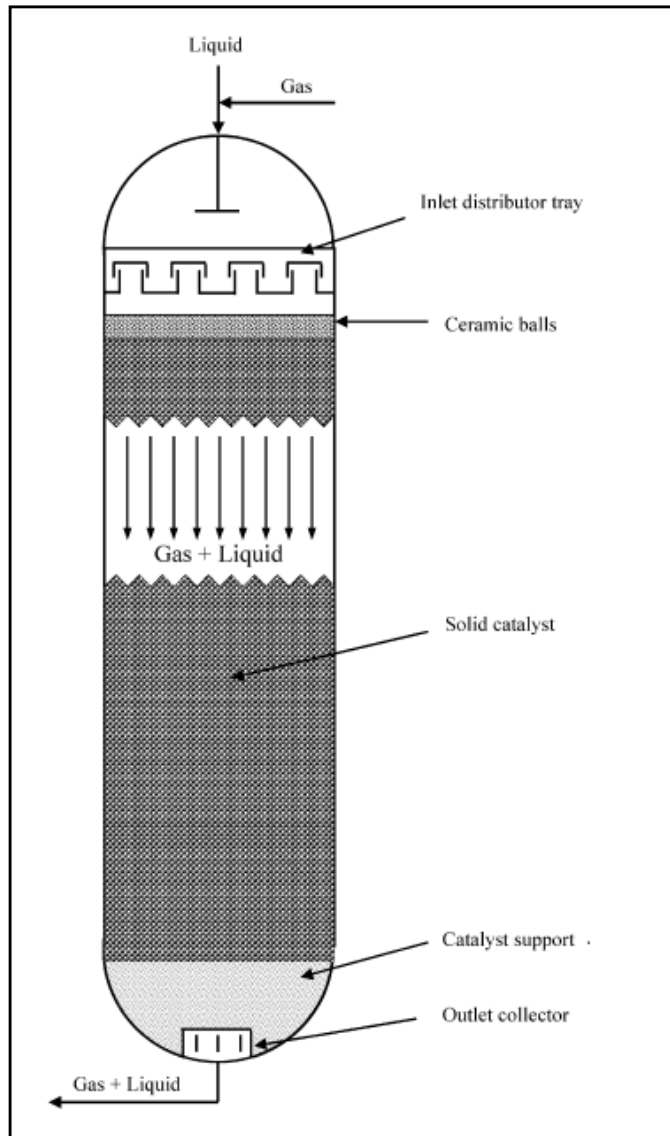


Figure 2.4: Schematic diagram of trickle bed reactor [15]

## 2.5 Reactor Hydrodynamics

In gas-liquid reactions, net reaction rate depends on:

- i. Mass transfer of reactants from gas to liquid
- ii. Mass transfer of reactants from liquid into the porous particle
- iii. Reaction at catalytic surface in the pores
- iv. Mass transfer of products in the pores of catalyst particle to liquid and gas.

Mass transfer rates depend on the interfacial area of contact and mass transfer coefficients which in turn depend on the relative velocity between the phases. Actual

gas and liquid velocities through the reactor depend on the phase holdups which can together be expressed as

$$\varepsilon_p + \varepsilon_L + \varepsilon_G = 1$$

where the sum of the volume fractions of the gas and liquid adds up to the bed porosity.

$$\varepsilon_L + \varepsilon_G = \varepsilon$$

Thus, conversions in trickle bed reactors depend on the reaction kinetics as well as reactor hydrodynamics [41].

Reactor hydrodynamics can be described using hydrodynamic parameters such as flow regime, flow rates, pressure drop, liquid holdup, mass transfer and heat transfer. Among them, liquid holdup and two phase pressure drop are the main parameters that impact interfacial mass transfer, reactor performance and power consumption for the operation [42]–[43]. Therefore, understanding of the hydrodynamics of trickle beds is essential for reliable scale up for process design and performance evaluation. A number of empirical correlations [44]–[46] and models such as relative permeability model [8], [47]–[49], slit model [9], [50]–[53], and CFD models [10], [54]–[56] have been proposed to explain trickle bed reactor hydrodynamics. A brief review of trickle bed reactor hydrodynamics is presented in the following section.

### **2.5.1 Hydrodynamic Regimes**

Flow regimes primarily depend on gas and liquid superficial velocities, together with the fluid properties as well as particles packing. They can be classified as low interaction regime (trickle flow regime) and high interaction regime (pulse, spray and bubble regimes) [57]. The flow regime boundaries with respect to gas and liquid flow rates are schematically shown in Figure 2.5.

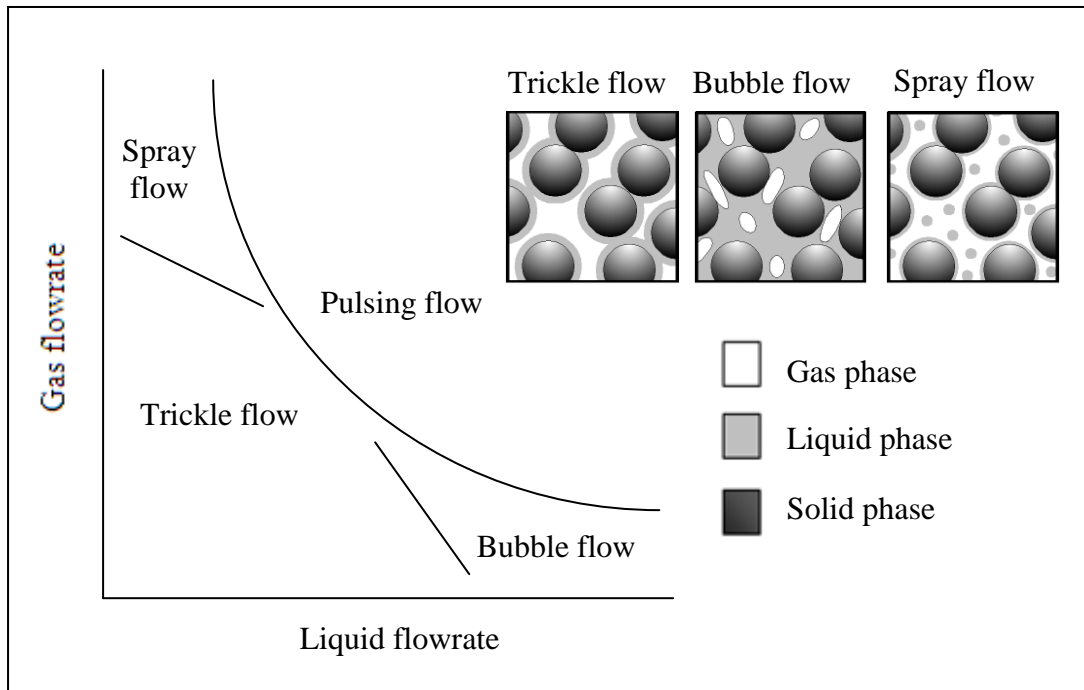


Figure 2.5: Schematic illustration of hydrodynamic regimes with respect to gas and liquid flowrates [58]

In the low interaction regime at low liquid and gas flow rates, the liquid trickles over the packing in the form of films and rivulets while the gas flows in the remaining void space as a continuous phase. This regime is known as trickle flow regime. In the high interaction regime at higher liquid flow rates and low gas flow rates, in bubble flow regime, liquid flows as a continuous phase and gas flows as dispersed bubbles. At higher gas flow rates and lower liquid flow rates, in the spray flow regime, gas flows as a continuous phase and liquid flows as dispersed drops. At high gas as well as liquid flow rates, in the pulse flow regime, both the phases flow as alternate pulses of slugs of gas and liquid. The pulsing flow regime has significantly higher pressure fluctuations and higher pressure drop. Reactors are often operated in the trickle regime closer to pulse flow regime [41], [57]–[58].

Trivizadakis et al. [35] investigated the effect of particle size and shape (spherical of diameter 3–6 mm and cylindrical of diameter 3mm) on flow transitions and observed that the flow transitions were not affected by the particle size. However, the location of trickling to pulsing transition boundary shifts to higher gas flowrates when cylindrical extrudates were employed.

## 2.5.2` Pressure Drop in Packed Beds

### 2.5.2.1 Single Phase Pressure Drop

Energy required to move fluid through the reactor and hence the operating cost depends on the pressure drop across the reactor. Pressure drop for single phase flow in packed beds can be estimated by Ergun's equation [59].

$$\frac{P_1 - P_2}{Z} = E_1 \frac{(1 - \varepsilon)^2}{\Phi^2 \varepsilon^3} \cdot \frac{u_o \mu}{d_p^2} + E_2 \frac{(1 - \varepsilon)}{\varepsilon^3} \cdot \frac{\rho u_o^2}{\Phi d_p} \quad (2.2)$$

The first term on right hand side represents the viscous energy losses in laminar flow while the second term represents kinetic energy losses in turbulent flow.  $(P_1 - P_2)$  is the pressure drop through the packed bed,  $Z$  is the bed length or height,  $\varepsilon$  is the bed voidage,  $u_o$  is the superficial velocity of fluid flow,  $\rho$  is the fluid density,  $\mu$  is the fluid dynamic viscosity,  $\Phi$  is the particle sphericity and  $d_p$  is the particle diameter. For spherical particles, the value of  $\Phi$  is 1. For beds with non-spherical particles and non uniform size particles, an equivalent particle diameter may be used. Bed porosity ( $\varepsilon$ ) is defined as void fraction in the bed.

$$\varepsilon = \frac{\text{volume of voids between particles in the bed}}{\text{total volume of bed}}$$

Note that a small change in bed voidage has a large effect on the pressure drop. Based on experimental data, Ergun [59] obtained the viscous flow constant ( $E_1$ ) and inertia flow constant ( $E_2$ ) as 150 and 1.75 respectively.

Over the past years, classical values of the Ergun constants (150 and 1.75) have been the subject of considerable debate. Different values for  $E_1$  and  $E_2$  have been reported by different investigators for different bed geometries. Macdonald et al. [60] proposed modified values of  $E_1=180$  and  $E_2=1.8$  based on large experimental data base. For rough particle shape, they suggested using a value of  $E_2=4.0$ . The numerical constants 180 and 1.8 have been used by other researchers (e.g. Saez and Carbonell [8] and Grosser et al. [61]). Kundu et al. [62] proposed values of 250 and 2.1 for spherical nonporous packing. Ozahi et al. [63] recommended values of 160

and 1.61 for predicting pressure drop through packed bed with circular or non-circular particle packing. Nemeč and Levec [32] claimed that the coefficients (150 and 1.75) in the Ergun equation are not constants but depend on the Reynolds number, porosity and particle shape. In view of this, they proposed an improvement to the original constants using empirical functions for non-spherical particles, where the original values were retained for spherical particles. Iliuta et al. [64] suggested neural network model to improve Ergun constants for various bed configurations.

#### *2.5.2.2 Pressure Drop for Two Phase Flow in Packed Beds*

Pressure drop for two phase flow through packed beds received great attention over the last several decades due to its importance in the design of packed bed absorbers, extractors and distillation units and trickle bed reactors [50]–[53], [64]–[66]. A variety of bed packing elements were developed for applications in absorption, distillation and extraction to increase bed voidage and external surface area per volume of bed. Voidage of a randomly packed bed of spherical particles is around 0.4 and voidage in modern structured metal packing can be as high as 0.98. Energy consumption in trickle bed reactors per a given throughput for a given conversion also decreases with increase in bed voidage [35], [67]. As the catalyst particles are highly porous in nature, their mechanical strength is low and restricts the level of voidage that can be employed (generally less than 0.6). In trickle bed reactors, size of catalyst particles need to be small to minimize pore diffusion effects. In view of this, multilobe catalyst extrudate particles are preferable [67] as higher effectiveness factor and lower pressure drop can be achieved.

Two phase pressure drop depends on velocities of gas and liquid phases, physical properties of the flowing fluids, operating variables and bed characteristics. Saroha and Khera [65] investigated the effect of gas and liquid velocities on two phase pressure drop in trickle beds. They observed that the pressure drop increases with increasing gas and liquid velocities. Aydin and Larachi [68] studied the effect of temperature, pressure (gas density) as well as gas and liquid velocities on bed pressure drop. They observed bed pressure drop decreases with temperature, increases with operating pressure and gas velocity. The effect of temperature was

more pronounced at higher gas and liquid velocities. Trivizadakis et al. [35] observed that bed pressure drop increases with decreasing particle size for spherical particles. They also observed that pressure drop with cylindrical particles was higher than with spherical particles.

#### *2.5.2.3 Pressure Drop Correlations for Two Phase Flow in Packed Beds*

There are many correlations for two phase pressure drop that were established on the basis of experimental data obtained in a wide range of operating conditions. One approach is based on the Lockhart-Martinelli concept according to which the ratio  $(\Delta P_{LG}/\Delta P_G)$  is correlated with the ratio  $(\Delta P_L/\Delta P_G)$  [69]. Some others adopted Ergun's equation for two phase flow in packed beds considering the presence of liquid holdup in the bed. Some of the correlations are summarized in Table 2.2.

Table 2.2: Some correlations for two phase flow in packed beds

Reference	Correlation
Larkins et al. [69]	$\log \left[ \frac{\Delta P_{LG}}{\Delta P_L + \Delta P_G} \right] = \frac{0.416}{0.66 + \left[ \log \sqrt{\frac{\Delta P_L}{\Delta P_G}} \right]^2}$
Turpin and Huntington [70]	$\ln F_{LG} = 7.96 - 1.34 \ln Z + 0.0021(\ln Z)^2 - 0.00078 (\ln Z)^3$ <p>where <math>F_{LG} = \left[ \frac{1}{3} d_p \varepsilon \frac{(-\Delta P_{LG})}{Z} \right] / \rho_G u_{oG}^2 (1 - \varepsilon)</math></p>
Ellman et al. [45]	$\frac{\Delta P}{Z} = \frac{2G^2}{d_h \rho_G} (200(X_G \delta)^{-1.2} + 85(X_G \delta)^{-0.5})$ <p>where <math>\delta = \frac{\text{Re}_L^2}{(0.001 + \text{Re}_L^{1.5})}</math>, <math>\text{Re}_L = \frac{\rho_L u_{oL} d_p}{\mu_L}</math>, <math>X_G = \frac{G}{L} \sqrt{\frac{\rho_L}{\rho_G}}</math>, <math>d_h = \left( \frac{16\varepsilon^3}{9\pi(1-\varepsilon)^2} \right)^{0.33} d_p</math></p>
Larachi et al. [46]	$\frac{\Delta P}{Z} = \frac{2G^2}{d_h \rho_G} \frac{1}{[(\text{Re}_L \text{We}_L)^{0.25} X_G]^{1.5}} \left[ 31.3 + \frac{17.3}{[(\text{Re}_L \text{We}_L)^{0.25} X_G]^{0.5}} \right]$ <p>where <math>\text{We}_L = \frac{\rho_L u_{oL}^2 d_p}{\sigma_L}</math></p> <p>The terms of <math>\text{Re}_L</math>, <math>X_G</math> and <math>d_h</math> are same as Ellman's correlation.</p>

### 2.5.3 Liquid Holdup

Liquid holdup is a prime hydrodynamic parameter as it determines the residence time of the liquid phase reactant in the reactor. The liquid holdup has direct or indirect affect on the following parameters [65]–[66], [68].

- i) actual gas and liquid velocities through the reactor
- ii) pressure drop
- iii) gas-liquid mass transfer
- iv) heat transfer
- v) degree of catalyst wetting
- vi) thickness of the liquid film covering the particles
- vii) provides thermal stability due to the high heat capacity of liquid phase

Total liquid holdup ( $\epsilon_L$ ) is defined as the total volume of liquid held in the reactor per volume of empty reactor. Liquid holdup in trickle beds with non porous particles was considered to be made up of two components which are static holdup ( $\epsilon_{Ls}$ ) and dynamic holdup ( $\epsilon_{Ld}$ ). Static holdup can be described as liquid fraction that could not be drained out by gravity while dynamic holdup is liquid freely flowing in between the particles [72]. In trickle beds with porous particles, liquid held inside the catalyst pores contributes to the liquid holdup and it is refer as internal holdup ( $\epsilon_{L,int}$ ) [72]. Thus, total liquid holdup can be expressed as

$$\epsilon_L = \epsilon_{Ls} + \epsilon_{Ld} + \epsilon_{L,int} \quad (2.3)$$

Some investigators present information as liquid saturation instead of liquid holdup. Liquid saturation is defined as the liquid volume contained in void volume of column. It can be described as

$$\beta = \frac{\epsilon_L}{\epsilon} \quad (2.4)$$

Most of the investigators reported measurement of liquid holdup in packed beds with non porous particles using liquid drainage [45], [73], [74], [75] or liquid tracer techniques [68], [72]. For packed beds with porous catalytic particles, Trivizadakis et al. [35] and Ayude et al. [76] employed tracer technique to measure the liquid holdup.

Basically, draining method is used to measure the dynamic saturation ( $\beta_d$ ) by simultaneously shutting off the gas and liquid input and collecting the liquid at the bottom of the bed. The flowing liquid holdup is determined by the balance of gravitational force, pressure drop over the column and resisting force (drag force at liquid solid interface and surface tension force). Static saturation ( $\beta_s$ ) is the amount of liquid remaining in the packed bed after the draining period [73]–[75]. For the tracer technique, liquid holdup is measured through RTDs for different reactor length. A tracer pulse is injected into the liquid flow that enters the bed. The tracer concentration continuously recorded using the conductance probes inserted in the bed to get RTD curves different axial positions. Liquid holdup is calculated from the mean liquid residence time and contrasted to the normalized conductance measured by each probe. Reviews on experimental installation and the procedure employed have been described by Ayude et al. [76].

The influence of the liquid and gas velocities on liquid holdup have been studied by several investigators (e.g. Saroha and Khera [65]; Guo and Al-Dahhan [66], Fu and Tan [72]; Xiao et al. [75]). Higher gas velocity results in lower liquid holdup while higher liquid velocity results in higher liquid holdup. Trivizadakis et al. [35] observed that liquid holdup with smaller porous cylindrical extrudates is higher than with larger spherical particles. Sidi-Boumedine and Raynal [77] investigated the effect of liquid viscosity on liquid holdup in structured packing under concurrent downflow with liquid viscosity varies from 1 to 20 cP. These authors observed that liquid holdup (both static and dynamic) increases with increasing liquid viscosity. Similar observations were also reported by Fu and Tan [72] and Xiao et al. [75]. However, Xiao et al. [75] noticed that the effect of liquid viscosity is more pronounced in trickling flow than pulsing flow. Guo and Al-Dahhan [66] investigated the influence of reactor pressures on the external liquid holdup in trickle beds with porous particle and found that liquid holdup decreases with increasing pressure. Aydin and Larachi [68] observed that liquid holdup decreased with an increase in temperature, pressure and gas velocity.

### 2.5.3.1 Liquid Holdup Correlations

Static holdup is due to interfacial forces holding the liquid weight. In most of studies so far, static holdup was not extensively investigated either experimentally or theoretically. Charpentier et al. [78] first presented a correlation for static holdup as

$$\varepsilon_{L_s} = \frac{1}{20 + 0.9E_o} \quad (2.5)$$

$$\text{with } E_o = \frac{\rho_L g d_p^2}{\sigma} \quad (2.6)$$

To account for the dependence of static holdup on void fraction, Saez and Carbonell [8] recommended modification of  $d_p$  to  $d_p(1-\varepsilon)$ . Kramer [71] recommended a correlation for static holdup based on assumption that static liquid is retained in liquid pendular bonds around contact point between touching spheres.

$$\varepsilon_{L_s} \approx 0.028 \frac{1-\varepsilon}{\varepsilon} \quad (2.7)$$

Sidi-Boumedine and Raynal [77] observed that static liquid holdup also can get affected by viscosity

$$\varepsilon_{L_s} = \varepsilon_{w_s} \left( \frac{\mu_L}{\mu_W} \right)^{0.333} \quad (2.8)$$

Over the years, a number of empirical correlations devoted to dynamic/total liquid holdup have been established, as listed in Table 2.3. Specchia and Baldi [73] made use of Davidson's model [79] based on liquid film flow and introduced a modified Galileo number in which the gas flow is taken into account by pressure gradient. Ellman et al. [45] proposed a correlation for dynamic liquid holdup for high interaction regime by incorporating a modified Lockhart-Martinelli parameter, Reynolds number and Weber number for the liquid phase. Later, Larachi et al. [46] measured total liquid holdup up to 8.1 MPa by means of tracer technique, and derived more simple correlation for them. Fu and Tan [72] proposed an equation considering the dependence of total liquid saturation ( $\beta_L$ ) on liquid viscosity and particle size. Xiao et al. [75] correlated dynamic liquid holdup in terms of interstitial velocity ratio.

Table 2.3: Empirical correlations of liquid holdup

Reference	Correlation
Specchi and Baldi [73]	<p>Dynamic liquid holdup in high interaction regimes</p> $\varepsilon_{Ld} = 3.86 \text{Re}_L^{0.55} \text{Ga}_L^{-0.42} \left( \frac{a_s d_p}{\varepsilon} \right)^{0.65} \varepsilon$ $\text{Ga}_L = d_p^3 \rho_L \left[ \rho_L g + \left( -\frac{\Delta P_{LG}}{Z} \right) \right] / \mu_L^2$
Ellman et al. [45]	<p>Dynamic liquid holdup in high interaction regimes</p> $\log_{10} \left( \frac{\varepsilon_{Ld}}{\varepsilon} \right) = 0.001 - \frac{0.42}{\left[ X_L^{0.5} \text{Re}_L^{-0.3} \left( \frac{a_s d_h}{1-\varepsilon} \right)^{0.3} \right]^{0.48}}$ $X_L = \frac{1}{\frac{G}{L} \sqrt{\frac{\rho_L}{\rho_G}}}$ $\text{Re}_L = \frac{\rho_L u_{oL} d_p}{\mu_L}$ $d_h = \left( \frac{16\varepsilon^3}{9\pi(1-\varepsilon)^2} \right)^{0.33} d_p$ $a_s = \frac{6(1-\varepsilon)}{d_p}$
Larachi et al. [46]	<p>Total saturation in all regimes</p> $\log_{10}(1-\beta) = -1.22 \frac{\text{We}_L^{0.15}}{X_G^{0.15} \text{Re}_L^{0.2}},$ $X_G = \frac{G}{L} \sqrt{\frac{\rho_L}{\rho_G}}$ $\text{Re}_L = \frac{\rho_L u_{oL} d_p}{\mu_L};$ $\text{We}_L = \frac{\rho_L u_{oL}^2 d_p}{\sigma_L}$

Table 2.3 (continued)

Reference	Correlation
Fu and Tan [72]	Liquid saturation for low regime $\beta = 1.505 \text{Re}_L^{0.29} \text{Ga}_L^{-0.32} d_h^{-0.22}$ <p>where <math>\beta = \frac{\varepsilon_L}{\varepsilon}</math></p>
Xiao et al. [75]	Dynamic liquid holdup $\varepsilon_{Ld} = 0.2277 + 0.6766 \left( \frac{u_G}{u_L} \right)^{0.8358}$
Ayude et al. [76]	Total liquid holdup $\varepsilon_L = \varepsilon_{Ls} + 0.046 \text{Re}_L^{0.49} \text{Re}_G^{-0.10}$
Wammes et al. [80]	Dynamic holdup $\frac{\varepsilon_{Ld}}{\varepsilon} = 3.8 \text{Re}_L^{0.55} \left[ \frac{d_p^3 \rho_L^2 g}{\mu_L^2} \left( 1 + \frac{\Delta P/Z}{\rho_L g} \right) \right]^{-0.42} \left( \frac{6(1-\varepsilon)d_p}{\varepsilon} \right)^{0.65}$ $\frac{(\Delta P/Z)d_p}{0.5\rho_G u_{oG}^2} = 155 \left[ \frac{\rho_g u_{oG} d_p \varepsilon}{\mu_G (1-\varepsilon)} \right]^{-0.37} \left[ \frac{1-\varepsilon}{\varepsilon(1-\beta)} \right]$

#### 2.5.4 Two Phase Flow Models

Many of the equations for pressure drop and liquid holdup were developed using dimensionless groups of the operating variables. The empirical correlations are applicable only in their specific narrow range of process conditions. Many attempts are being made to model the multiphase flow in trickle bed reactors to develop predictive equations. Most of the models were formulated based on continuity and momentum equations for the gas and liquid phases, coupled with the drag forces between the fluid phases and particles. The drag forces were described by using appropriate closure terms. These models do have some adjustable parameters that need to be determined experimentally.

#### 2.5.4.1 Relative Permeability Model

Saez and Carbonell [8] have modified the Ergun equation for single phase flow in packed beds to model two phase flows through a porous media by introducing relative permeability concept ( $k_a$ ) in the expression of drag force for each phase.

$$\frac{F_\alpha}{\varepsilon_\alpha} = \frac{1}{k_\alpha(\beta_\alpha)} \left[ E_1 \frac{\text{Re}_\alpha}{\text{Ga}_\alpha} + E_2 \frac{\text{Re}_\alpha^2}{\text{Ga}_\alpha} \right] \rho_\alpha g \quad (2.9)$$

$$\text{where } \beta_\alpha = \frac{\varepsilon_\alpha}{\varepsilon}$$

The constants  $E_1$  and  $E_2$  in eq. (2.9) are the Ergun constants for single phase flow in the packed beds [59].  $\text{Re}_\alpha$  and  $\text{Ga}_\alpha$  are Reynolds and Galileo numbers for  $\alpha$  phase respectively.

$$\text{Re}_\alpha = \frac{\rho_\alpha u_\alpha d_e}{\mu_\alpha (1 - \varepsilon)} \quad (2.10)$$

$$\text{Ga}_\alpha = \frac{\rho_\alpha^2 g d_e^3 \varepsilon^3}{\mu_\alpha^2 (1 - \varepsilon)^3} \quad (2.11)$$

$$d_e = 6 \frac{V_p}{S_p} \quad (2.12)$$

Saez and Carbonell [8] related gas relative permeability to gas saturation and liquid relative permeability to reduced saturation and developed the following correlations based on the literature data

$$k_G = \beta_G^{4.80}, \quad \beta_G = \frac{\varepsilon - \varepsilon_{Ls}}{\varepsilon} \quad (2.13)$$

$$k_L = \delta_L^{2.43}, \quad \delta_L = \frac{\varepsilon_L - \varepsilon_{Ls}}{1 - \varepsilon_{Ls}} \quad (2.14)$$

They assumed that the flow is one-dimensional and the liquid holdup is independent of reactor length. Liquid holdup and pressure drop thus can be evaluated as

$$\frac{1}{k_L} \left[ E_1 \frac{\text{Re}_L}{\text{Ga}_L} + E_2 \frac{\text{Re}_L^2}{\text{Ga}_L} \right] - \frac{1}{k_G} \left[ E_1 \frac{\text{Re}_G}{\text{Ga}_G} + E_2 \frac{\text{Re}_G^2}{\text{Ga}_G} \right] \frac{\rho_G}{\rho_L} = 1 \quad (2.15)$$

$$\frac{-\Delta P / Z}{\rho_G g} = \frac{1}{k_G} \left[ E_1 \frac{\text{Re}_G}{\text{Ga}_G} + E_2 \frac{\text{Re}_G^2}{\text{Ga}_G} \right] \quad (2.16)$$

This model was extended by Lakota et al. [47], Nemeč et al. [48], and Nemeč and Levec [49] by proposing new closure laws for relative permeabilities. Lakota et al. [47] proposed

$$k_L = \delta_L^{2.92}, \quad \delta_L \geq 0.3 \quad (2.17)$$

$$k_L = 0.4\delta_L^{2.12}, \quad \delta_L < 0.3 \quad (2.18)$$

for the liquid phase regardless of the particle shape and size, and

$$k_G = \beta_G^n, \quad n = \lambda + 0.0478 \times (\text{Re}_G)^{0.774} \quad (2.19)$$

for the gas phase. The constant  $\lambda$  for spheres is 4.37 while for extrudates is 3.31.

Nemeč et al. [48] have conducted experimental studies and found that the correlation for gas phase permeability given by Lakota et al. [47] as presented in eq. (2.23) underpredicts the experimental observations. Thus, they proposed a correlation for gas relative permeability which explained the experimental data reasonably well.

$$k_G = 0.5\beta_G^{3.9} \quad (2.20)$$

Nemeč and Levec [49] confirmed through their extensive experimental studies in a wide range of operating conditions and shapes and sizes of particles that the relative permeabilities are functions of the phase saturation. They proposed new correlations for gas phase

$$k_G = 0.4\beta_G^{3.6}; \quad \beta_G \leq 0.64 \quad (2.21)$$

$$k_G = \beta_G^{5.5}; \quad \beta_G > 0.64 \quad (2.22)$$

#### 2.5.4.2 Slit model

Holub et al. [9] visualized two phase flow in trickle beds as equivalent to two phase flow in tortuous channels. They considered two phase flow through an inclined slit (Figure 2.6). They assumed no shear stress at gas-liquid interface.

$$\Psi_L = \frac{\Delta P/Z}{p_L g} + 1 = \left( \frac{\varepsilon}{\varepsilon_L} \right)^3 \left[ \frac{E_1 \text{Re}_L}{Ga_L} + \frac{E_2 \text{Re}_L^2}{Ga_L} \right] \quad (2.23)$$

$$\Psi_G = \frac{\Delta P/Z}{\rho_G g} + 1 = \left( \frac{\varepsilon}{\varepsilon - \varepsilon_L} \right)^3 \left[ \frac{E_1 \text{Re}_G}{Ga_G} + \frac{E_2 \text{Re}_G^2}{Ga_G} \right] \quad (2.24)$$

$$\Psi_L = 1 + \frac{\rho_L}{\rho_G} (\Psi_G - 1) \quad (2.25)$$

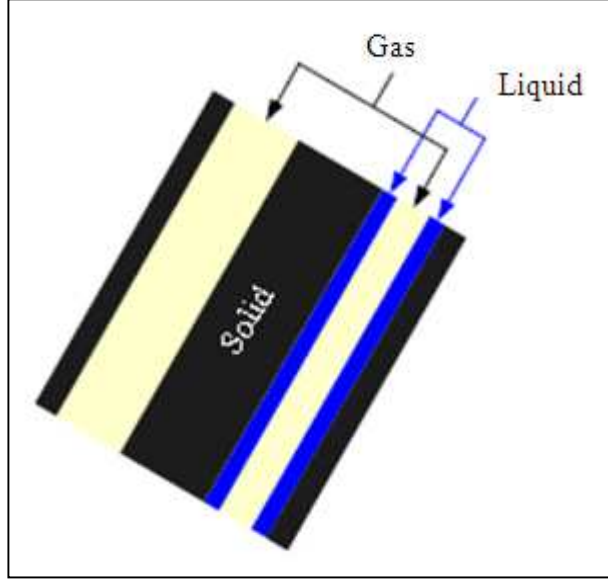


Figure 2.6: Schematic representative of slit model [9]

Their model compared well with experimental observations with a better accuracy than the existing correlations (i.e. Ellman et al. [45] and Larachi et al. [46]). However, Al-Dahhan and Dudukovic [43] observed that the Holub model underpredicts at high pressure and high gas flowrates due to interaction at the gas-liquid interface is not accounted in the model. Al-Dahhan et al. [51] extended the Holub model by incorporating empirical velocity and shear slit factors between the phases to improve the predictions.

$$\Psi_L = \left( \frac{\varepsilon}{\varepsilon_L} \right)^3 \left[ \frac{E_1 \text{Re}_L}{Ga_L} + \frac{E_2 \text{Re}_L^2}{Ga_L} \right] + f_s \frac{\varepsilon_G}{\varepsilon_L} \left( 1 - \frac{\rho_L}{\rho_G} - \Psi_L \right) \quad (2.26)$$

$$\Psi_G = \left( \frac{\varepsilon}{\varepsilon - \varepsilon_L} \right)^3 \left[ \frac{E_1 (\text{Re}_G - f_v \varepsilon_G \text{Re}_L)}{Ga_G} + \frac{E_2 (\text{Re}_G - f_v \varepsilon_G \text{Re}_L)^2}{Ga_G} \right] \quad (2.27)$$

where  $f_s = -4.4 \times 10^{-2} \text{Re}_G^{0.15} \text{Re}_L^{0.15}$

$$f_v = -2.3 \text{Re}_G^{0.05} \text{Re}_L^{-0.05}$$

Iliuta and Larachi [52] generalized Holub slit model by considering partial wetting. Iliuta et al. [53] developed a slit model by incorporating wall effect functions into the drag force equations

$$\Psi_L = \left( \frac{\varepsilon}{\varepsilon_L} \right)^3 \left[ \eta_e^2 \frac{E_1 \text{Re}_L}{Ga_L} + \eta_e \frac{E_2 \text{Re}_L^2}{Ga_L} \right] + f_s \eta_e \frac{\varepsilon - (\varepsilon_L / \eta_e)}{\varepsilon_L} \left( 1 - \frac{\rho_L}{\rho_G} - \Psi_L \right) \quad (2.28)$$

$$\Psi_G = \left( \frac{\varepsilon^3}{(\varepsilon - (\varepsilon_L / \eta_e))^2 (\varepsilon - \varepsilon_L)} \right) \left[ \frac{E_1 (\text{Re}_G - f_v (\varepsilon - (\varepsilon_L / \eta_e))) \text{Re}_i}{Ga_G} + \frac{E_2 (\text{Re}_G - f_v (\varepsilon - (\varepsilon_L / \eta_e)))^2 \text{Re}_i^2}{Ga_G} \right] \quad (2.29)$$

#### 2.5.4.3 Fluid-fluid Interaction Force Model

Attou et al. [10] modeled trickle flow by annular flow pattern in which the gas and the liquid flow are completely separated by a smooth and stable interface. The drag force on each phase is contributed from fluid-fluid interaction as well as from the particle-fluid interactions.

$$F_{LS} = A_{LS} \mu_L u_{oL} + B_{LS} \rho_L u_{oL}^2 \quad (2.30)$$

$$F_{GL} = \varepsilon_G (A_{GL} \mu_G u_r + B_{GL} \rho_G u_r^2) \quad (2.31)$$

$$\text{where } u_r = u_G - \left( \frac{\varepsilon_G}{1 - \varepsilon_G} \right) u_L$$

Boyer et al. [74] extended the Attou's model by incorporating two phase flow tortuosity in liquid-solid drag force.

$$F_{LS} = (1 - \varepsilon_G) (A_{LS} \mu_L u_L + B_{LS} \rho_L u_L^2) (1 - \varepsilon_G)^n + (A_{GL} \mu_G u_G + B_{GL} \rho_G u_G^2) \quad (2.32)$$

The exponent  $n$  was found to be -0.54 for aqueous fluids and -0.02 for organic fluids.

#### *2.5.4.4 Computational Fluid Dynamic Model*

In recent times, application of Computational Fluid Dynamics (CFD) techniques to simulate two phase flow in packed beds is being attempted. Most of the previous studies applied fluid-fluid interaction force model as closure model in CFD calculations for simulating the flow through packed bed [54]–[56], [81]. Jiang et al. [81] developed a two dimensional CFD model including variation of bed porosity. Souadnia and Latafi [82] used the CFD model for predicting liquid saturation and pressure drop in the trickling flow.

Gunjal et al. [54] developed 3-dimensional CFD model to predict liquid phase mixing and liquid flow distribution. Gunjal et al. [55] adopted CFD model to simulate spray flow regime and hysteresis on pressure drop in trickle bed reactors. Atta et al. [56] developed a two phase Eulerian CFD model for gas-liquid flow in packed beds by applying relative permeability concept as closure terms. The simulation results compared well with the experimental data from literature. Table 2.4 summarized various approaches towards hydrodynamic models for two phase flow in trickle beds.

Table 2.4: Various approaches for hydrodynamics modeling in trickle beds

Approaches	Remark
<p><i>Relative permeability model</i>                      Saez and Carbonell [8], Lakota et al. [47], Nemeč et al. [48], Nemeč and Levec [49]</p>	<p>Ergun equation has been modified to account the presence of second flowing phase by incorporation of relative permeability in each phase.</p>
<p><i>Slit model</i>                      Holub et al. [9], Holub et al. [50], Al-Dahhan and Dudukovic [43], Al-Dahhan et al. [51], Iliuta and Larachi [53]</p>	<p>A modified form of Ergun equation. The model represents the complex geometry of the actual void space in a packed bed of particles as a simple inclined slit.</p>
<p><i>Fluid-fluid interfacial force model</i>                      Attou et al. [10], Boyer et al. [74], Narasimhan et al. [83]</p>	<p>Fully wetted flow of gas and liquid phases                      The drag force on each phase are comprised of particle-fluid and fluid-fluid interactions.</p>
<p><i>Computational fluid dynamics</i>                      Gunjal et al. [54], Gunjal et al. [55], Atta et al. [56], Jiang et al. [79], Souadnia and Latifi [82]</p>	<p>Relatively complex and computationally expensive. Boundary conditions are empirical (closure problems). Capable of dealing 2 and 3 dimensions</p>

#### 2.5.4.5 Comparisons of Two Phase Flows Models

Various approaches for predicting liquid holdup and pressure drop in trickle bed reactors (relative permeability model, slit model, fluid-fluid interfacial model and empirical correlation) have been compared with experimental data in trickling regime by Larachi et al. [46] to evaluate the models. The deviations between the models developed by various authors and experimental data are shown in Table 2.5.

Table 2.5: Mean absolute relative error for liquid holdup and pressure drop [46]

Correlations	Liquid holdup (%)	Pressure drop (%)
Saez and Carbonell [8]	19	53
Holub et al. [9]	18	70
Attou et al. [10]	20	61
Ellman et al. [45]	25	70
Larachi et al. [46]	20	72
Al-Dahhan et al. [51]	13	68

As can be seen in Table 2.5, none of the models are reliable in spite of the empirical correlations incorporated into the models. Among the models, slit model provides a reasonable estimate for liquid holdup while relative permeability model provides a reasonable estimate for pressure drop. Still, it is necessary to look for alternate approaches to describe two phase flow in trickle bed reactors as well as packed bed absorbers, distillation units and extractors.

## 2.6 Reaction Kinetics of Hydrodesulfurization.

### 2.6.1 Representation of Sulfur Compounds

Sulfur is present in crude oil in the form many types of hydrocarbon compounds. Quantitative evaluation of reaction kinetics of hydrodesulfurization of the various sulfur compounds is an immense task. Some investigators grouped various sulfur compounds in terms of a few lumps (e.g. Ma et al. [84] and Shabina et al. [85]). Quantitative modeling of the performance of hydrodesulfurization reactor with so many lumps also can be formidable. To minimize the difficulty, a few considered sulfur compounds as a single lump in developing models to explain the performance of industrial units (e.g. Bhaskar et al. [12], Rodriguez and Ancheyta [13] and Murali et al. [14]). Desulfurization of dibenzothiophene is less reactive among sulfur organic

compounds and it can be taken as the controlling compound to represent reaction kinetics of desulfurization of sulfur compounds in crude oil.

### 2.6.2 Reaction Kinetics

Two main models to kinetically model HDS are the power law and Langmuir Hinshelwood. Macias and Ancheyta [29] and Ancheyta et al. [86] conducted experimental studies to determine kinetics of HDS reaction described by power-law model.

$$-\frac{dC_A}{d(1/LHSV)} = kC_A^n \quad (2.33)$$

The value of  $n$  depends on the type and distribution of sulfur compounds in the oil fraction as well as on the catalyst employed. The apparent rate constant was calculated from the  $n^{\text{th}}$  order rate equation.

$$k = \frac{1}{n-1} \left[ \frac{1}{S_p^{n-1}} - \frac{1}{S_f^{n-1}} \right] (LHSV)^{-n} \quad (2.34)$$

where  $k$  is apparent rate constant for hydrodesulfurization,  $n$  is order of reaction,  $S_p$  is sulfur in product (wt%) and  $S_f$  is sulfur in feed (wt%).

The Power Law model is simple but it unable to account for inhibition in the reaction processes. On the other hand, the Langmuir-Hinshelwood model is complex but has advantage of taking into account the inhibition in reaction processes. Most of the kinetic studies of hydrotreating that using Langmuir-Hinshelwood are based on sulfur and nitrogen model compounds which include hydrogen sulfide ( $H_2S$ ) and ammonia ( $NH_3$ ) as inhibiting species. The general reaction steps for Langmuir-Hinshelwood model are as follows [87];

- 1) Adsorption of the reactant ( $A$ ) on the active site of the catalyst with an adsorption factor;  $K_A$
- 2) Reaction of  $A$  on the surface of catalyst with other reactants adsorbed on other sites
- 3) Desorption of the products from the active sites into the bulk fluid.

Broderick and Gates [88] analyzed the reaction kinetics of both the hydrodesulfurization and the hydrogenation reactions of dibenzothiophene using an isothermal plug-flow reactor, and recommended the reaction kinetics is based on Langmuir-Hinshelwood expression. Korsten and Hoffmann [89] presented a single lump model with Langmuir-Hinshelwood kinetics to account for hydrogen sulfide inhibition. Froment [21] proposed kinetics for hydrogenation and hydrodesulfurization reactions by accounting the adsorption of various reacting species on two types of active sites. Table 2.6 presents different models of kinetic equations of Langmuir-Hinshelwood and power type.

Table 2.6: Selected kinetic models for hydrodesulfurization reaction

Model	Reaction kinetic
Froment [21]	$r_{DBT-BPH} = \frac{k_1 K_{DBT\sigma} K_{H_2,\sigma} C_{DBT} C_{H_2}}{1 + K_{DBT\sigma} C_{DBT} + \sqrt{K_{H_2,\sigma} C_{H_2} + K_{H_2S,\sigma} (C_{H_2S}/C_{H_2})}}^3$
Van Hasselt et al. [40]	$r_A = \frac{K_r C_{DBT}^2 C_{H_2}}{(1 + K C_{H_2S})}$
Broderick and Gates [88]	$r_{DBT-\tau} = \frac{k_2 C_{DBT} C_{H_2}}{(1 + K_{DBT} C_{DBT}) + (1 + K_{H_2} C_{H_2})}$
Korsten and Hoffman [89]	$r_{HDS} = \frac{k_{HDS} C_S C_{H_2}^{0.45}}{(1 + K_{H_2S} C_{H_2S})^2}$
Girgis and Gates [90]	$r_{HDS} = \frac{k' K'_{DBT} K'_{H_2} C_{DBT} C_{H_2}}{1 + K'_{DBT} C_{DBT}}$
Tsamatsoulis and Papayannakos [91]	$r_{HDS} = \frac{k_{HDS} P_{H_2} C_S^{2.16}}{(1 + K_{H_2S} P_{H_2S} + K_{H_2} P_{H_2})}$
Chen and Ring [92]	$r_A = K C_A^{1.12} C_{H_2}^{-0.85}$
Cotta et al. [93]	$r_{HDS} = K_S C_{DBT}^{1.2} P_{H_2}^{1.5}$

where  $r$  is the reaction rate,  $k$  is the rate constant,  $K_i$  are equilibrium constants;  $P_i$  are pressure values; and the subscripts  $DBT$ ,  $H_2$ ,  $H_2S$  and  $S$  refer to dibenzothiophene, hydrogen, hydrogen sulfide and sulfur respectively.

## 2.7 Experimental Information on HDS Reactor Performance

A lot of experimental studies have been performed to investigate the impact of process variables on HDS reactor performance. Jimenez et al. [27] conducted an experimental study on hydrodesulfurization of vacuum gas oil (VGO) in the ranges of operating conditions; for temperature 330–390°C, pressure 6–10MPa, and liquid hourly space velocity (LHSV) 1–3h<sup>-1</sup> and gas/oil ratio 4.6–6.25. Experimental observations show that high temperature and pressure while low LHSV improve the sulfur conversion. Similar studies also have been performed by other researchers by changing pressure, H<sub>2</sub>/CH ratio and LHSV, and keeping other parameters constant [13], [14], [25]. They found the similar observations as Jimenez's, and used the results for estimating kinetic parameters. Table 2.7 provides some published experimental data from various investigators on reactor performance.

Table 2.7: Experimental data on hydrodesulfurization performance

Process conditions	Results
<p>Rodriguez and Ancheyta [13]  <math>H_2/HC = 2000\text{ft}^3/\text{bbl}</math>  <math>LHSV = 2\text{h}^{-1}</math>  <math>\text{Pressure} = 54\text{kg}/\text{cm}^2</math>  <math>\text{Temperature} = 340\text{--}380^\circ\text{C}</math></p> <p>Murali et al. [14]  <math>H_2/HC = 200\text{--}600\text{Nm}^3/\text{m}^3</math>  <math>LHSV = 0.8\text{--}2.6\text{h}^{-1}</math>  <math>\text{Pressure} = 4.0\text{--}6.0\text{MPa}</math>  <math>\text{Temperature} = 340\text{--}365^\circ\text{C}</math></p> <p>Sertic-Bionda et al. [25]  <math>H_2/HC = 0.118, 0.354 \text{ and } 0.590 \text{ Nm}^3/\text{kg}</math>  <math>LHSV = 1.0\text{--}2.5\text{h}^{-1}</math>  <math>\text{Pressure} = 40\text{--}65 \text{ bar}</math>  <math>\text{Temperature} = 300^\circ\text{C}</math></p> <p>Jimenez et al. [27]  <math>H_2/HC = 4.5\text{--}6.25</math>  <math>LHSV = 1.0\text{--}3.0\text{h}^{-1}</math>  <math>\text{Pressure} = 6\text{--}10\text{MPa}</math>  <math>\text{Temperature} = 330\text{--}390^\circ\text{C}</math></p>	<p>All the experimental studies confirmed that high temperature and pressure while low LHSV improve the sulfur and nitrogen conversion</p>

## 2.8 Hydrodesulfurization Reactor Models

It is prudent to say that hydrodesulfurization process is very complex. Most of the HDS reactor models have used continuum concept for describing hydrodesulfurization phenomenon in the reactor. These models were developed based on conservation equations of mass and energy and assume plug flow for each

phase which subsequently led to the system of non-linear differential-algebraic equations. The available information on HDS reactor models is reviewed.

Korsten and Hoffman [89] adopted trickle bed reactor modeling technique to hydrotreating processes operated under isothermal conditions. This model incorporated hydrodynamics, mass transfer at gas-liquid and liquid-solid interfaces considering the properties of oil and gases. Langmuir-Hinshelwood type reaction kinetics was adopted. The simulation results were in good agreement with experimental data over a wide range of temperature, pressure, space velocity, and gas-oil ratio. Bhaskar et al. [12] used the model of Korsten and Hoffmann [88] to simulate the HDS of an atmospheric gas oil fraction under adiabatic conditions. The model incorporates mass and energy balances as well as partial wetting.

Besides, Murali et al. [14] and Mederos and Ancheyta [36] developed trickle bed reactor model for hydrotreating reactions considering heat release effects. With rise in the level of sulfur content in the crudes, the reactor temperature can be higher and can be controlled by quenching the catalyst beds with cooler hydrogen injection. Alvarez and Ancheyta [24] also applied the model of Korsten and Hoffmann [88] to simulate the behavior of hydrotreating reaction system with and without the injection of four quench fluids; VGO, diesel, hydrogen and water. Jimenez et al. [27] modeled simultaneous HDS, HDN and HDO. Macias and Ancheyta [29] modeled the HDS reactor considering the effect of particle shape in an isothermal reactor. They found that particle size and pore geometry have significant effect on reactor performance. Liu et al. [26] and Mederos et al. [94] developed a system dynamic model for hydrotreating for optimization studies.

The HDS reactor models developed so far are quite complex and not modular in structure. It is felt that developing a HDS reactor model in terms of cells-in-series structure can be simpler and helpful in utilization of nonlinear parameters such as oil and gas properties, heat and mass transfer parameters.

## 2.9 Conclusions

With the depletion of good quality light crudes, processing of heavier crudes with higher sulfur content is becoming necessary. The possibility of desulfurization of heavier sour crudes in trickle bed reactor is receiving much attention in recent times. Strategies for improved design, operation and optimization can be worked using a reliable reactor model through simulation.

Liquid holdup is an important hydrodynamic parameter that defines the residence time for liquid phase in the reactor and hence the degree of conversion. Many investigators reported experimental measurements on liquid holdup. Some empirical correlations are available. Equations based on physically realistic model are still not available. An attempt to develop a physically realistic model for liquid holdup and pressure drop in trickle beds is made in the present work.

A few researchers proposed models for the performance of trickle bed reactors. Models based on continuum concepts to describe the multiphase flow contact in trickle beds with nonlinear reaction kinetics, exothermic reactions and transport model parameters are unrealistic and solution by even numerical methods is tough. It is necessary to develop simpler model to describe the already complex problem. In view of this, an attempt is made to develop one dimensional cells-in-series model to describe the desulfurization of crudes in trickle bed reactors.

## Notation

$a_s$	Liquid-solid interfacial area per unit volume of the reactor
$A$	Reactant
$A_i, B_i$	Interfacial momentum transfer coefficients
$C_A$	Concentration of $a$ in product
Co	Cobalt
$d_p$	Particle diameter
$d_h$	Hydraulic diameter
$d_e$	Equivalent particle diameter
DBT	Dibenzothiophene
$E_o$	Eötvös number, $\rho_L g d_p^2 / \sigma$
$E_1$	Constant in the viscous term of Ergun type equation
$E_2$	Constant in the inertia term of Ergun type equation
$F_\alpha$	Drag force on the $\alpha$ phase per unit volume
$f_s$	Phase interaction parameter (shear)
$f_v$	Phase interaction parameter (velocity)
$g$	Gravitational acceleration
$G$	Gas superficial mass velocity
$Ga_\alpha$	Galileo number of $\alpha$ phase, $\rho_\alpha^2 g d_e^3 \varepsilon^3 / \mu_\alpha^2 (1 - \varepsilon)^3$
H <sub>2</sub>	Hydrogen
H <sub>2</sub> S	Hydrogen sulfide
HC	Hydrocarbon
HDS	Hydrodesulfurization
HDN	Hydrodenitrogenation
HDO	Hydrodeoxygenation
HDT	Hydrotreating
$k$	Apparent rate constant
$k_\alpha$	Relative permeability of $\alpha$ phase
$K$	Equilibrium constant

$L$	Liquid superficial mass velocity
LHSV	Liquid hourly space velocity
Mo	Molybdenum
Ni	Nickel
$n$	Reaction order
$P$	Pressure
$-\Delta P$	Pressure drop
$Re_\alpha$	Reynolds number of $\alpha$ phase, $\rho_\alpha u_\alpha d_e / \mu_\alpha (1 - \varepsilon)$
$Re_i$	Interfacial Reynolds number
$r_{HDS}$	Reaction rate of hydrodesulfurization
RTD	Residence time distribution
$S_p$	Surface area of particle
S	Sulfur
TBR	Trickle Bed Reactor
$u_{oG}$	Gas superficial velocity
$u_{oL}$	Liquid superficial velocity
$u_r$	Reference superficial velocity associated to the gas-liquid slip motion
$u_G$	Gas interstitial velocity
$u_L$	Liquid interstitial velocity
$V_p$	Volume of particle
$We_L$	Liquid Weber number
$X$	flow factor
$Z$	Bed length

### *Greek Symbols*

$\beta$	Saturation
$\varepsilon$	Bed voidage
$\varepsilon_G$	Gas holdup
$\varepsilon_L$	Total liquid holdup

$\varepsilon_{Ld}$	Dynamic liquid holdup
$\varepsilon_{Ls}$	Static liquid holdup
$\varepsilon_p$	Particle volume fraction
$\delta_L$	Reduced saturation of liquid phase
$\eta_e$	Wetting efficiency
$\rho_G$	Gas density
$\rho_L$	Liquid density
$\mu_L$	Liquid viscosity
$\sigma$	Surface tension
$\chi$	Larkin's correlating variable
$\Psi_\alpha$	Dimensionless body force on $\alpha$ phase
$\Phi$	Sphericity of particle

*Subscripts and Superscripts*

$i$	Gas-liquid interface
$\alpha$	Gas or liquid
TP	Two phase
W	Water
G	Gas
L	Liquid
LG	Gas-liquid (two phase flow)

## CHAPTER 3

### MODEL FOR DYNAMIC LIQUID HOLDUP

Liquid holdup in a trickle bed reactor defines the residence time of the liquid phase in the reactor and hence will have a direct bearing on the degree of conversion. Dependence of liquid holdup on various parameters was investigated extensively and empirical correlations were proposed. There have been attempts to model the flow in trickle beds to develop semi-empirical correlations (e.g. Saez and Carbonell [8], Holub et al. [9], Al-Dahhan et al. [51], Attao et al. [10], etc.). New models to estimate liquid holdup and gas phase pressure drop in trickle bed reactors are presented in section 3.1. The models are compared with the literature data in the section 3.2. To account for the deviation in gas phase pressure drop estimates from experimental observations, effect of gas phase volume fraction on tortuosity of gas flow is incorporated into the model equation in section 3.3. Section 3.4 concludes the chapter.

#### **3.1 Submerged Particle Model for Dynamic Liquid Holdup**

In trickle beds, the liquid flows in the form of film over the particles while the gas flows continuously in the void space between liquid film covered particles (Figure 3.1). As liquid trickles down over the catalyst particles by gravitational force, it experiences drag force opposing its flow at the liquid-solid interface. Under steady state, gravitational force acting on the flowing liquid ( $\epsilon_{Ld}$ ) is in equilibrium with the resistance due to drag force experienced by the liquid at the surface of all the particles.

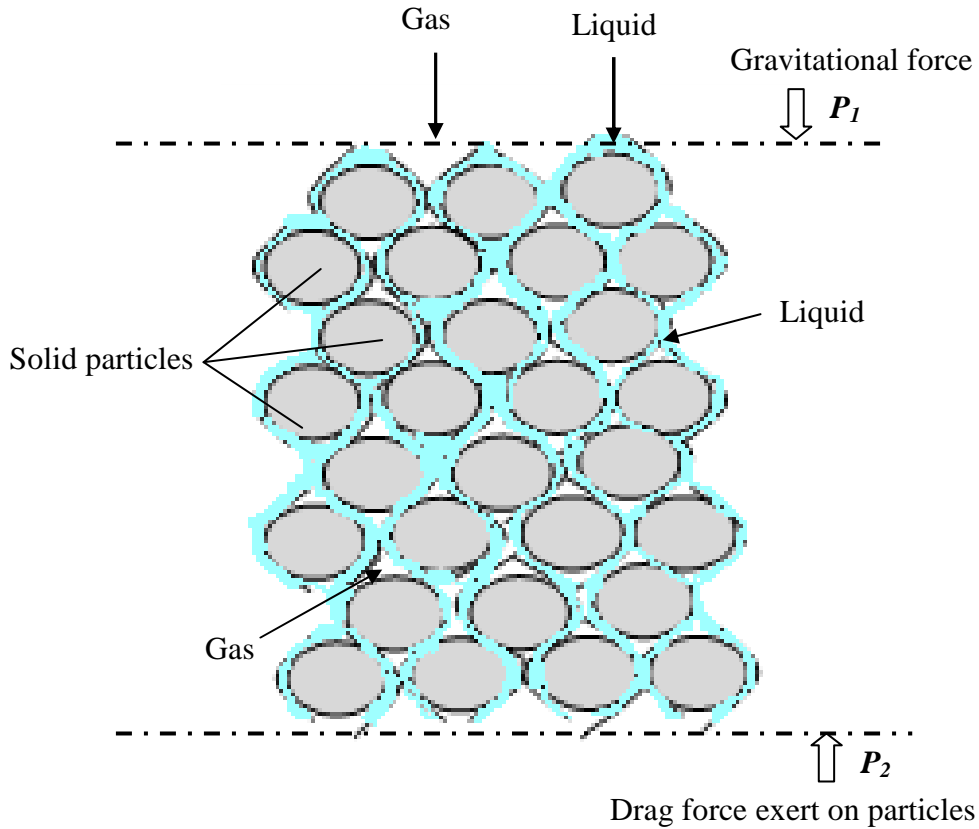


Figure 3.1: Schematic representation of the concurrent gas-liquid downward flow through the void space of the packed bed

From a macro-balance over the trickle bed,

$$AZ\epsilon_{Ld}(\rho_L - \rho_G)g = N_p \cdot C_{Dm} A_p \frac{\rho_L u_L^2}{2} \quad (3.1)$$

*Gravitational force = number of particles  $\times$  drag force of a particle*

where  $N_p = \frac{AZ\epsilon_p}{V_p}$

The liquid flows downward by gravitational force. Gas flows from the higher pressure ( $P_1$ ) to the lower pressure ( $P_2$ ) acting on the area of gas phase. The pressure drop for gas flow is ( $P_1 - P_2$ ). Momentum transfer between gas and liquid at gas-liquid interface by shear is generally accepted to be negligible. The pressure difference ( $P_1 - P_2$ ) acts also on the area of liquid phase enveloping particle phase ( $\epsilon_L + \epsilon_p$ ). This force can assist the gravitational force acting on liquid phase in concurrent gas-liquid flows to increase the liquid velocity in the downward direction. In

the case of countercurrent flows (liquid flowing downward and gas flowing upwards), gas pressure drop acting on the area of liquid phase enveloping the particle phase ( $\varepsilon_L + \varepsilon_p$ ) can reduce the liquid velocity leading to flooding. Thus, momentum balance for two phase flow in packed beds can be expressed as follows

$$AZ\varepsilon_{Ld}(\rho_L - \rho_G)g \pm (P_1 - P_2)_{TP} A(\varepsilon_p + \varepsilon_{Ld}) = AZ \frac{\varepsilon_p}{V_p} C_{Dm} A_p \frac{\rho_L u_{oL}^2}{2\varepsilon_{Ld}^2} \quad (3.2)$$

*Gravitational force*  $\pm$  *Drag force exerted* = *Drag force at liquid-particle interface on liquid by gas*

The sign (+) is for concurrent operation (trickle beds) while the sign (-) is for countercurrent operation. To simplify the momentum balance for two phase flow in packed beds (eq. 3.2), we first note that

$$V_p = \frac{\pi d_p^3}{6} \quad (3.3)$$

$$A_p = \frac{\pi d_p^2}{4} \quad (3.4)$$

Then, substitute eqs. (3.3) and (3.4) into eq. (3.2), this equation can be rearranged as

$$\varepsilon_{Ld}^3 = \frac{3}{4} C_{Dm} \cdot \frac{\rho_L}{\rho_L - \rho_G} \cdot \left[ \frac{\varepsilon_p u_{oL}^2}{d_p g \left\{ 1 \pm \left[ \frac{\rho_L (\varepsilon_p + \varepsilon_{Ld})}{(\rho_L - \rho_G) \varepsilon_{Ld}} \right] \frac{(P_1 - P_2)_{TP}}{Z\rho_L g} \right\}} \right] \quad (3.5)$$

### 3.1.1 Evaluation of $C_{Dm}$

The factor  $C_{Dm}$  is the drag coefficient on a particle embedded in a packed bed. Considering that the drag force in a packed bed is due to the drag force on an individual particle ( $F_{Dm}$ ) multiplied by the number of particles ( $N_p$ ) in the bed, drag force can be expressed as

$$F_D = N_p F_{Dm} \quad (3.6)$$

$$(P_1 - P_2)A\varepsilon = \frac{AZ\varepsilon_p}{V_p} C_{Dm} A_p \frac{\rho_L u_o^2}{2\varepsilon^2} \quad (3.7)$$

Rearranging eq. (3.7) would give equation for the factor  $C_{Dm}$

$$\frac{3}{4} C_{Dm} = \frac{(P_1 - P_2)}{Z} \frac{\varepsilon^3}{(1 - \varepsilon)} \frac{d_p}{\rho u_o^2} \quad (3.8)$$

Comparing eq. (3.8) with Ergun equation for flow through packed beds with empirical Ergun constants recommended by Macdonald et al. [60]

$$\frac{(P_1 - P_2)}{Z} \frac{\varepsilon^3}{(1 - \varepsilon)} \frac{d_p}{\rho u_o^2} = \frac{180(1 - \varepsilon)\mu}{d_p \rho u_o} + 1.8 \quad (3.9)$$

The factor  $C_{Dm}$  can be obtained as

$$\frac{3}{4} C_{Dm} = \frac{180(1 - \varepsilon)\mu}{d_p \rho u_o} + 1.8 \quad (3.10)$$

For non spherical and non uniform particles, particle diameter ( $d_p$ ) can be estimated as an equivalent surface volume mean diameter ( $d_e$ ) given by

$$\frac{6}{d_e} = \sum \frac{S_p}{V_p} \quad (3.11)$$

where  $S_p$  = surface area of a particle

$V_p$  = volume of a particle

### 3.1.2 Dynamic Liquid Holdup

From equations (3.5) and (3.10), equation for dynamic liquid holdup can be obtained as

$$\varepsilon_{Ld} = \left[ \left( \frac{\varepsilon_p u_{oL}^2}{d_p g} \right) \cdot \frac{\rho_L}{\rho_L - \rho_G} \cdot \left( \frac{180\mu_L \varepsilon_p}{d_p \rho_L u_{oL}} + 1.8 \right) \right]^{1/3} \left( \frac{1}{\left\{ 1 \pm \left[ \frac{\rho_L (\varepsilon_p + \varepsilon_{Ld})}{(\rho_L - \rho_G) \varepsilon_{Ld}} \right] \frac{(P_1 - P_2)_{TP}}{Z \rho_L g} \right\}} \right)^{1/3} \quad (3.12)$$

The first term in the right hand side of this equation brings out the dependence of dynamic liquid holdup on particle volume fraction, particle size, liquid velocity and

properties. The second term brings out the effect of gas flow on dynamic liquid holdup. For countercurrent flow this equation suggests that

$$\text{as } \left[ \left\{ \frac{\rho_L}{(\rho_L - \rho_G)} \frac{(\varepsilon_p + \varepsilon_{Ld})}{\varepsilon_{Ld}} \right\} \frac{(P_1 - P_2)_{TP}}{Z\rho_L g} \right] \text{ approaches 1,}$$

dynamic liquid holdup can increase drastically with increase in gas flow rate leading to flooding. It is well known that flooding takes place at around 2 inches of water head per foot of bed length and this corresponds to a value of (1/6) for the factor  $\frac{(P_1 - P_2)_{TP}}{Z\rho_L g}$ . The factor  $\left[ \frac{\rho_L}{(\rho_L - \rho_G)} \frac{(\varepsilon_p + \varepsilon_{Ld})}{\varepsilon_{Ld}} \right]$  is expected to be around 6. Thus, this equation can adequately explain the point of flooding for countercurrent operation. For the case of co-current flow as in trickle bed reactors, increase in gas flow decreases the dynamic liquid holdup and there is no limitation like flooding.

### 3.1.3 Model for Pressure Drop in Trickle Bed Reactors $(P_1 - P_2)_{TP}$

Ergun equation is widely used to estimate pressure drop for gas flow through packed beds.

$$\frac{(P_1 - P_2)}{Z} \frac{\varepsilon_G^3}{(1 - \varepsilon_G)} \frac{d_p}{\rho_G u_{oG}^2} = \frac{180(1 - \varepsilon_G)\mu_G}{d_p \rho_G u_{oG}} + 1.8 \quad (3.13)$$

This equation can be adopted to estimate pressure drop for gas flow in gas-liquid flow in trickle beds as well. Presence of liquid in the voids between particles reduces the void space for gas flow.

$$\varepsilon_G = 1 - \varepsilon_p - \varepsilon_L \quad (3.14)$$

Due to the presence of liquid film on the particles, the gas flows over particles having an effective diameter,  $d_p'$  greater than actual diameter  $d_p$  (Figure 3.2). The relation can be expressed as

$$\left( \frac{d_p'}{d_p} \right)^3 = \frac{(\varepsilon_p + \varepsilon_L)}{\varepsilon_p} \quad (3.15)$$

$$d_p' = \left( \frac{\varepsilon_p + \varepsilon_L}{\varepsilon_p} \right)^{1/3} d_p \quad (3.16)$$

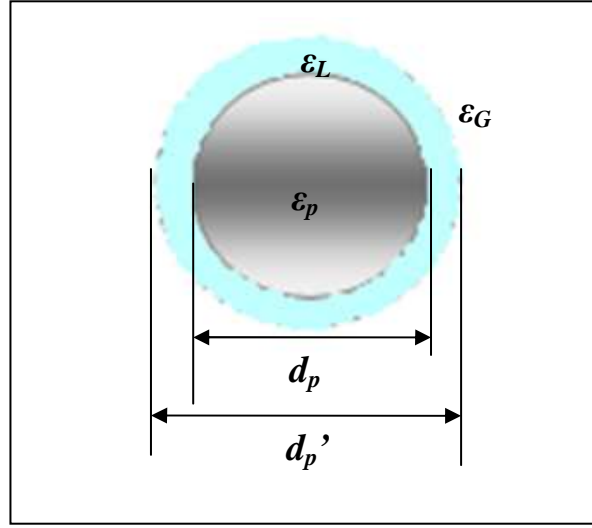


Figure 3.2: Schematic representation of effective diameter particle,  $d_p'$

Incorporating these modifications into Ergun equation (eq. 3.13)

$$\frac{(P_1 - P_2)_{TP}}{Z} \frac{\varepsilon_G^3}{(\varepsilon_L + \varepsilon_p)} \frac{d_p'}{\rho_G u_{oG}^2} = \frac{180(\varepsilon_L + \varepsilon_p)\mu_G}{d_p' \rho_G u_{oG}} + 1.8 \quad (3.17)$$

where

$$\varepsilon_L = \varepsilon_{Ld} + \varepsilon_{Ls} \quad (3.18)$$

Rearranging eq. (3.17), pressure drop for gas flow in trickle beds with two phase flow can be expressed as

$$\frac{(P_1 - P_2)_{TP}}{Z} = \left[ \frac{180\mu_G (\varepsilon_p + \varepsilon_{Ld} + \varepsilon_{Ls})^{2/3} \varepsilon_p^{1/3}}{d_p u_{oG} \rho_G} + 1.8 \right] \cdot \left[ \frac{\rho_G u_{oG}^2 \varepsilon_p^{1/3} (\varepsilon_p + \varepsilon_{Ld} + \varepsilon_{Ls})^{2/3}}{\varepsilon_G^3 d_p} \right] \quad (3.19)$$

The pressure gradient depends on the bed characteristics, velocities of both phases and the physicochemical properties of the flowing gas (gas density and gas viscosity). Eqs. (3.12) and (3.19) can be solved simultaneously to estimate liquid holdup and pressure gradient in trickle beds as the value of other parameters are known.

### **3.2 Results and Discussion**

Effect of particle size, shape, liquid properties, and operating conditions such as gas and liquid velocities, temperature and pressure on dynamic liquid holdup have been reported in the literature. In this section, the submerged particle model equation developed for dynamic liquid holdup (eq. 3.12) is compared with the experimental observations of various investigators as listed in Table 3.1. The two Ergun parameters, 180 and 1.8 are the only fitted constants that were used for model evaluation. The experimental observations on liquid holdup are compared with the model equation in Figures 3.3–3.8.

Table 3.1: Details of operating conditions used for Submerged Particle Model validation

References	System			Liquid velocity (cm/s)	Gas velocity (cm/s)	Packing	Material
	Gas/liquid	Temperature (K)	Pressure (MPa)			Diameter (mm)	
Fu and Tan [72]	H <sub>2</sub> /n-hexane H <sub>2</sub> /cyclohexane	311	3.45	0.465-0.31	0.1-0.3	0.5-1.9	NP
Xiao et al. [75]	air/water	293	0.1	0.8-1.6	7.0-36.0	2.0-3.0	NP
Saroha and Khera [65]	air/water	298	0.1	0.72-2.05	2.0-14.4	4	NP
Aydin and Larachi [68]	air/water air-CMC/water	298-363	0.3-0.7	0.188-1.41	5.0-21.0	3	NP
Al-Dahhan et al. [51]	N <sub>2</sub> /water N <sub>2</sub> /hexane	298	3.55	0.122-0.5498	8.75	1.1	NP
Specchia and Baldi [49]	air/water	293	0.1	0.28	20-80	2.7	NP
Wammes et al. [80]	N <sub>2</sub> /water Helium/water	293	6	0.1-1.2	9.0-36.0	3	NP
Gunjal et al. [55]	air/water	293	0.1	0.17-0.92	22	6	NP
Trivizadakis et al. [35]	air/water	298	0.1	0.2407-0.6148	0.0-30.83	1.5-6.0	P, NP
Ayude et al. [76]	air/water	293	0.1	0.15-0.655	1.4-3.0	3.1	P

### 3.2.1 Submerged Particle Model Validation

#### 3.2.1.1 Effect of Particle Diameter, Shape and Liquid Viscosity on Liquid Holdup

Fu and Tan [72] reported experimental observations on the liquid saturation as a function of liquid mass flow rate for three nonporous spherical particle sizes (0.5mm, 0.9mm and 1.9mm) with hydrogen-hexane and hydrogen-cyclohexane systems. The liquid saturation,  $\beta_L$  can be defined as

$$\beta_L = \frac{\varepsilon_L}{\varepsilon}$$

These observations are compared with the model equation in Figure 3.3. Figure 3.3a illustrates hydrogen-hexane system with viscosity of 0.22cp while Figure 3.3b shows hydrogen-cyclohexane system with viscosity of 0.76cp. They observed that

- i. Liquid holdup increases with liquid mass flowrate
- ii. Liquid holdup is higher for smaller packing size
- iii. Liquid holdup is higher for higher liquid viscosity

The model equation compares well with the experimental data of Fu and Tan [72].

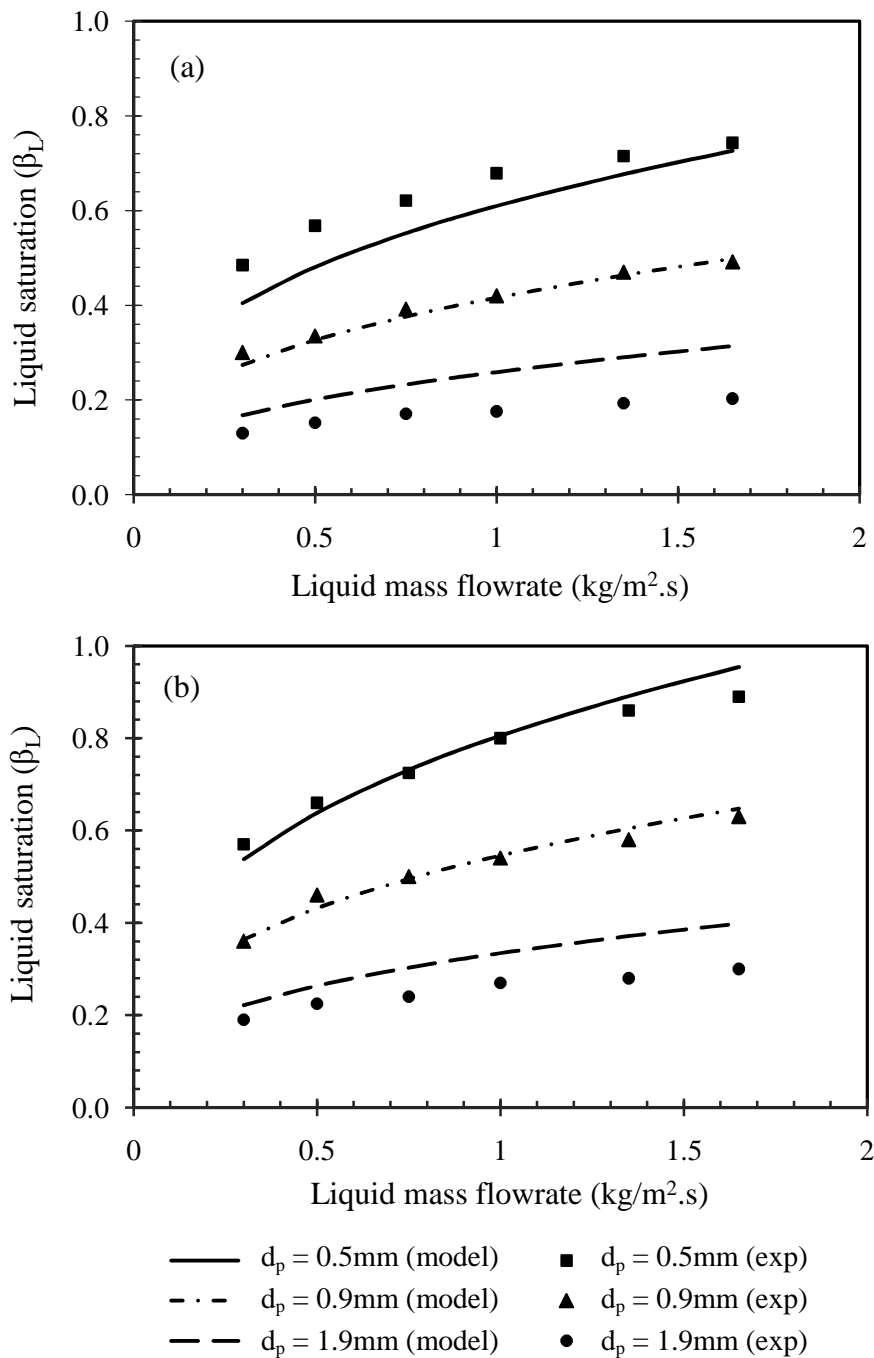


Figure 3.3: Effect of particle size and liquid viscosity on liquid holdup (a) hydrogen-hexane system,  $\mu_L = 0.22$ cp (b) hydrogen-cyclohexane system,  $\mu_L = 0.76$ cp. Data are plotted from Fu and Tan [72]

Trivizadakis et al. [35] reported data on liquid holdup for 3mm spherical particles and 1.5mm diameter  $\times$  3.11mm long cylindrical extrudates. Equivalent surface volume mean diameter of the extrudates is calculated using eq. 3.11 as 1.81mm. Model equation explains the data for spherical particles (Figure 3.4a) reasonably well. Surprisingly, data of Trivizadakis et al. [35] on liquid holdup with extrudates (Figure 3.4b) appears to be independent on liquid flow rate. The model equation predicts the observations well for liquid mass velocity of  $4.27\text{kg/m}^2\cdot\text{s}$ . However, the model equation slightly underpredicts for liquid mass velocity rate of  $2.4\text{kg/m}^2\cdot\text{s}$ .

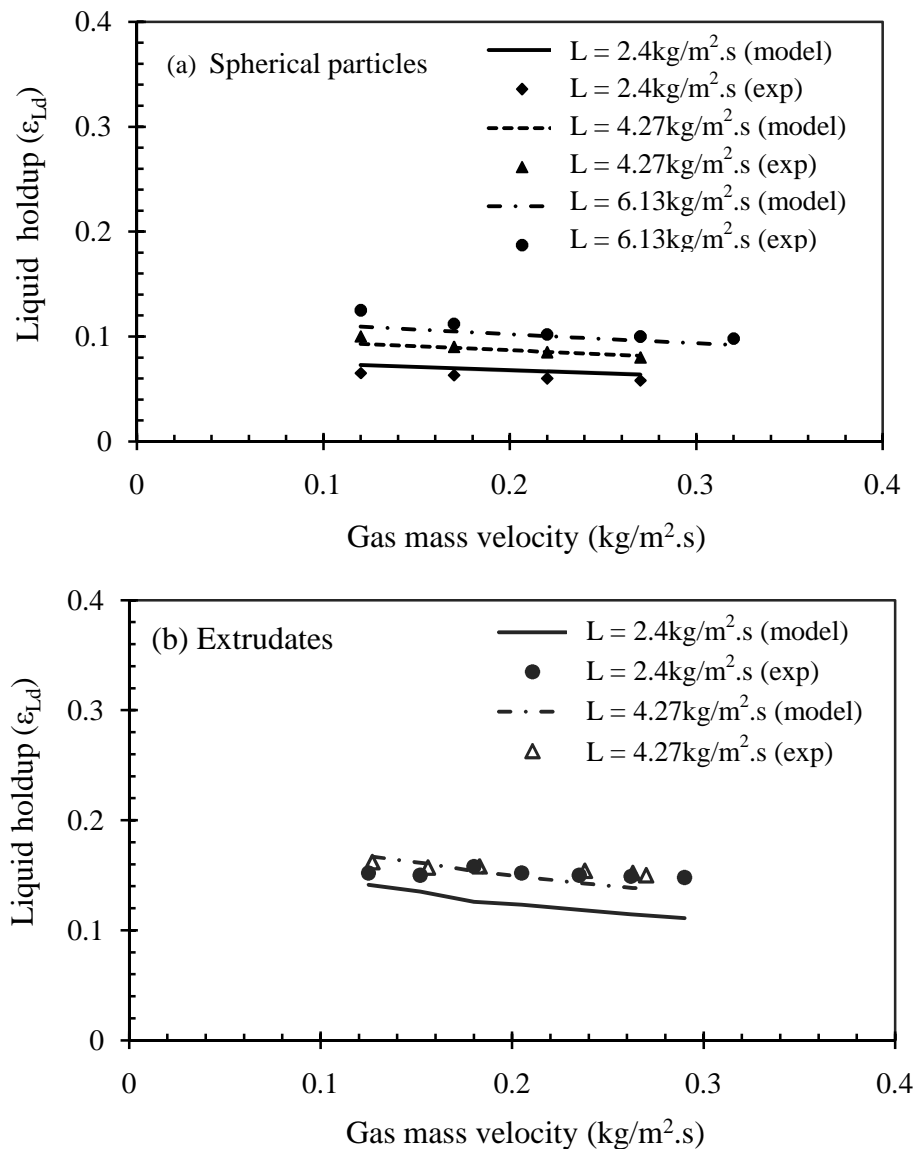


Figure 3.4: Liquid holdup versus gas flux for various liquid mass velocities (a) Spherical,  $d_p = 3\text{mm}$  (b) Cylindrical extrudates,  $d_p = 1.5\text{mm}$ . Data are plotted from Trivizadakis et al. [35]

### 3.2.1.2 Effect of Gas Velocity on Liquid Holdup

Figure 3.5 presents the dependence of liquid holdup on gas and liquid velocities for beds with non-porous packing. Liquid holdup increases with increasing liquid velocity and decreases with increasing gas velocity. Higher liquid velocity increase the volume of liquid held in the reactor. Presence of gas phase increased the shear stress exerted on liquid phase and hence decreased the liquid film thickness and liquid holdup. Model predictions compares well with the observations of Saroha and Khera [65] as shown in Figure 3.5.

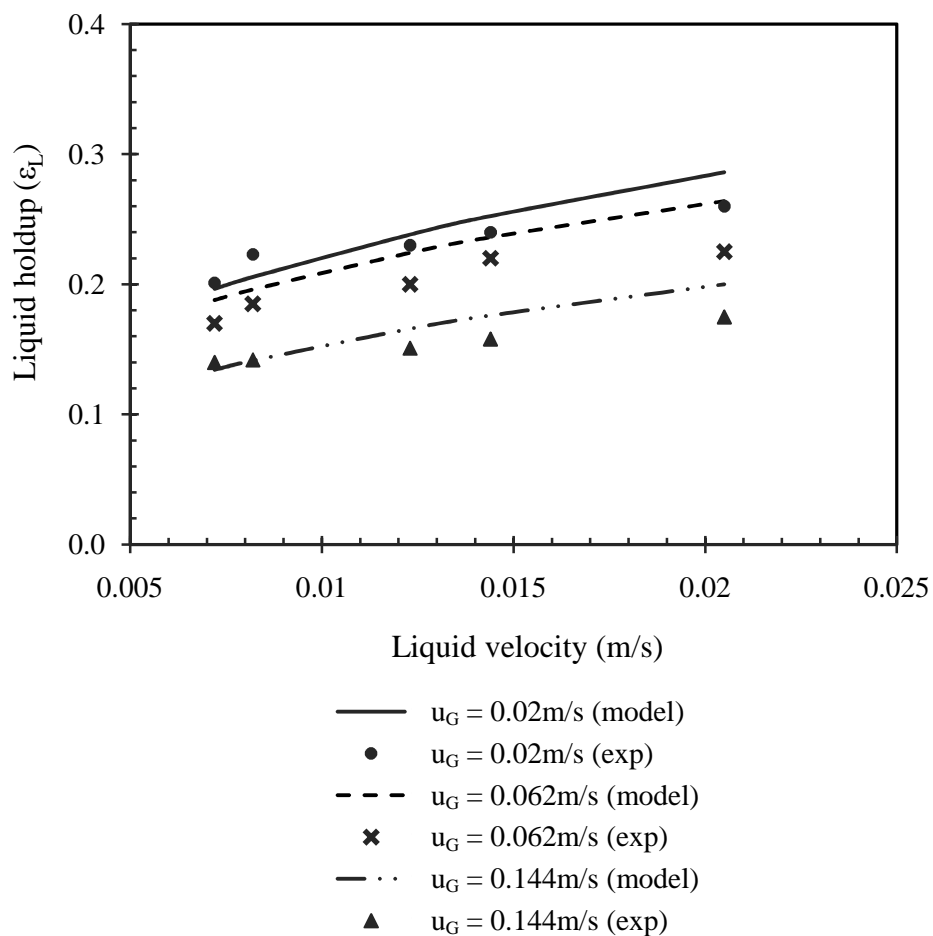


Figure 3.5: Influences of gas and liquid velocities on liquid holdup. Data are plotted from Saroha and Khera [65]

Comparison of the model estimates with the data of Ayude et al. [76] on the dependence of liquid holdup on gas and liquid velocities for porous packing is shown in Figure 3.6. Similar to the results for non-porous packing (Figure 3.5), liquid holdup increases with liquid velocity and decreases with gas velocity. The effect of gas velocity is not that prominent compared to the effect of liquid velocity. Model estimates compares well with experimental observations of Ayude et al. [76].

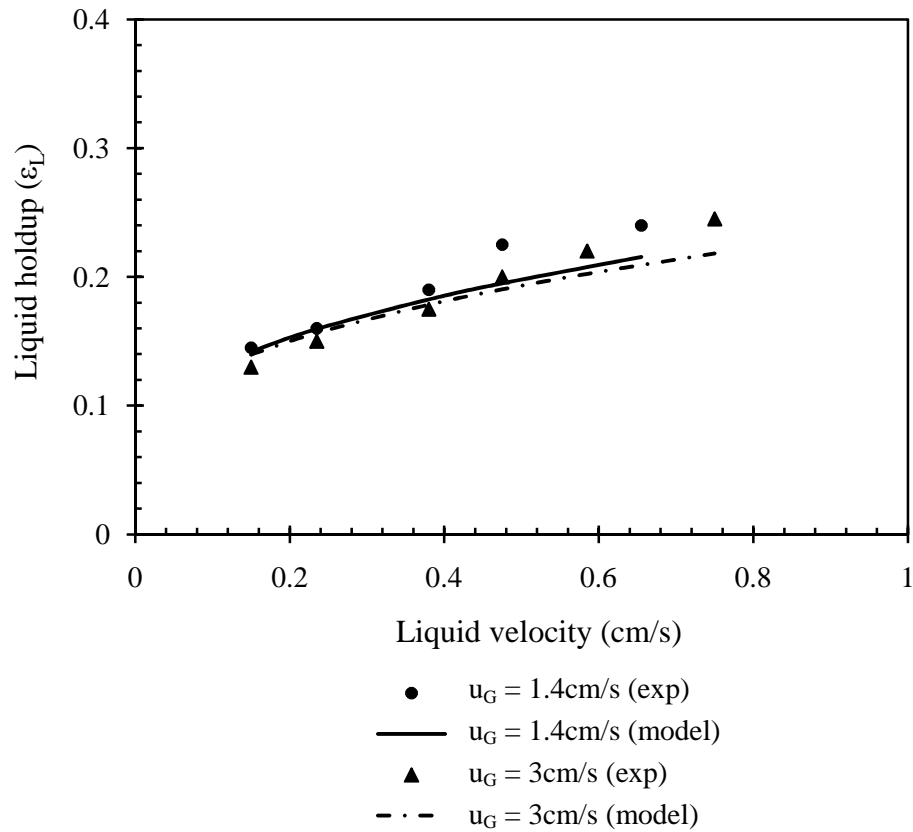


Figure 3.6: Effect of gas and liquid velocities on liquid holdup for porous packing.

Data are plotted from Ayude et al. [76]

### 3.2.1.3 Effect of Temperature and Pressure on Liquid Holdup

Experimental observations of Aydin and Larachi [68] on the effect of reactor temperature and pressure on liquid holdup for air-CMC/water system are compared with the model equation of liquid holdup in Figure 3.7. It shows that at a given superficial gas and liquid velocities, liquid holdup decreases with increasing temperature and pressure. Increase in temperature reduces viscosity. Increase in pressure increases gas density and hence gas drag. The model underpredicts the experimental data of Aydin and Larachi [68] although the estimates are in the right direction.

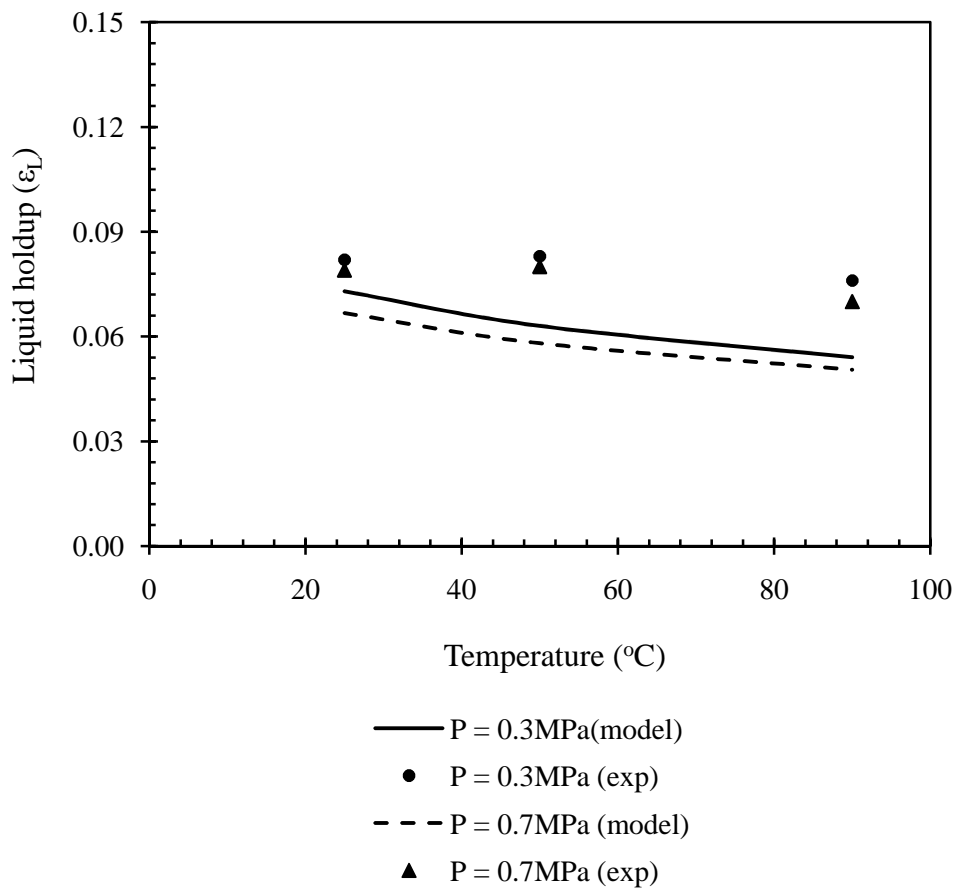


Figure 3.7: Effect of temperature and pressure on liquid holdup for air-CMC/water system. Data are plotted from Aydin and Larachi [68]

### 3.2.1.4 Parity Plot

Comparisons of the model prediction for liquid holdup with the experimental data from the literature are summarized in Figure 3.8. It can be seen that there is a good agreement with a deviation approximately 30%.

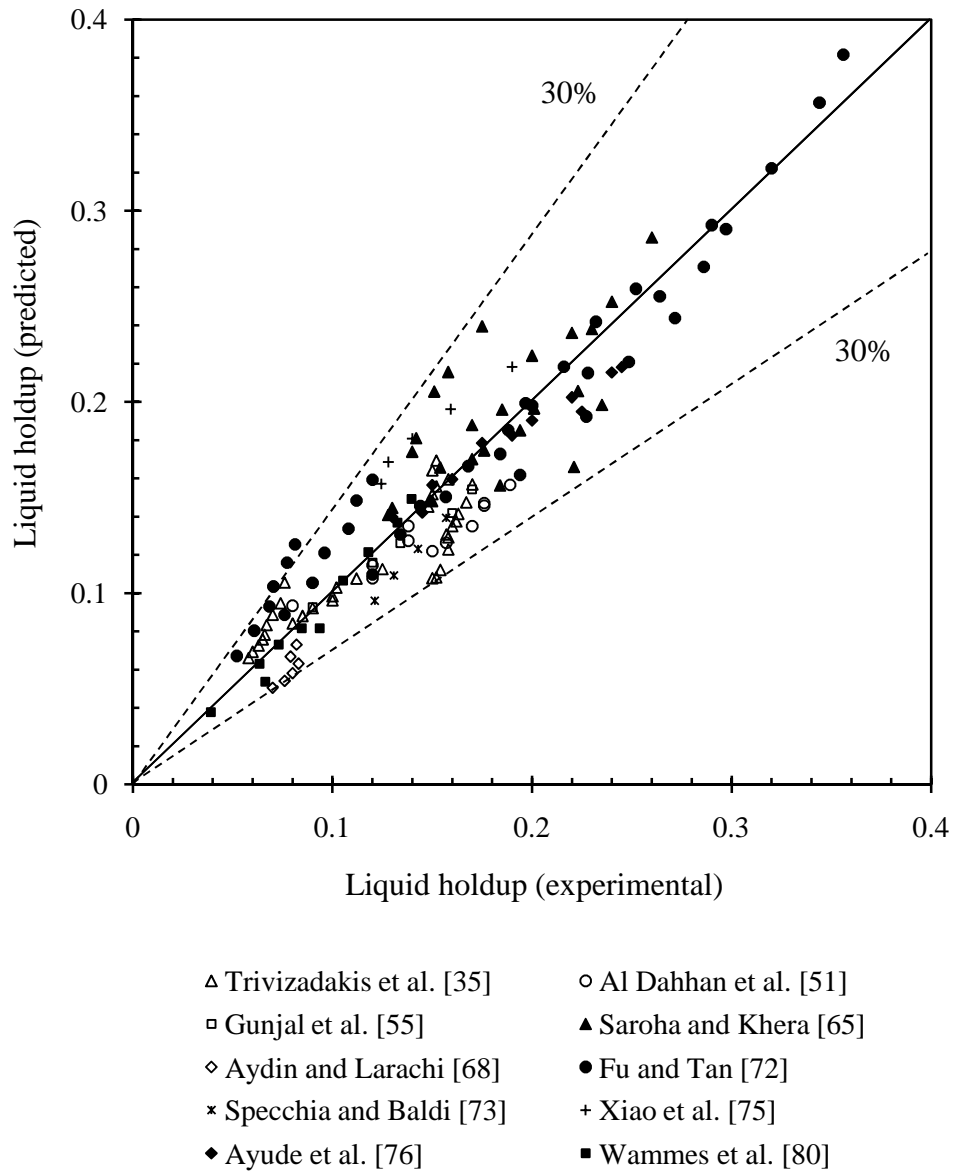


Figure 3.8: Comparison of experimental data on liquid holdup with values predicted by Submerged Particle Model

### 3.2.2 Validation of the Model for Gas Phase Pressure Drop

The model estimates (eq. 3.19) for gas phase pressure drop in packed beds through Ergun's equation modified for the presence of liquid holdup is compared with the experimental observations of various investigators (listed in Table 3.2). Experimental data of Specchia and Baldi [73] and Rao et al. [95] on the effect of gas velocity on bed pressure drop along with the model predictions are presented in Figure 3.9. Experimental observations of Szady and Sundaresan [96] and Iliuta et al. [97] on the effect of liquid velocity on pressure drop are compared with the model equation in Figure 3.10. Though the predictions of the model equation on the effects of gas and liquid velocities on pressure drop are in the right direction, the model underpredicts the experimental data. This could be due to the possibility of Ergun constants getting affected by the presence of liquid in the catalyst bed as they are dependent on the tortuosity of gas flow path. Presence of liquid holdup increases the gas flow path and gas tortuosity.

Table 3.2: Details of operating conditions used for pressure drop model validation

References	System			packing			
	Gas/liquid	Temperature (K)	Pressure (MPa)	Liquid velocity (cm/s)	Gas velocity (cm/s)	Diameter (mm)	Material
Al-Dahhan and Dudukovic [43]	N <sub>2</sub> /water	298	0.31–3.55	0.12–0.37	8.75	1.14	NP
Specchia and Baldi [73]	air/water	293	0.1	0.28	20–88	2.7	NP
Gunjal et al. [55]	air/water	293	0.1	0.17–0.92	22	6	NP
Aydin and Larachi [68]	air/water air-CMC/water	298–363	0.3–0.7	0.188–1.41	5.0–21.0	3	NP
Wammes et al. [80]	N <sub>2</sub> /water	293	6	0.1–1.2	11	3.1	NP
	helium/water	293	6	0.5–0.9	13–39	3.1	NP
Szady and Sundaresan [95]	air/water	293	0.1	0.2–0.8	22	3	NP
Iliuta et al. [96]	air/water	298	0.1	0.5	8.0–42.0	3	NP
Rao et al. [94]	air/water	298	0.1	0.004–0.008	0.13–0.4	6.72	NP
Trivizadakis et al. [35]	air/water	298	0.1	0.2407–0.6148	0.0–30.83	1.5–6.0	P, NP

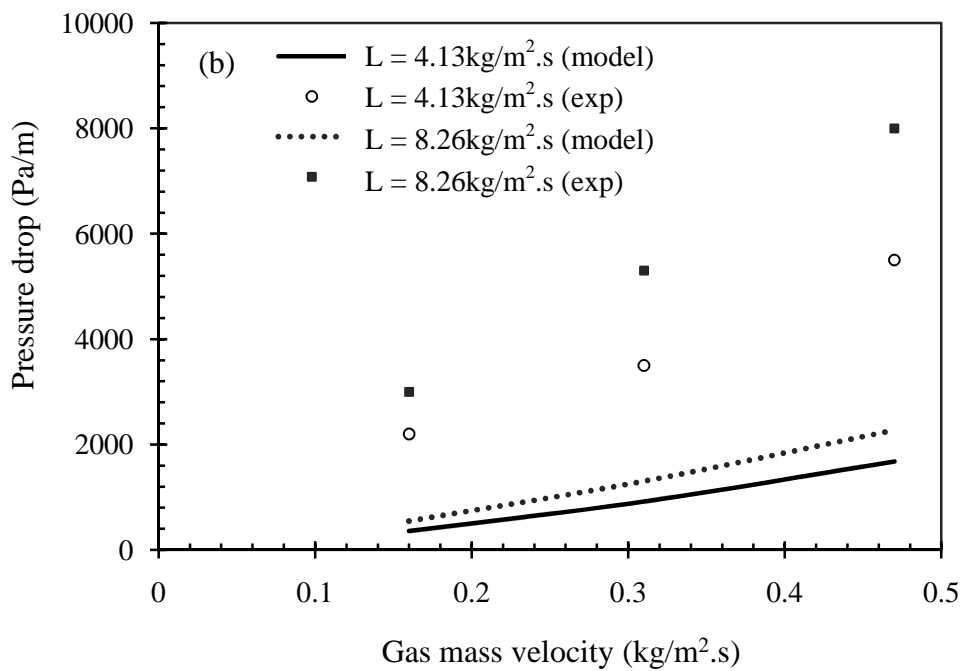
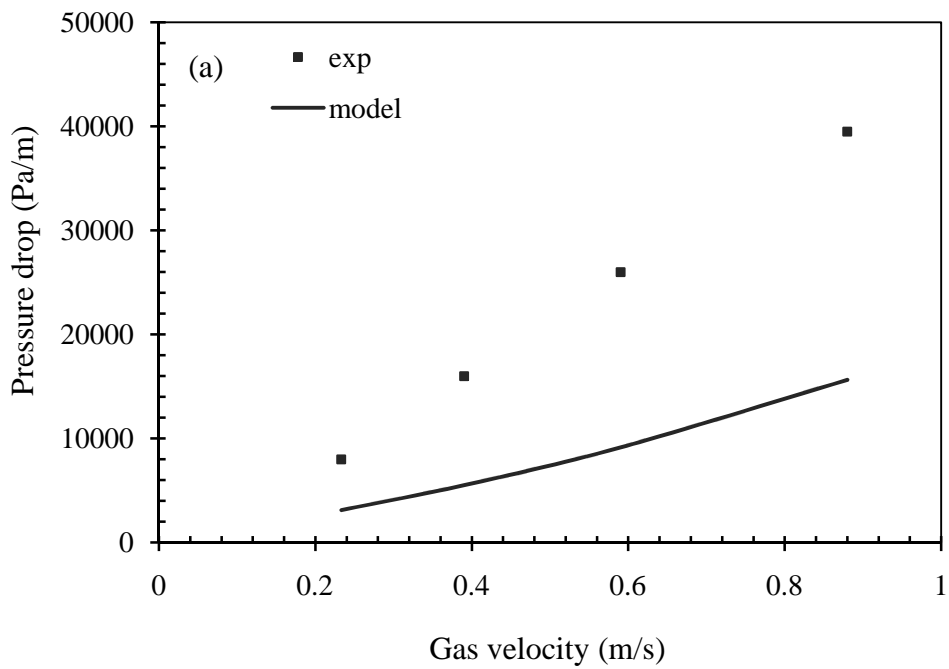


Figure 3.9: Effect of gas velocity on pressure drop. Data are plotted from  
 (a) Specchia and Baldi [73], (b) Rao et al. [95]

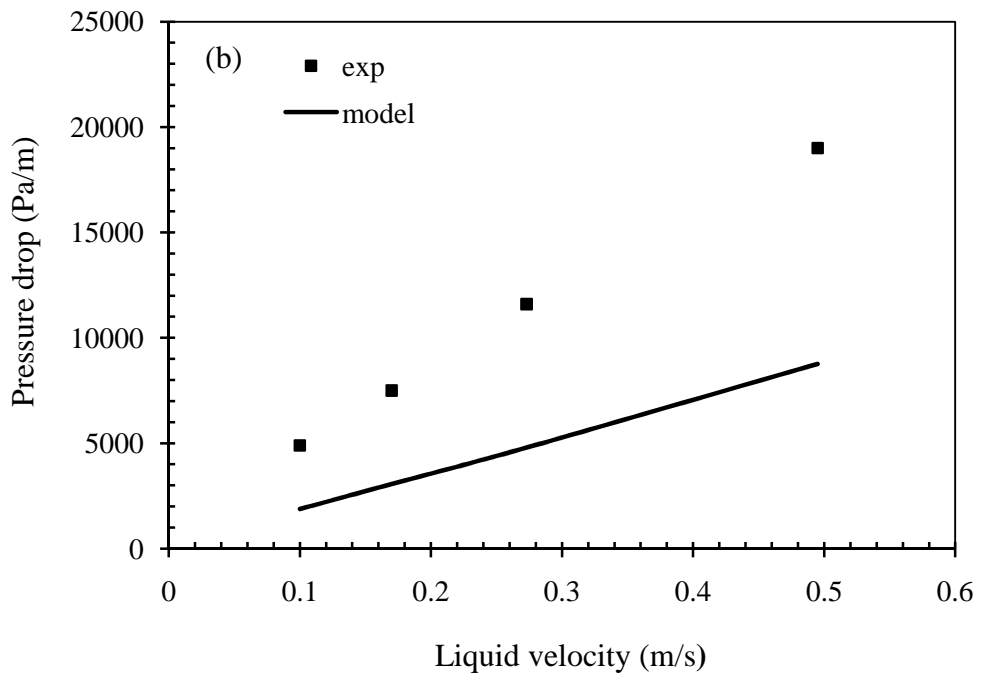
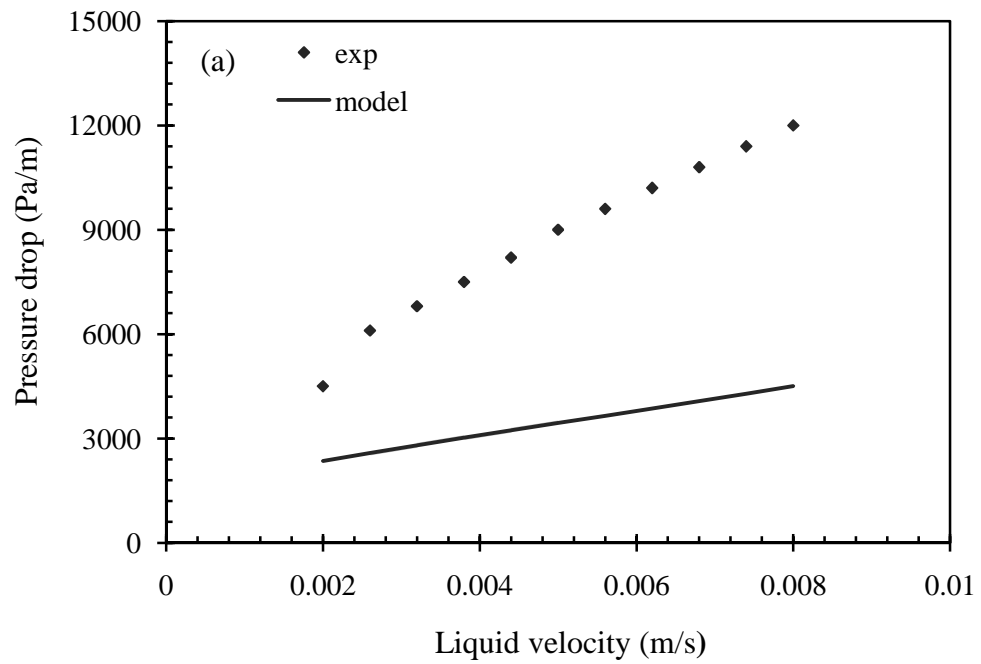


Figure 3.10: Effect of liquid velocity on pressure drop. Data are plotted from (a) Szady and Sundaresan [96], (b) Iliuta et al. [97]

Comparisons of experimental data on pressure drop with values predicted by modified Ergun’s equation with standard Ergun’s parameter is presented in Figure 3.11. It can be seen that the model under predicts the experimental data with deviation approximately 70%. The standard Ergun equation 180 and 1.8 may not be the best values to explain the pressure drop phenomenon in two phase flow. An attempt to improve the accuracy of pressure drop prediction in two phase flow is made in the next section by considering the dependence of two Ergun constants on gas flow tortuosity.

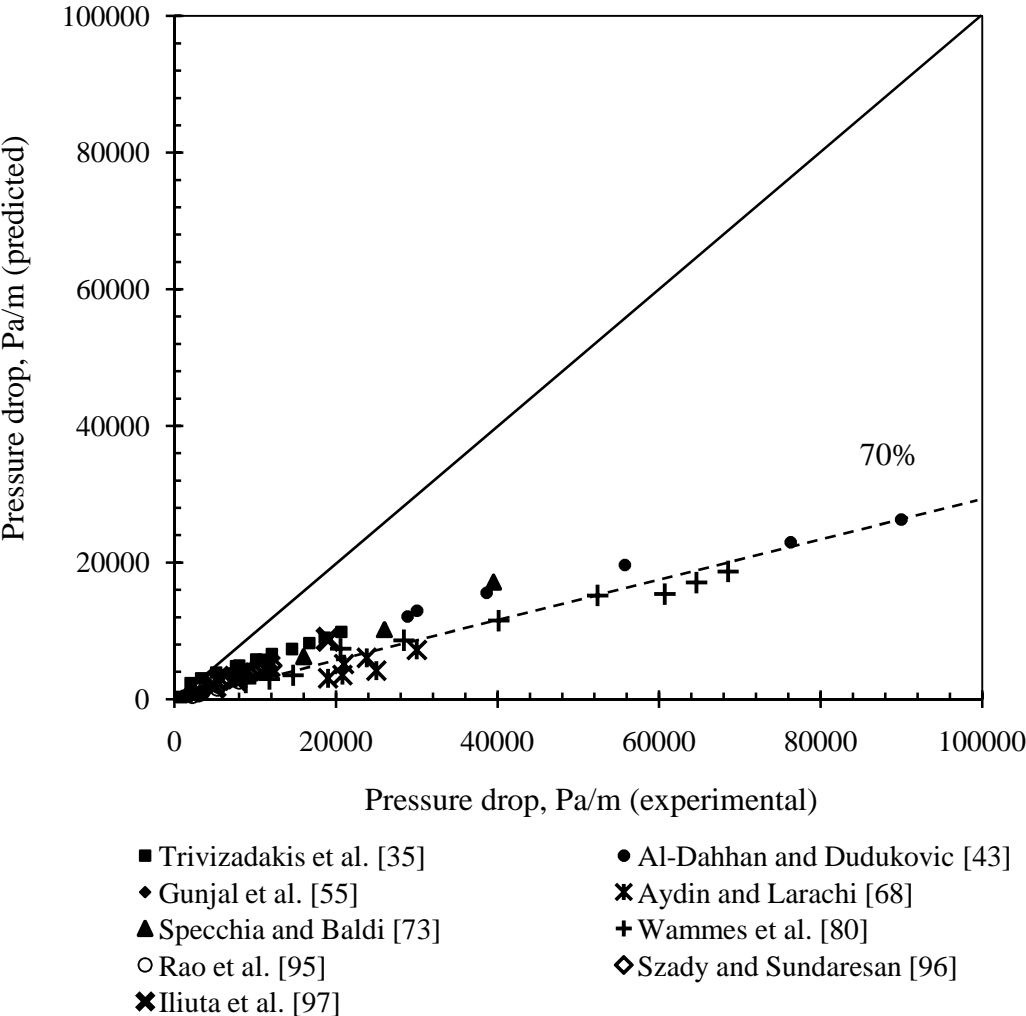


Figure 3.11: Comparison of experimental data on pressure drop with values predicted by modified Ergun’s equation with standard Ergun’s parameter ( $E_1=180, E_2=1.80$ )

### 3.3 Tortuosity of Gas Flow Path

The widely used Ergun's equation for pressure drop was derived among the packed beds to be a bundle of parallel straight tubes through by such fluid flow [98]. The fluid flows through a tortuous path through the bed of particles. However, length of tortuous flow path was assumed to be equal to packed bed length in the original Ergun's equation. Tortuosity in a packed bed can be defined as

$$\tau = \frac{\text{Length of voids}}{\text{Length of bed}}$$

With this, bed voidage can be expressed as

$$\varepsilon = \frac{\text{Volume of voids}}{\text{Volume of bed}} = \frac{\text{Cross sectional area of voids}}{\text{Cross sectional area of bed}} \times \frac{\text{length of voids}}{\text{length of bed}} = \varepsilon_A \tau$$

Thus, ratio of cross sectional area of voids to bed can be obtained as

$$\varepsilon_A = \frac{\text{Cross sectional area of voids}}{\text{Cross sectional area of bed}}$$

This parameter effects actual velocity and bed pressure drop as

$$u_G = \frac{u_{oG}}{\varepsilon_A} = \frac{u_{oG}\tau}{\varepsilon}; \quad F_D = (-\Delta P)A\varepsilon_A = (-\Delta P)A\frac{\varepsilon}{\tau} \quad (3.20)$$

With these parameter, Ergun equation may be obtained as

$$\frac{-\Delta P}{Z} \frac{\varepsilon_G^3}{(1-\varepsilon_G)} \frac{d_p}{\rho_G u_{oG}^2} = \frac{36k_1\tau^2\mu_G(1-\varepsilon_G)}{d_p u_{oG}\rho_G} + 6k_2\tau^3 \quad (3.21)$$

With  $\tau=1$ , this equation reduces to standard Ergun Equation. The constant  $k_1$  is expected to be 2 for laminar flow through a straight pipe [99]. Macdonald et al. [60] recommended the numerical values of the Ergun constants for a bed randomly packed with uniform spherical particles as;

$$36k_1\tau^2 = 180 \quad (3.22)$$

$$6k_2\tau^3 = 1.8$$

$$(3.23)$$

The corresponding values for  $\tau$  and  $6k_2$  are 1.58 and 0.455 respectively. With these values, Ergun's equation can be written in a generalized form considering the tortuosity coefficients as

$$\frac{-\Delta P}{Z} \frac{\varepsilon_G^3}{(1-\varepsilon_G) \rho_G u_{oG}^2} \frac{d_p}{\rho_G u_{oG}^2} = \frac{72\tau^2 \mu_G (1-\varepsilon_G)}{d_p u_{oG} \rho_G} + 0.455\tau^3 \quad (3.24)$$

The tortuosity for gas flow is expected to increase as gas flow path gets restricted with increase in liquid holdup. The exact dependence of Ergun parameters on gas holdup needs to be investigated in the light of experimental observations on pressure drop and it is expected to be inversely proportional to gas holdup. For the present, it is proposed that tortuosity for gas flow can be estimated as

$$\tau = \frac{1}{\varepsilon_G^n} \quad (3.25)$$

Incorporating these modifications into eq. (3.19), the two phase pressure drop thus is expressed as

$$\frac{(P_1 - P_2)_{TP}}{Z} = \left[ \frac{72}{\varepsilon_G^{2n}} \frac{\mu_G (\varepsilon_p + \varepsilon_{Ld})^{2/3} \varepsilon_p^{1/3}}{d_p u_{oG} \rho_G} + \frac{0.455}{\varepsilon_G^{3n}} \right] \cdot \left[ \frac{\rho_G u_{oG}^2 \varepsilon_p^{1/3} (\varepsilon_p + \varepsilon_{Ld})^{2/3}}{\varepsilon_G^3 d_p} \right] \quad (3.26)$$

The empirical constant  $n$  needs to be fitted to match the experimental results. It was found that a value of  $n=0.75$  appears to explain the experimental observations reasonably well and the results are presented in Figures 3.12–3.16.

### 3.3.1 Pressure drop Model Validation (New Ergun Constants)

In this section, experimental observations reported by various investigators are compared with the predictions of the Ergun's equation with the new parameters. Predictions by the model equation with the standard Ergun constants (180 and 1.8) are presented as well for comparison.

### *3.3.1.1 Effect of Gas and Liquid Velocities on Pressure Drop*

Experimental observations of Rao et al. [95] (Figure 3.12a) and Szady and Sundaresan [96] (Figure 3.12b) on the effect of gas and liquid velocities on pressure drop are shown in Figure 3.12 along with the predictions by modified Ergun's equation with the new Ergun parameters (eq. 3.25). It shows that pressure drop increases as increasing gas and liquid velocities. For comparison, predictions by Ergun's equation with standard Ergun constants (eq. 3.19) are also presented. Model equation with new Ergun parameters compares well with the experimental observations of Rao et al. [95] and Szady and Sundaresan [96].

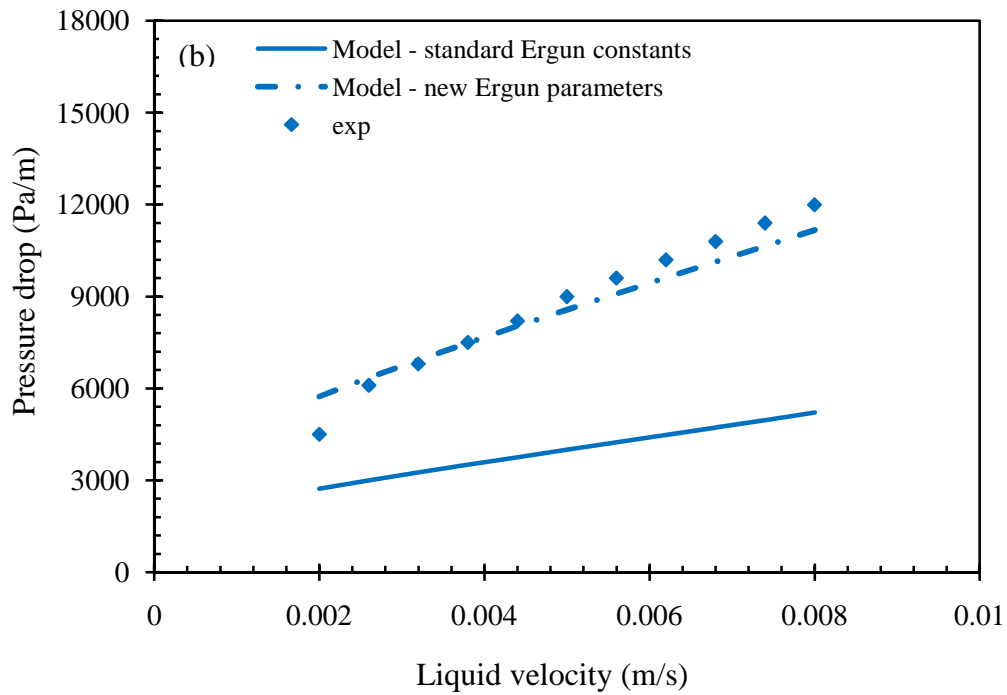
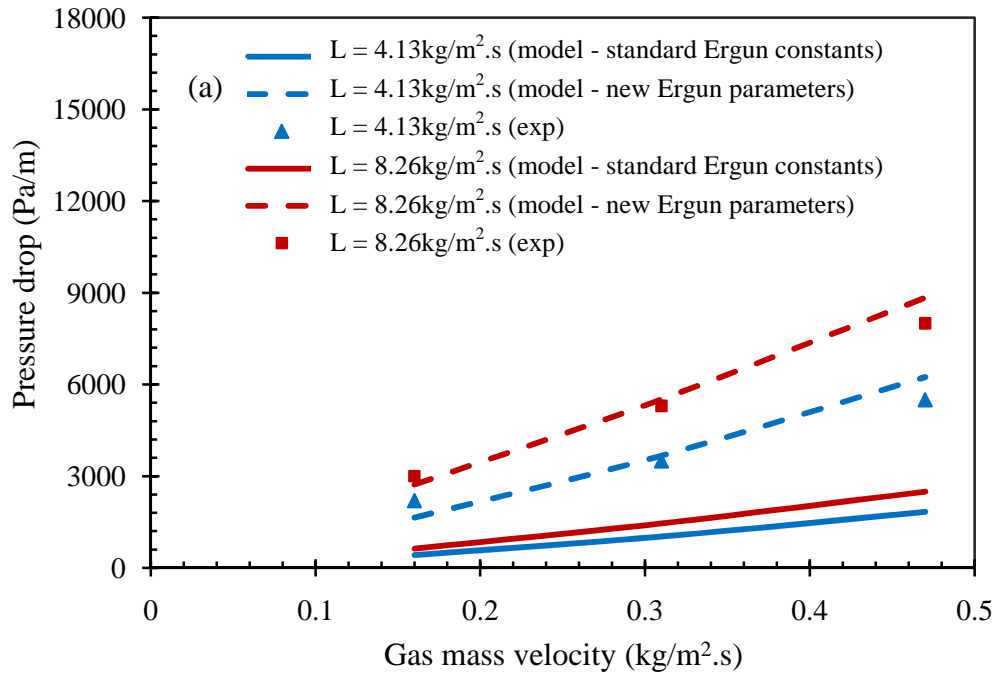


Figure 3.12: Effect of gas and liquid velocities on pressure drop. Data are plotted from (a) Rao et al. [95], (b) Szady and Sundaresan [96]

### 3.3.1.2 Effect of Pressure on Pressure Drop

Al-Dahhan and Dudukovic [43] reported experimental observations on dimensionless pressure drop as a function of liquid mass velocity for two pressures, 0.31MPa and 3.55MPa. The experimental observations are compared with the model equation in Figure 3.13. They observed that pressure drop increases with increasing pressure and liquid mass velocity. An increase in pressure results in higher gas density and hence higher interfacial drag force exerted on liquid phase. The deviation in pressure drop prediction by model equation with new Ergun parameters is reduced significantly. The model equation with new Ergun parameters predicts the observations well for pressure of 0.31MPa. However, the model slightly underpredicts for the pressure of 3.55MPa.

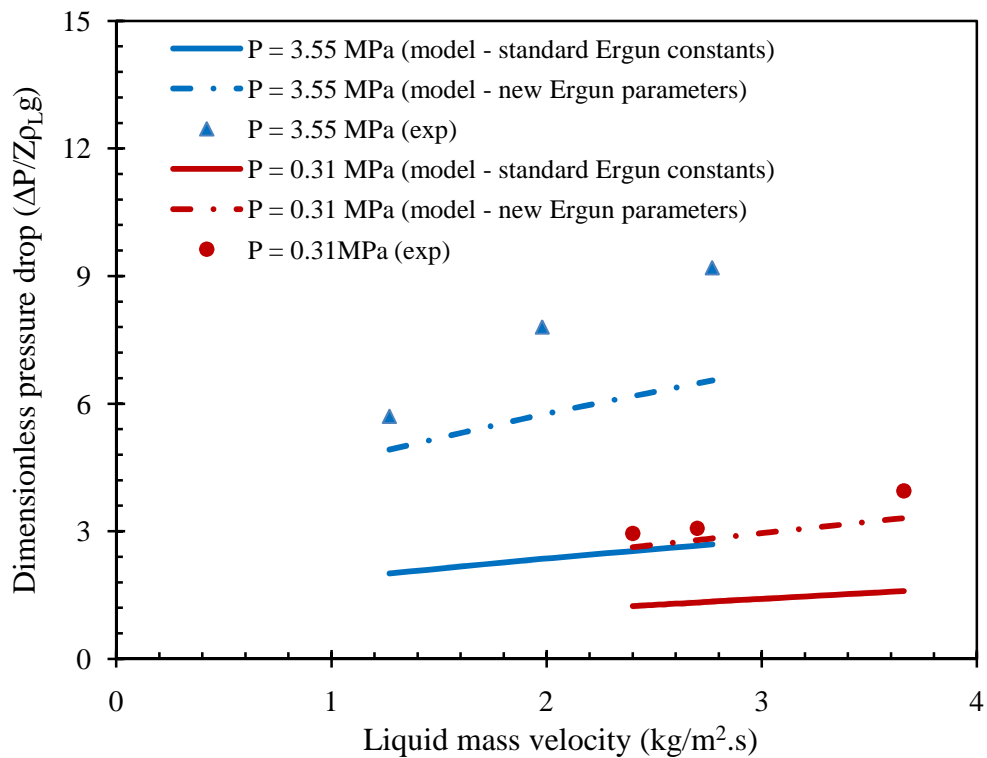


Figure 3.13: Influences of operating pressure on pressure drop. Data are plotted from Al-Dahhan and Dudukovic [43]

### 3.3.1.3 Effect of Temperature on Pressure Drop

Experimental observation of Aydin and Larachi [68] on the effect of temperature on pressure drop is illustrated in Figure 3.14. At a given gas and liquid velocities, pressure drop decreases with increasing temperature. Increase in temperature leads to reduction of gas density and hence low interfacial drag force exerted on liquid phase. The model predictions with new Ergun parameters compares well with the observation of Aydin and Larachi [68].

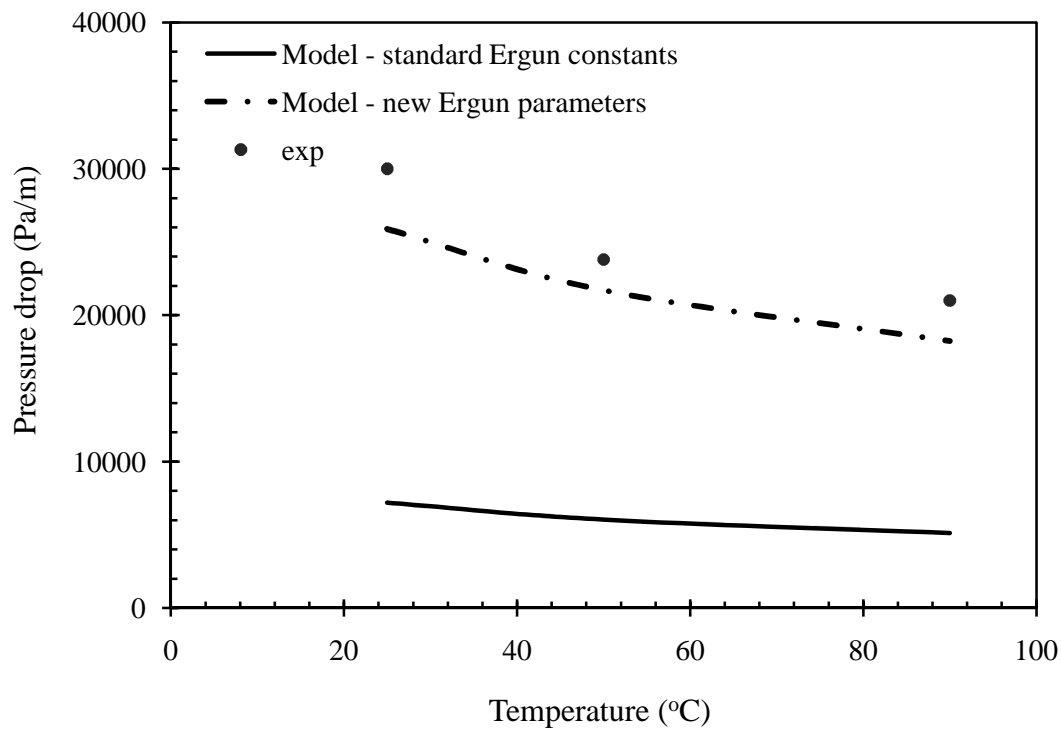


Figure 3.14: Effect of temperature on pressure drop. Data are plotted from Aydin and Larachi [68]

### 3.3.1.4 Effect of Particle Size on Pressure Drop

Comparison of the model estimates with the data of Trivizadakis et al. [35] on the effect of particle diameter and shape on pressure drop for spherical particles (3mm and 6mm) and cylindrical extrudates (1.5mm diameter  $\times$  3.11mm) are shown in Figure 3.15. As observed, particle size has significant effect on pressure drop. Smaller particle size results in higher pressure drop. Model predictions with new Ergun constants explain the data for spherical and extrudates reasonably well.

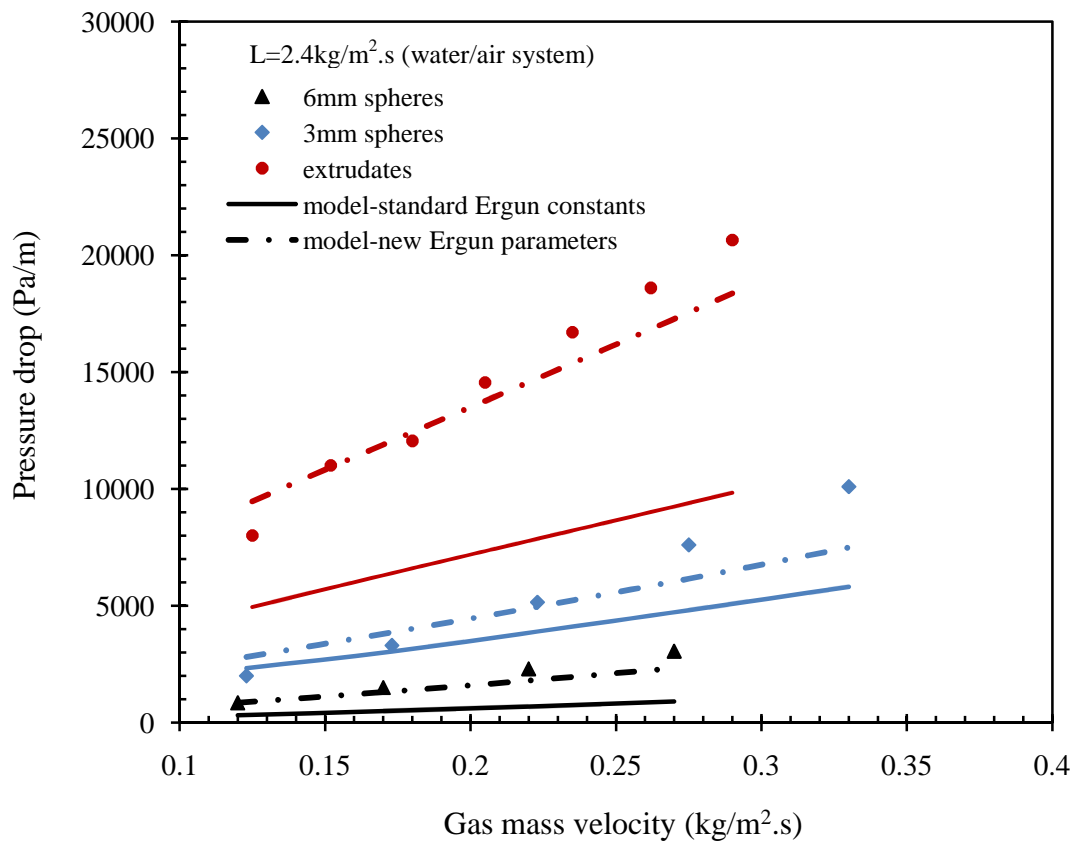


Figure 3.15: Pressure drop versus gas mass velocity for spherical and cylindrical extrudates. Data are plotted from Trivizadakis et al. [35]

### 3.3.1.5 Parity Plot

Model predictions for pressure drop and liquid holdup with experimental observations reported in the literature over a wide range of operating data in terms of liquid and gas velocities, liquid viscosity, packing sizes, temperature and operating pressure are compared in parity plots shown in Figures 3.16 and 3.17. As can be seen, the accuracy of pressure drop prediction has improved significantly with relative error decreased from 70% to 40% (Figures 3.11 and 3.16). Still, the model predictions of pressure drop are lower compared to the experimental data.

Ergun’s equation used is for gas or liquid flow in packed beds. The Ergun constants for gas flow over wetted particles can be lower as wall shear at gas-liquid boundary reduces to zero. In view of this, the Ergun constants could be lower than 180 and 1.8. This needs further research to identify suitable Ergun constants for gas flow on liquid wetted particles.

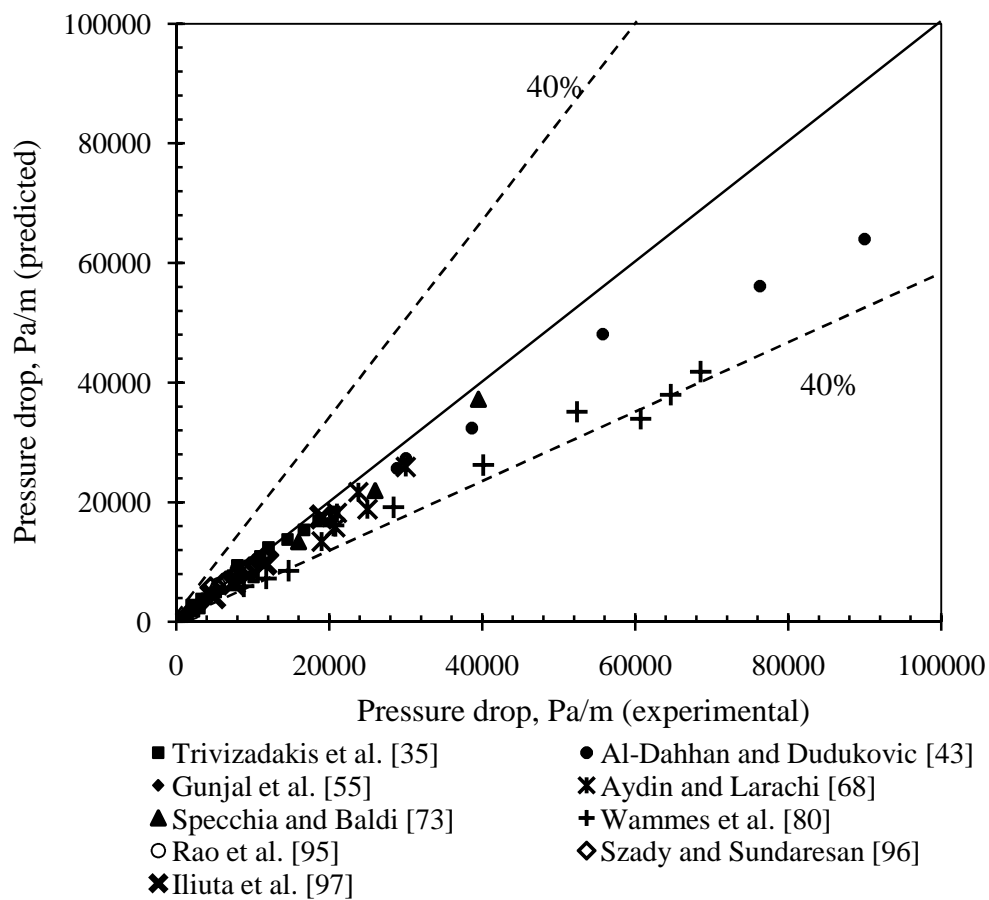


Figure 3.16: Comparison of experimental data on pressure drop with values predicted by modified Ergun’s equation with new Ergun parameters

Liquid holdup prediction remained within the same range of predictability as that by model estimates with standard Ergun constants, as shown in Figure 3.8 (standard Ergun constants for pressure drop prediction) and Figure 3.17 (new Ergun parameters for pressure drop prediction).

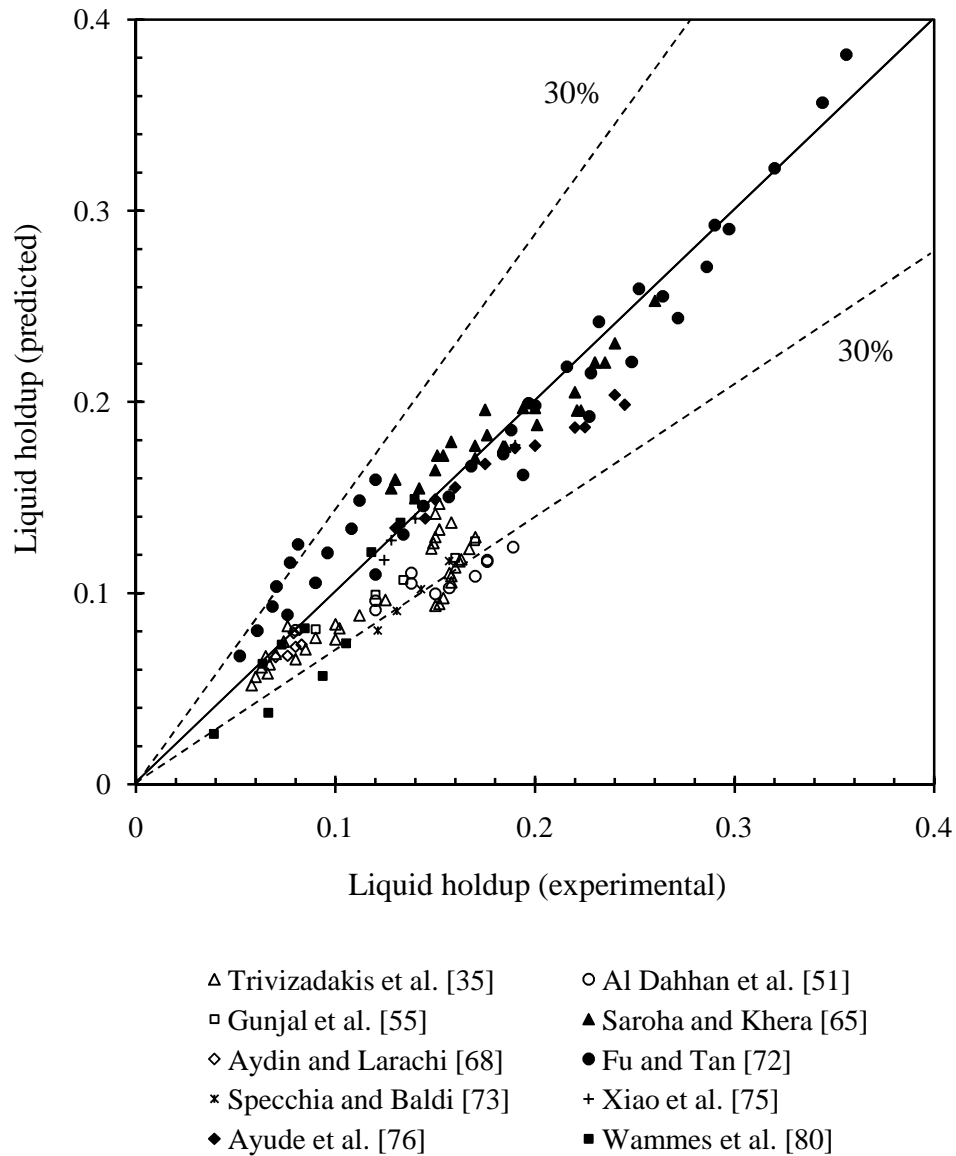


Figure 3.17: Comparison of experimental data on liquid holdup with values predicted by submerged particle model coupled with modified Ergun's equation and new Ergun parameters

### 3.4 Conclusions

In this chapter, a submerged particle model for estimating dynamic liquid holdup and two phase pressure drop in a trickle bed reactor was developed. Liquid holdup enhances the tortuosity of gas flow path which in turn increases pressure drop. The model equations were validated with the experimental data available in literature on liquid holdup and pressure drop as a function of gas and liquid velocities, liquid viscosity, operating temperature and pressure, and particle diameter. The main conclusions are:

- 1) The submerged particle model equation (eq. 3.12) explains the experimental observations for liquid holdup reasonably well. Liquid holdup increases with increasing liquid velocity and liquid viscosity. On the other hand, liquid holdup decreases with increasing gas velocity, particle size, pressure and temperature.
- 2) Ergun equation was adopted to estimate gas phase flow in trickle beds by incorporating the presence of liquid holdup which reduces the cross sectional area for gas flow and increases the size of particles over which gas flows. This equation (eq. 3.19) with usually used Ergun constants (180 and 1.8) underpredicts the experimental observations.
- 3) Deviation of two phase pressure drop from experimental observation significantly decreased as the effect of the gas phase volume fraction on the tortuosity of gas flow is incorporated into the model equation (eq. 3.26).
- 4) Pressure drop increases with increasing gas and liquid velocities as well as operating pressure. On the other hand, pressure drop decreases with increasing temperature and particle size.

## Notation

$A$	Cross section area of reactor ( $\text{m}^2$ )
$A_p$	Projected area of particle ( $\text{m}^2$ )
$d_p$	Particle diameter (m)
$d_p'$	Effective particle diameter (m)
$d_e$	Equivalent surface volume mean diameter (m)
$C_{Dm}$	Drag coefficient on a particle
$F_{Dm}$	Drag force for single particle ( $\text{kg.m/s}^2$ )
$g$	Gravitational acceleration ( $\text{m/s}^2$ )
$G$	Gas mass velocity ( $\text{kg/m.s}^2$ )
$L$	Liquid mass velocity ( $\text{kg/m.s}^2$ )
$N_p$	Number of particles
$-\Delta P$	Pressure drop (Pa)
$P$	Pressure (Pa)
$S_p$	Surface area of particle ( $\text{m}^2$ )
$u_L$	Interstitial liquid velocity (m/s), $\frac{u_{oL}}{\epsilon_L}$
$u_{oL}$	Liquid superficial velocity (m/s)
$u_{oG}$	Gas superficial velocity (m/s)
$V_p$	Volume of particle ( $\text{m}^3$ )
$Z$	Bed length (m)

## Greek letters

$\epsilon$	Bed porosity
$\epsilon_L$	Total liquid holdup
$\epsilon_{Ld}$	Dynamic liquid holdup
$\epsilon_G$	Gas holdup
$\epsilon_p$	Particle volume fraction

$\rho_L$	Liquid density (kg/m <sup>3</sup> )
$\rho_G$	Gas density (kg/m <sup>3</sup> )
$\mu_L$	Liquid dynamic viscosity (Pa.s)
$\mu_G$	Gas dynamic viscosity (Pa.s)
$\tau$	Tortuosity

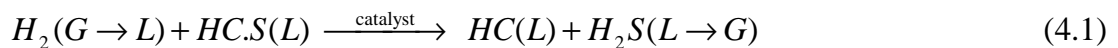
### *Subscripts*

$G$	Gas
$L$	Liquid
$TP$	Two phase
exp	Experiment

## CHAPTER 4

### MODEL FOR TRICKLE BED REACTOR

Trickle bed reactors are widely used for hydrotreating of hydrocarbons with hydrogen in presence of catalyst particles in a packed bed. In hydrodesulfurization reaction, sulfur atoms attached to the hydrocarbon molecules react with the dissolved hydrogen at the surface of solid catalyst to form hydrogen sulfide. Sulfur compounds in hydrocarbons are lumped together and represented as HC.S. The reaction can be represented as



Trickle bed reactors are multiphase in nature, the reactions are exothermic, heat and mass transfer processes are non linear. In view of these, the models formulated on continuum concepts (e.g. Rodriguez and Ancheyta [13], Murali et al. [14], Mederos et al. [15], Jimenez et al. [27], Mederos and Ancheyta [36], etc.) are not realistic. Hence, an attempt is made to develop a one-dimensional cell-in-series model to explain the performance of hydrodesulfurization process.

A new one-dimensional cells-in-series model to describe hydrodesulfurization reaction in trickle bed reactor is developed in section 4.1. In section 4.2, model governing equations to establish the reactor model are formulated. Kinetic reactions as well as correlations to estimate hydrodynamics and feed properties are presented in section 4.3 and 4.4. The calculation procedure is presented in section 4.5. In section 4.6, the reactor model is validated with the experimental data reported in literature. In section 4.7, the validated model is applied to simulate HDS commercial unit to investigate the effect of various parameters on the reactor performances. Section 4.8 concludes the chapter.

#### 4.1 1-D Cells in Series Model

A trickle bed reactor, with gas and liquid flowing co-currently downward through a catalytic packed bed to undergo chemical reactions, operating under steady state is considered. Figure 4.1 presents schematic representative of one-dimensional cells-in-series model for trickle bed reactor. The reactor is assumed to consist of  $N$  cells in series along the axial direction. Each cell consists of three phases - gas phase, liquid phase and solid phase - well mixed with in each phase. The variables for each phase are distinguished with subscripts  $G$  for gas phase,  $L$  for liquid phase and  $S$  for solid phase. The axial distance of each cell ( $\Delta z$ ) is assumed to be equal with the diameter of catalyst particle.

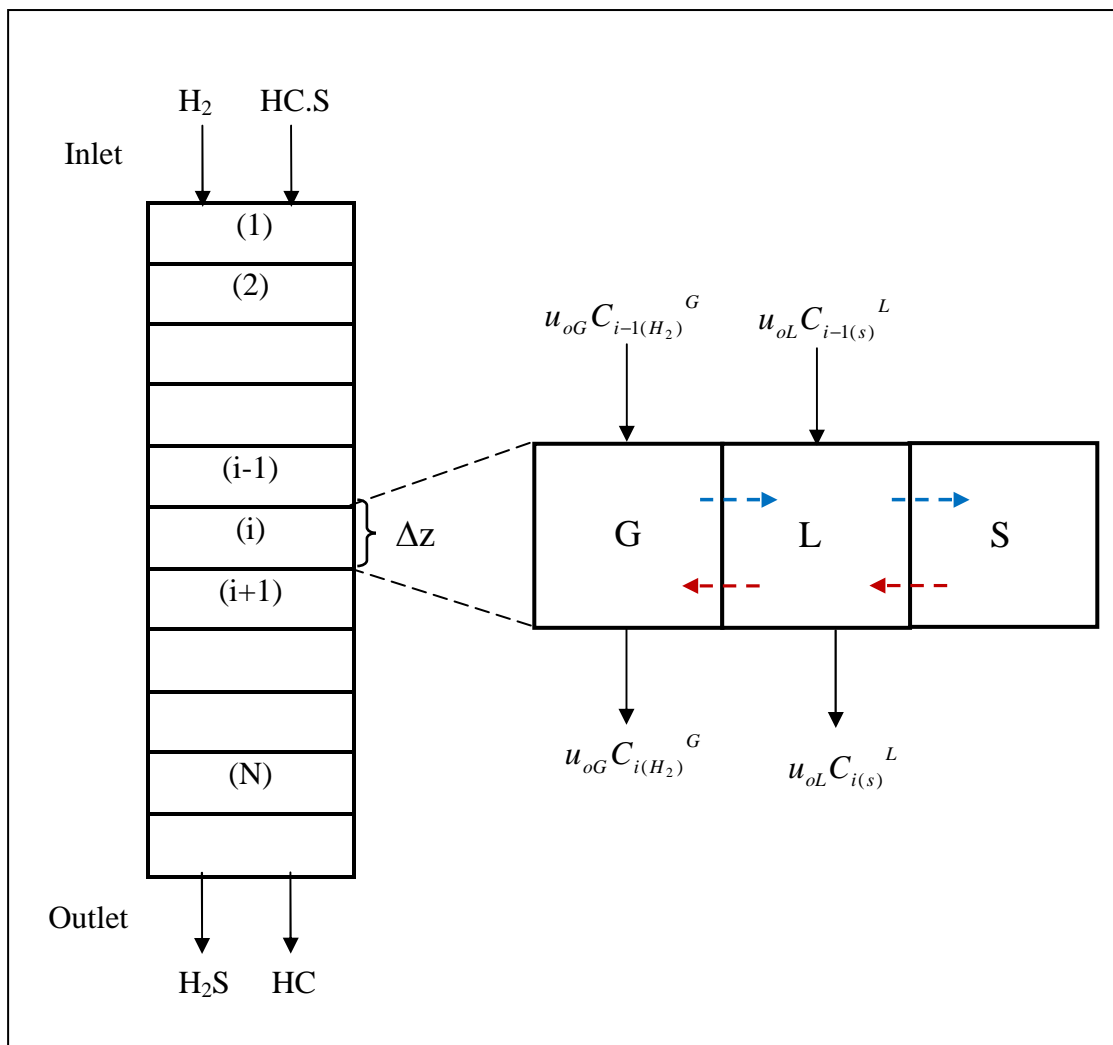


Figure 4.1: 1-D Cells-in-Series Model

Processes taking place in the  $i^{\text{th}}$  cell between the three phases are highlighted in Figure 4.1. The value of “ $i$ ” can be from 1 to  $N$ . Gas and liquid from  $(i-1)^{\text{th}}$  cell flow through the  $i^{\text{th}}$  cell over the catalyst to  $(i+1)^{\text{th}}$  cell. In the  $i^{\text{th}}$  cell, the steps occur are:

1. Hydrogen in the gas phase diffuses into the liquid phase by mass transfer.
2. Dissolved hydrogen and sulfur in the liquid phase diffuse into the solid phase.
3. Dissolved hydrogen and sulfur in the solid phase react to produce dissolved hydrogen sulfide. The reaction is exothermic and hence heat is generated and temperature of solid phase increases.
4. Dissolved hydrogen sulfide in the solid phase diffuses to liquid phase by mass transfer. Temperature of liquid phases increases because of heat transfer from solid phase to liquid phase (heat transfer coefficient is assumed to be very large).
5. Dissolved hydrogen sulfide from liquid phases diffuses to gas phase. Temperature of gas phase increases by heat transfer from liquid phase to gas phase (heat transfer coefficient is assumed to be very large).

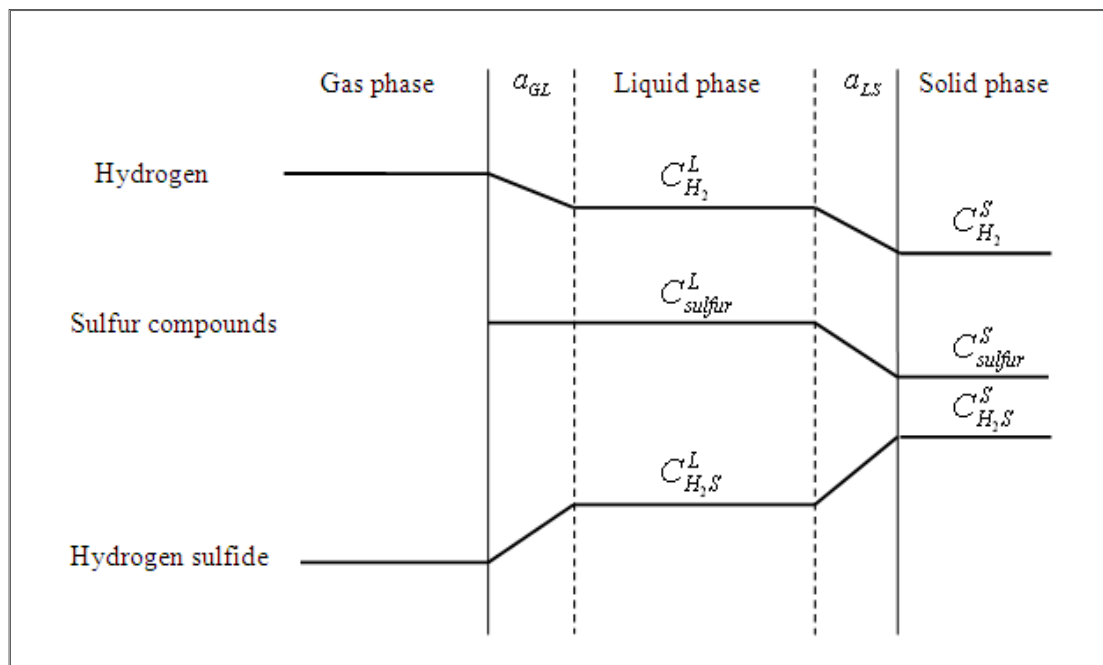


Figure 4.2: Concentrations profile of reactants and product  
The following assumptions were considered for formulating the reactor model

- Steady state operation
- Reactor is operated adiabatically
- No evaporation of the liquid
- Catalyst deactivation is insignificant
- The reaction occur only in the porous solid catalyst uniformly wetted by the liquid
- Gas and liquid velocities are constant across the reactor
- The reactor is assumed to operate at a constant pressure.

## 4.2 Model Equations

The mass and heat balance equations over a cell with interphase mass and heat transfer with chemical reaction are formulated. These equations are solved by incorporating properties of the materials, hydrodynamic and reaction kinetic parameters. These parameters such as mass transfer coefficients, gas solubility and properties of oil under process conditions are estimated by using correlations taken from the literature as described in section 4.4. Then, the resulting algebraic equations are solved for extent of reaction and rise in temperature over the cell “i” based on inlet conditions. This was extended to the subsequent cells to estimate the extent of reaction and rise in the temperature along the length of the reactor.

### 4.2.1 Mass Balance Equations

#### 4.2.1.1 Gas Phase

As shown in Figure 4.3, the change in gas molar flow from (i-1)<sup>th</sup> to i<sup>th</sup> cell for component hydrogen is equal to mass transfer rate to the liquid phase in i<sup>th</sup> cell as there is no consumption/formation by chemical reaction in the gas phase.

$$\frac{u_{oG} P_{i-1(H_2)}^G}{RT} = \frac{u_{oG} P_{i(H_2)}^G}{RT} + k_{GL_{H_2}} a_{GL} \left( \frac{P_{i(H_2)}^G}{H_{i(H_2)}} - C_{i(H_2)}^L \right) \Delta z \quad (4.2)$$

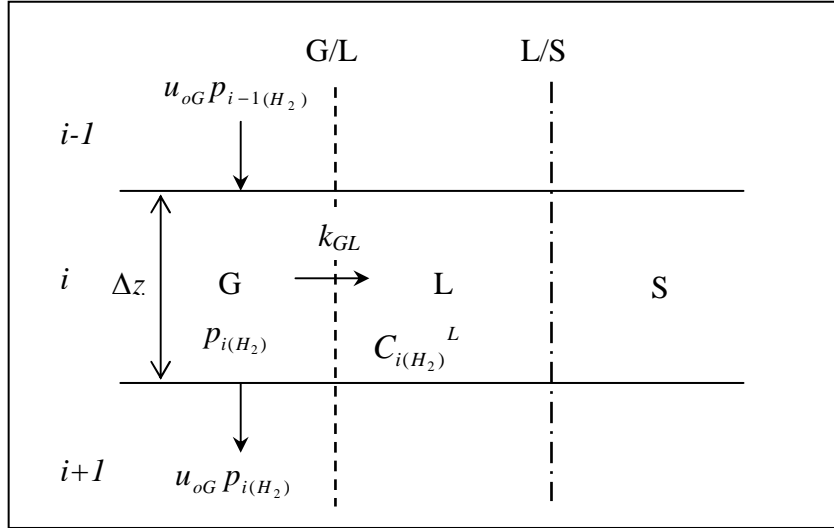


Figure 4.3: Mass balance for hydrogen in gas phase

Hydrogen and sulfur compounds in the liquid phase diffuse into the solid phase where they are converted to hydrogen sulfide. The hydrogen sulfide generated then diffuses back to the liquid phase and eventually to the gas phase. Thus, as shown in Figure 4.4, the change in hydrogen sulfide concentration in the gas phase from  $(i-1)^{\text{th}}$  cell to  $i^{\text{th}}$  cell is due to mass transfer of hydrogen sulfide from liquid phase to gas phase in  $i^{\text{th}}$  cell.

$$\frac{u_{oG} P_{i-1(H_2S)}^G}{RT} = \frac{u_{oG} P_{i(H_2S)}^G}{RT} - k_{GL_{H_2S}} a_{GL} \left( \frac{P_{i(H_2S)}^G}{H_{i(H_2S)}} - C_{i(H_2S)}^L \right) \Delta z \quad (4.3)$$

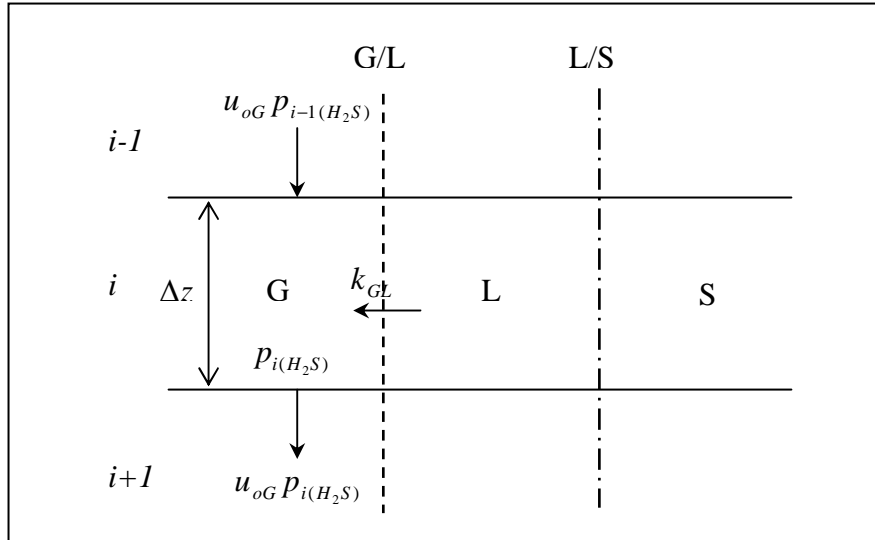


Figure 4.4: Mass balance for hydrogen sulfide in gas phase

#### 4.2.1.2 Gases in Liquid Phase

Concentration of dissolved hydrogen gas in the liquid phase as shown in Figure 4.5, is due to balance of (1) mass transfer in from gas phase to liquid phase in  $i^{\text{th}}$  cell; (2) mass transfer out from liquid phase to solid phase in  $i^{\text{th}}$  cell; (3) dissolved gas in the liquid flow in from  $(i-1)^{\text{th}}$  cell to  $i^{\text{th}}$  cell; (4) dissolved gas in the liquid flow out from  $i^{\text{th}}$  cell to  $(i+1)^{\text{th}}$  cell. Mass balance equation for hydrogen in the liquid phase can be written as follows

$$u_{oL} C_{i-1(H_2)}^L + k_{GL(H_2)} a_{GL} \left( \frac{P_{i(H_2)}^G}{H_{i(H_2)}} - C_{i(H_2)}^L \right) \Delta z = u_{oL} C_{i(H_2)}^L + k_{LS(H_2)} a_{LS} (C_{i(H_2)}^L - C_{i(H_2)}^S) \Delta z \quad (4.4)$$

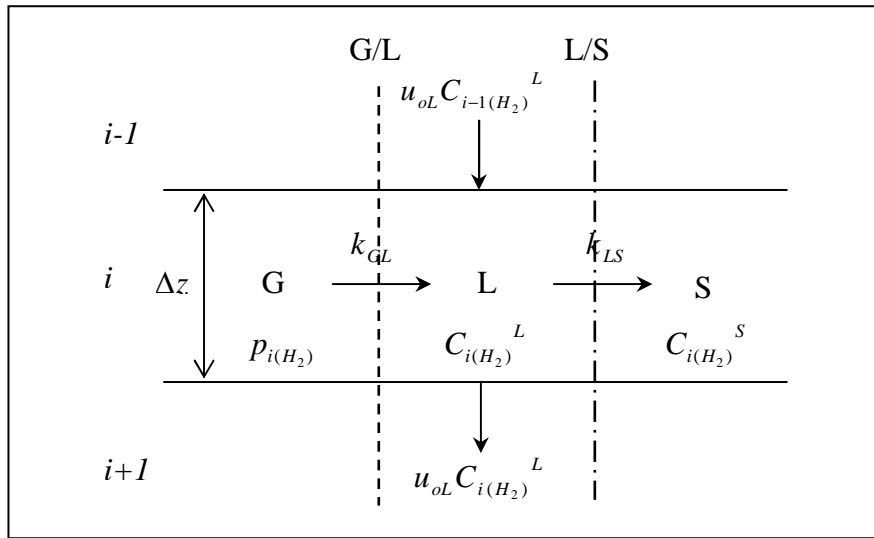


Figure 4.5: Mass balance for hydrogen in liquid phase

A similar equation as eq. 4.4 can also be written for hydrogen sulfide to describe concentration of hydrogen sulfide in the liquid phase in  $i^{\text{th}}$  cell, as shown in Figure 4.6. It should be noted that hydrogen sulfide is transferred from the solid to the liquid phase and eventually to the gas phase.

$$u_{oL} C_{i-1(H_2S)}^L - k_{LS(H_2S)} a_{LS} (C_{i(H_2S)}^L - C_{i(H_2S)}^S) \Delta z = u_{oL} C_{i(H_2S)}^L - k_{GL(H_2S)} a_{GL} \left( \frac{P_{i(H_2S)}^G}{H_{i(H_2S)}} - C_{i(H_2S)}^L \right) \Delta z \quad (4.5)$$

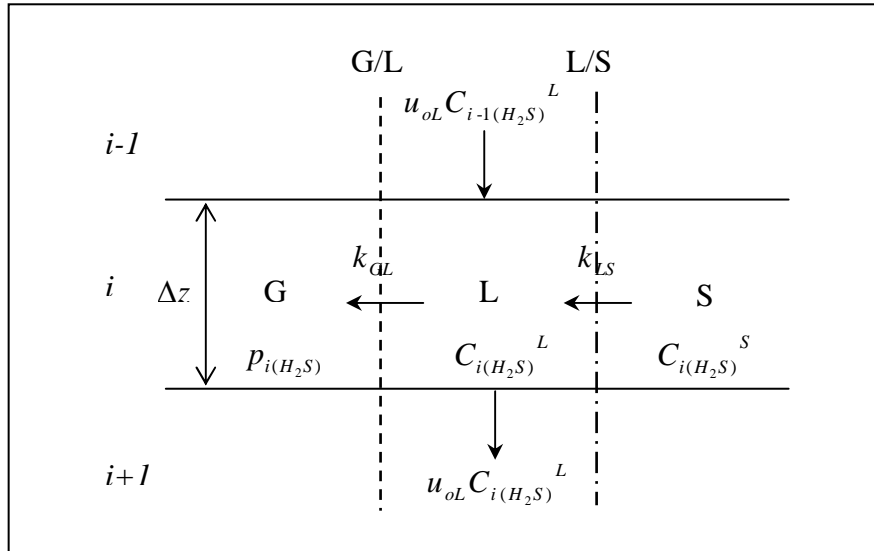


Figure 4.6: Mass balance for hydrogen sulfide in liquid phase

#### 4.2.1.3 Sulfur in Liquid Phase

Concentration of sulfur compounds in the liquid phase in  $i^{\text{th}}$  cell is due to balance of (1) sulfur compounds in the liquid flow in from  $(i-1)^{\text{th}}$  cell to  $i^{\text{th}}$  cell; (2) sulfur compounds in the liquid flow out from  $i^{\text{th}}$  cell to  $(i+1)^{\text{th}}$  cell; (3) mass transfer out from liquid phase to solid phase in  $i^{\text{th}}$  cell; as shown in Figure 4.7. Mass balance equation for sulfur compounds in the liquid phase assuming no evaporation of the feed, can be expressed as follows

$$u_{oL} C_{i-1(s)}^L = u_{oL} C_{i(s)}^L + k_{LS(s)} a_{LS} (C_{i(s)}^L - C_{i(s)}^S) \Delta z \quad (4.6)$$

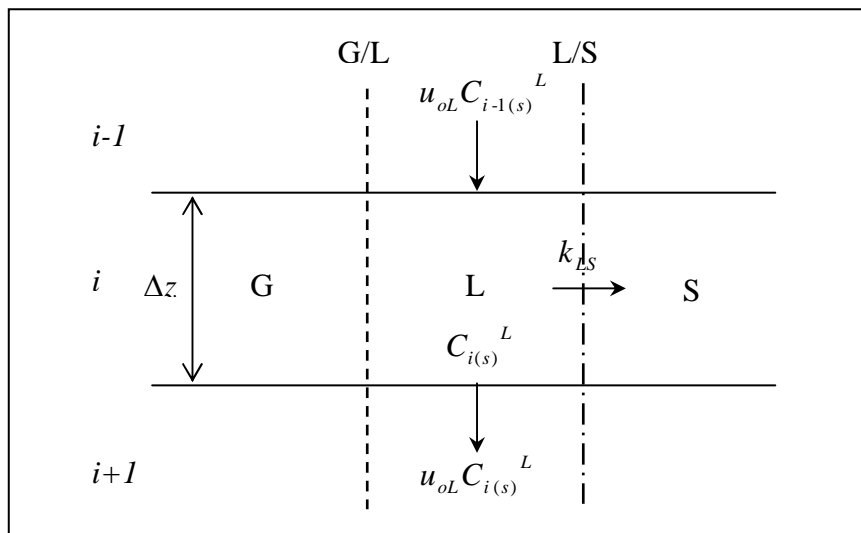


Figure 4.7: Mass balance for sulfur compound in liquid phase

#### 4.2.1.4 Reaction in Solid Phase

The sulfur compounds and hydrogen transported from the liquid phase to the solid phase are consumed by the chemical reaction at the surface of the catalyst as shown in Figure 4.8. Mass balance equation at the solid phase can be written as follows:

$$k_{LS(H_2)} a_{LS} (C_{i(H_2)}^L - C_{i(H_2)}^S) \Delta z + k_{LS(s)} a_{LS} (C_{i(s)}^L - C_{i(s)}^S) \Delta z = \rho_p \varepsilon_p \eta \Delta z r_{HDS} \quad (4.7)$$

$$r_{HDS} = k_{HDS} \frac{(C_S^s)(C_{H_2}^s)^{0.45}}{(1 + K_{H_2S}^s C_{H_2S}^s)^2} \quad (4.8)$$

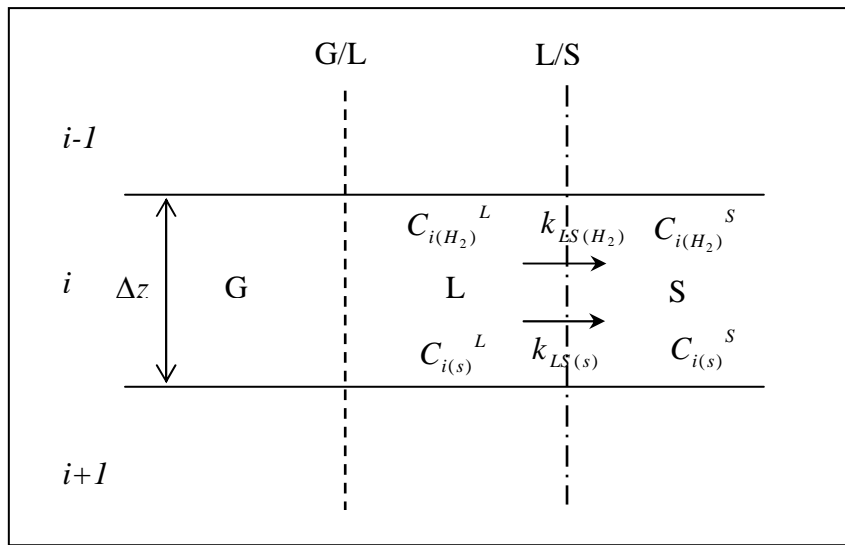


Figure 4.8: Mass balance in solid phase

Hydrogen sulfide transported between solid phase and liquid phase is produced by the chemical reaction. Mass balance for hydrogen sulfide in the solid phase can be estimated as

$$k_{LS(H_2S)} a_{LS} (C_{i(H_2S)}^S - C_{i(H_2S)}^L) \Delta z = \rho_p \varepsilon_p \eta \Delta z r_{HDS} \quad (4.9)$$

The set of equations 4.2 to 4.9 are solved for cells 1 to N in a marching technique. The detailed calculation procedure is discussed in section 4.5.

### 4.2.2 Energy Balance Equations

Hydrodesulfurization reactor is generally operated adiabatically with no heat exchange between the reactor and its surrounding. Heat generated by the reaction in the catalyst causes rise in the catalyst temperature and heat transfer to the liquid phase. Assuming no temperature gradient within the catalyst particle, heat transfer from the catalyst to liquid phase can be expressed as

$$\Delta z \rho_p \varepsilon_p \eta r_{HDS} (-\Delta H_{HDS}) = h_{LS} a_{LS} \Delta z (T_{Si} - T_{Li}) \quad (4.10)$$

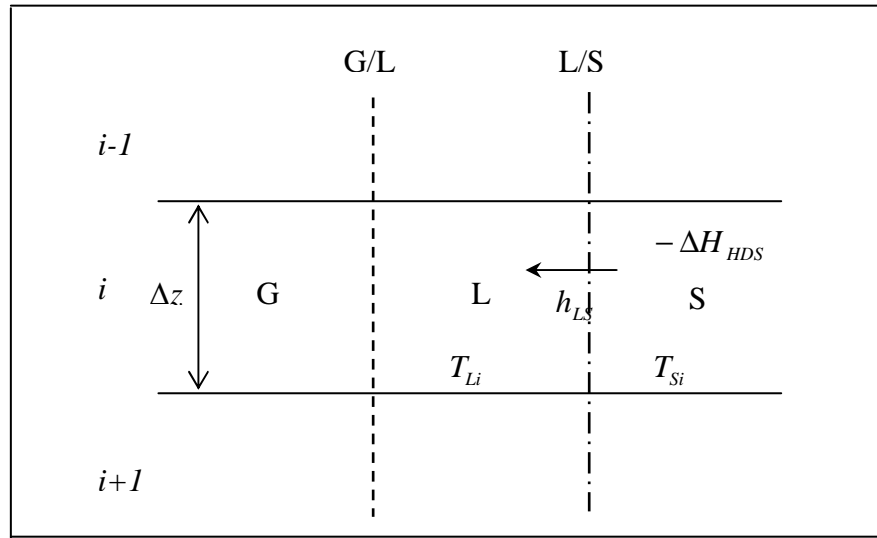


Figure 4.9: Heat transfer from solid phase to liquid phase

Temperature in the liquid phase in  $i^{\text{th}}$  cell is due to balance of (1) in flow of heat with liquid flow from  $(i-1)^{\text{th}}$  cell to  $i^{\text{th}}$  cell; (2) heat transfer from solid phase to liquid phase by convection in  $i^{\text{th}}$  cell; (3) out flow of heat with liquid flow from  $i^{\text{th}}$  cell to  $(i+1)^{\text{th}}$  cell; and (4) heat transfer from liquid phase to gas phase by convection in  $i^{\text{th}}$  cell, as shown in Figure 4.10. Energy balance for liquid phase can be obtained as

$$u_{oL} \rho_L c_p^L T_{Li-1} + h_{LS} a_{LS} (T_{Si} - T_{Li}) \Delta z = u_{oL} \rho_L c_p^L T_{Li} + h_{GL} a_{GL} (T_{Li} - T_{Gi}) \Delta z \quad (4.11)$$

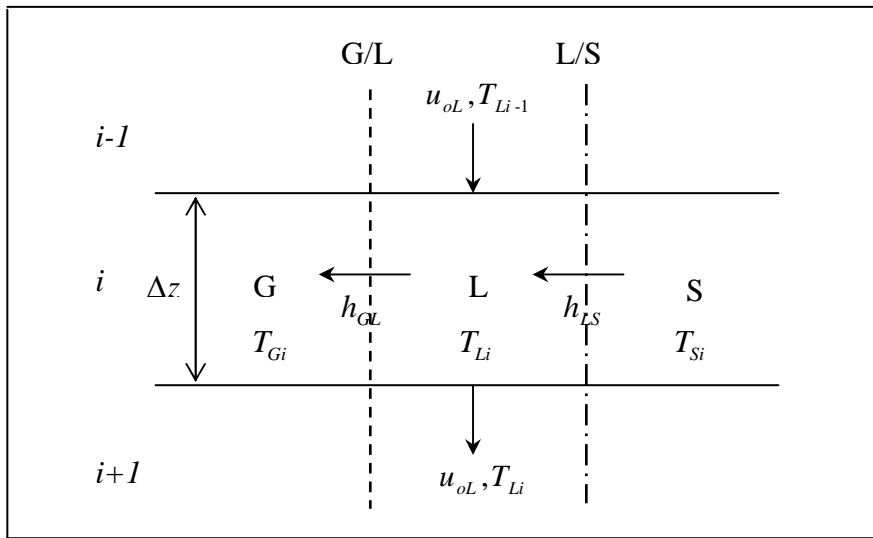


Figure 4.10: Energy balance in liquid phase

Increase in the enthalpy of gas phase as it flows from  $(i-1)^{\text{th}}$  cell to  $(i+1)^{\text{th}}$  cell through the  $i^{\text{th}}$  cell is equal to heat transfer from liquid phase to gas phase by convection as shown in Figure 4.11. From the energy balance on the gas phase

$$u_{oG}\rho_Gc_p^G T_{Gi-1} = u_{oG}\rho_Gc_p^G T_{Gi} + h_G a_{GL} (T_{Li} - T_{Gi}) \Delta z \quad (4.12)$$

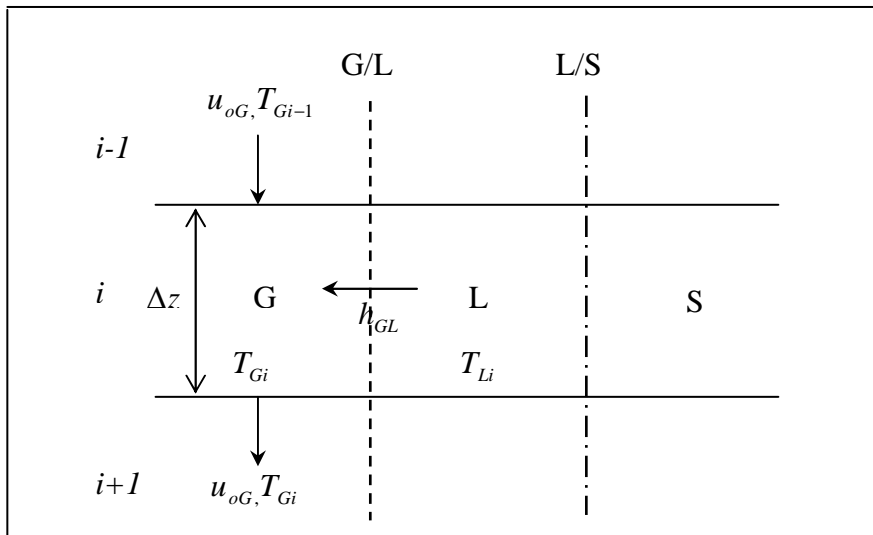


Figure 4.11: Energy balance in gas phase

Assuming high interphase heat transfer coefficients between the phases, the temperature of the three phases will be equal ( $T_{Gi} = T_{Li} = T_{Si} = T_i$ ). Therefore, equations (4.10)-(4.12) can be combined as

$$(u_{oG}\rho_G c_p^G + u_{oL}\rho_L c_p^L)(T_i - T_{(i-1)}) = \Delta z \rho_p \varepsilon_p \eta_j r_{HDS} (-\Delta H_{HDS}) \quad (4.13)$$

### 4.3 Reaction Kinetics

Langmuir-Hinshelwood type reaction kinetics as recommended by Korsten and Hoffman [89] is used to describe hydrodesulfurization reaction in one-dimensional cell-in-series model. The kinetics data are presented in Table 4.1.

Table 4.1: Kinetics and thermodynamic data [89]

Kinetic model (J/mol)	$E_a$ (J/mol)	$k_o$	$\Delta H_R$
$r_{HDS} = k_{HDS} \frac{(C_S^s)(C_{H_2}^s)^{0.45}}{(1 + K_{H_2S} C_{H_2S}^s)^2}$	131993	$4.266 \times 10^9 \text{ cm}^3 \text{ g}^{-1} \text{ s}^{-1}$	-251000
$K_{H_2S}(T) = k_{oH_2S} \exp\left(\frac{E_a}{RT}\right)$	2761	$41769.84 \text{ cm}^3 \text{ mol}^{-1}$	

$k_{HDS}$  is the reaction rate constant for HDS reaction,  $K_{H_2S}$  is adsorption equilibrium constant for hydrogen sulfide ( $\text{cm}^3/\text{mol}$ ),  $k_o$  is frequency factor,  $E_a$  is adsorption enthalpy of hydrogen sulfide. Hydrodesulfurization reaction is inhibited by the hydrogen sulfide whereas the inhibition effect from other compounds ( $\text{N}_2$ , aromatic, etc.) are negligible. The kinetic model includes an adsorption equilibrium constant of hydrogen sulfide,  $K_{H_2S}$  described by the van't Hoff equation to account for the effect of the temperature.

### 4.4 Estimation of Hydrodynamics and Physical Properties

The reactor model makes use of selected available industrial engineering correlations to estimate various parameters such as density, gas solubility, diffusivity, dynamic viscosity, mass transfer coefficients and properties of oil and gas at process condition. These equations are given by eqs. (4.14)–(4.34).

#### 4.4.1 Oil Density

Density for liquid petroleum fractions is usually reported in terms of specific gravity (SG), defined as the ratio of liquid density to that of water at standard conditions. The standard conditions adopted by petroleum industry are 60°F (15.5°C) and 1 atm. Another unit for specific gravity of liquid petroleum fraction is defined by the American Petroleum Institute (API) in terms of API gravity.

$$API \text{ gravity} = \frac{141.5}{SG \text{ (at } 60^\circ \text{ F)}} - 131.5 \quad (4.14)$$

The correlation of liquid density reported in literature incorporate the correction for high pressure and temperature [36].

$$\rho_L(P, T) = \rho_0 + \Delta\rho_P - \Delta\rho_T \quad (4.15)$$

$$\Delta\rho_P = \left[ 0.167 + 16.181 \times 10^{-0.0425\rho_0} \right] \left( \frac{P}{1000} \right) - 0.01 \left[ 0.299 + 263 \times 10^{-0.0603\rho_0} \right] \left( \frac{P}{1000} \right)^2 \quad (4.16)$$

$$\Delta\rho_T = \left( 0.0133 + 152.4 [\rho_0 + \Delta\rho_P]^{-2.45} \right) (T_L - 520) - \left( 8.1 \times 10^{-6} - 0.0622 \times 10^{-0.764[\rho_0 + \Delta\rho_P]} \right) (T - 520)^2 \quad (4.17)$$

where  $\rho_0$  (lb/ft<sup>3</sup>) is liquid density at standard condition,  $P$  is reactor pressure (psia) and  $T$  is reactor temperature in Rankine (°R).

#### 4.4.2 Gas Solubility

The solubility of hydrogen (H<sub>2</sub>) and hydrogen sulfide (H<sub>2</sub>S) in liquid phase depend on temperature and they can be estimated from the following relations [13], [36].

$$\lambda_{H_2} = -0.559729 - 0.42947 \times 10^{-3} T_L + 3.07539 \times 10^{-3} \left( \frac{T_L}{\rho_{20}} \right) + 1.94593 \times 10^{-6} T_L^2 + \frac{0.835783}{\rho_{20}^2} \quad (4.18)$$

$$\lambda_{H_2S} = \exp(3.367 - 0.00847 T_L) \quad (4.19)$$

where  $\lambda_{H_2}$  and  $\lambda_{H_2S}$  are solubility of hydrogen and hydrogen sulfide respectively (NI/MPa kg oil),  $T_L$  is liquid temperature in degree Celsius (°C),  $\rho_{20}$  is liquid density at 20°C (g/cm<sup>3</sup>).

Henry's law coefficients for hydrogen and hydrogen sulfide were calculated from the equations reported in the literature [36].

$$H_i = \frac{v_N}{\lambda_i \rho_L} \quad (4.20)$$

where  $H_i$  is Henry coefficient (Pa.m<sup>3</sup>/mol),  $v_N$  is molar gas volume at standard condition,  $\rho_L$  is liquid density at process conditions.

#### 4.4.3 Dynamic Liquid Viscosity

At low and moderate pressure, effect of pressure on liquid viscosity generally is assumed to be negligible. Liquid viscosity change with temperature appreciably. Viscosity of liquids decreases with an increase in temperature. Prediction of viscosity of crude oils can be estimated using Glaso's correlation [17], [100].

$$\mu_L = 3.141 \times 10^{10} (T - 460)^{-3.444} \left[ \log_{10}(API)^a \right] \quad (4.21)$$

$$a = 10313 \left[ \log_{10}(T - 460) \right] - 36447 \quad (4.22)$$

where  $\mu_L$  is liquid viscosity in mPa.s, T is temperature in Rankine (°R) and API is the oil gravity. In general, heavier oils (lower API gravity) exhibit higher viscosity.

#### 4.4.4 Diffusivity

The correlation for molecular diffusivity of solute  $i$  in the liquid petroleum fraction is given by Poling et al. [101] for organic and hydrocarbons system, derived from Tyn and Calus equation.

$$D_i^L = 8.93 \times 10^{-8} \left( \frac{v_L^{0.267}}{v_i^{0.433}} \right) \left( \frac{T}{\mu_L} \right) \quad (4.23)$$

where  $D_i^L$  is diffusion coefficient of solute in the liquid ( $\text{cm}^2/\text{s}$ ),  $T$  is temperature in Kelvin (K),  $\mu_L$  is dynamic viscosity (mPa.s),  $v_i$  and  $v_L$  are molar volumes of solute and liquid solvent respectively at its normal boiling point ( $\text{cm}^3/\text{mol}$ ).  $v_i$  and  $v_L$  can be calculated from critical specific volume as given as follows [36].

$$v_i = 0.285 v_c^{1.048} \quad (4.24)$$

$$v_c^m = 7.5214 \times 10^{-3} T_{MeABP}^{0.2896} d_{15.6}^{-0.7666} \quad (4.25)$$

where  $v_c$  is critical specific volume ( $\text{cm}^3/\text{mol}$ ),  $T_{MeABP}$  is mean average boiling point in Rankine ( $^{\circ}\text{R}$ ),  $d_{15.6}$  is specific gravity at  $15.6^{\circ}\text{C}$  while  $v_c^m$  ( $\text{ft}^3/\text{lb}$ ) to  $v_c$  is carried out by multiplication with molecular weight.

#### 4.4.5 Mass Transfer Coefficients

The gas-liquid mass transfer and the liquid-solid mass transfer are estimated using correlations taken from Korsten and Hoffman [89].

i. Gas-liquid mass transfer coefficient

$$\frac{k_{GL_i} a_{GL}}{D_i^L} = 7 \left( \frac{\rho_L u_L}{\mu_L} \right)^{0.4} \left( \frac{\mu_L}{\rho_L D_i^L} \right)^{0.5} \quad (4.26)$$

ii. Liquid-solid mass transfer coefficient

$$\frac{k_{LS_i}}{D_i^L a_{LS}} = 1.8 \left( \frac{\rho_L u_L}{a_{LS} \mu_L} \right)^{0.5} \left( \frac{\mu_L}{\rho_L D_i^L} \right)^{0.333} \quad (4.27)$$

In both correlations,  $k_{GL_i}$  and  $k_{LS_i}$  (cm/s) are the functions of molecular diffusivity,  $D_i^L$  (cm<sup>2</sup>/s); liquid density,  $\rho_L$  (g/cm<sup>3</sup>); liquid viscosity,  $\mu_L$  (mPa.s); superficial velocity,  $u_{oL}$  (cm/s); and the diameter of catalyst particle,  $d_p$  (cm).

#### 4.4.6 Heat Capacity

The heat capacity of liquid hydrocarbon is evaluated through the correlation of API method [17].

$$c_p^L = A_1 + A_2T + A_3T^2 \quad (4.28)$$

$$A_1 = -4.90383 + (0.099319 + 0.104281 SG)K_w + \left( \frac{4.81407 - 0.194833 K_w}{SG} \right) \quad (4.29)$$

$$A_2 = (7.53624 + 6.214610K_w) \times \left( 1.12172 - \frac{0.27634}{SG} \right) \times 10^{-4} \quad (4.30)$$

$$A_3 = -(1.35652 + 1.11863K_w) \times \left( 2.9027 - \frac{0.70958}{SG} \right) \times 10^{-7} \quad (4.31)$$

$$K_w = \frac{(1.8T_b)^{1/3}}{SG} \quad (4.32)$$

where  $c_p^L$  is heat capacity of liquid (J/g. K),  $K_w$  is the Watson characterization factor,  $T_b$  is normal boiling point (K).

Ideal gas properties do change with temperature significantly. The gas heat capacity has been correlated to temperature in the following form [17].

$$\frac{c_p^G}{R} = A + BT + CT^2 + DT^3 + ET^4 \quad (4.33)$$

where  $R$  is the gas constant,  $c_p^G$  is the molar heat capacity in the same unit with  $R$ , and  $T$  is temperature in Kelvin.

#### 4.4.7 Wetting Efficiency

The catalyst wetting efficiency is estimated using the correlation of Al-Dahhan and Dudukovic [102] that applicable for high operating pressure.

$$\eta = 1.104 \text{Re}_L^{1/3} \left[ \frac{1 + (\Delta P/Z)/\rho_L g}{Ga_L} \right]^{1/9} \quad (4.34)$$

where

$$\text{Re}_L = \frac{\rho_L u_{oL} d_p}{\mu_L}, \quad Ga_L = \frac{d_p^3 \rho_L^2 g}{\mu_L^2}$$

Pressure drop ( $\Delta P/Z$ ) can be estimated from modified Ergun equation that was developed in Chapter 3.

#### 4.5 Solution Scheme for 1-D Reactor Model

The model equations were solved by rearranging the mass and the energy balance equations to obtain the axial concentrations of components and temperature for a cell. To simplify the simulation work, eq. (4.2) is rearranged to obtain expression for partial pressure of hydrogen in the gas phase for  $i$  cell ( $p_{i(H_2)}^G$ ).

$$p_{i(H_2)}^G = \frac{\frac{u_{oG} p_{i-1(H_2)}^G}{RT} + k_{GL_{H_2}} a_{GL} C_{i(H_2)}^L \Delta z}{\frac{u_{oG}}{RT} + \frac{k_{GL_{H_2}} a_{GL} \Delta z}{H_{i(H_2)}}} \quad (4.35)$$

By considering mass transfer resistance of hydrogen between liquid and solid catalyst is negligible, eq. (4.4) can be rearranged to give expression for hydrogen concentration in the liquid phase.

$$C_{i(H_2)}^L = \frac{u_{oL} C_{i-1(H_2)}^L + k_{GL_{(H_2)}} a_{GL} \frac{p_{i(H_2)}^G}{H_{i(H_2)}} \Delta z}{u_{oL} + k_{GL_{(H_2)}} a_{GL} \Delta z} \quad (4.36)$$

Substituted eq. (4.36) into eq. (4.35) and rearranged them, equation for hydrogen partial pressure in gas phase can be obtained as

$$P_{i(H_2)}^G = \frac{u_{oG} P_{i-1(H_2)}^G + \frac{u_{oL} C_{i-1(H_2)}^L k_{GLH_2} a_{GL} \Delta z RT}{u_{oL} + k_{GLH_2} a_{GL} \Delta z}}{u_{oG} H_{i(H_2)} + k_{GLH_2} a_{GL} \Delta z RT} - \frac{(k_{GLH_2} a_{GL} \Delta z)^2 RT}{H_{i(H_2)} [u_{oL} + k_{GLH_2} a_{GL} \Delta z]} \quad (4.37)$$

Since mass transfer resistance of hydrogen between liquid and solid catalyst is negligible, mass balance at the solid phase as presented in eq. (4.7) can be obtained as follows

$$k_{LS(s)} a_{LS} (C_{i(s)}^L - C_{i(s)}^S) \Delta z = \eta \rho_p \varepsilon_p k_{HDS} \frac{(C_S^s)(C_{H_2}^s)^{0.45}}{(1 + K_{H_2S}^s C_{H_2S}^s)^2} \Delta z \quad (4.38)$$

Rearranging eq. (4.38), sulfur concentration in solid phase can be obtained as

$$C_{i(s)}^S = \frac{k_{LS(s)} a_{LS} C_{i(s)}^L}{k_{LS(s)} a_{LS} + \eta \rho_p \varepsilon_p k_{HDS} \frac{(C_{H_2}^s)^{0.45}}{(1 + K_{H_2S}^s C_{H_2S}^s)^2}} \quad (4.39)$$

By substituted eq. (4.39) into eq. (4.6), sulfur concentration in the liquid phase can be estimated as

$$C_{i(s)}^L = \frac{u_{oL} C_{i-1(s)}^L}{u_{oL} + k_{LS(s)} a_{LS} \Delta z \left( 1 - \frac{k_{LS(s)} a_{LS}}{k_{LS(s)} a_{LS} + \eta \rho_p \varepsilon_p k_{HDS} \frac{(C_{H_2}^s)^{0.45}}{(1 + K_{H_2S}^s C_{H_2S}^s)^2}} \right)} \quad (4.40)$$

Hydrogen sulfide produced as HDS reaction occurs between hydrogen and sulfur in the solid phase. Rearranging eq. (4.3), equation for partial pressure of hydrogen sulfide in gas phase can be obtained as

$$P_{i-1(H_2S)}^G = \frac{\frac{u_{oG} P_{i-1(H_2S)}^G}{RT} + k_{GL_{H_2S}} a_{GL} C_{i(H_2S)}^L \Delta z}{\frac{u_{oG}}{RT} + \frac{k_{GL_{H_2S}} a_{GL} \Delta z}{H_{i(H_2S)}}} \quad (4.41)$$

Substituted eq. 4.41 and eq. 4.9 into eq. 4.5 and rearranging them, equation for hydrogen sulfide concentration in liquid phase can be obtained as

$$C_{i(H_2S)}^L = \frac{u_{oL} C_{i-1(H_2S)}^L + \eta \rho_p \varepsilon_p k_{HDS} \frac{(C_{H_2}^s)^{0.45}}{(1 + K_{H_2S}^s C_{H_2S}^s)^2} \Delta z + \frac{u_{oG} P_{i-1(H_2S)}^G k_{GL_{(H_2S)}} a_{GL} \Delta z}{u_{oG} H_i + k_{GL_{(H_2S)}} a_{GL} \Delta z RT}}{u_{oL} + k_{GL_{(H_2S)}} a_{GL} \Delta z \left[ 1 - \frac{k_{GL_{(H_2S)}} a_{GL} \Delta z RT}{u_{oG} H_i + k_{GL_{(H_2S)}} a_{GL} \Delta z RT} \right]} \quad (4.42)$$

#### 4.6 Model Validation and Simulation Results

In order to validate the proposed 1-D cell in series model, experimental data on hydrotreating of vacuum gas oil (VGO) over NiMo/Al<sub>2</sub>O<sub>3</sub> catalyst on pilot plant scale, reported by Mederos and Ancheyta [36] as listed in Table 4.2 were used for simulating the behavior of reaction system. The present model only takes into consideration the HDS reaction. The simulation was performed under the conditions of a pressure of 5.3MPa and temperature 380°C. The model simulation results also are compared with the simulation of Mederos and Ancheyta [36].

Microsoft Excel was used to solve the governing equations. The reactor was divided into a number of cells (N=126) along the axial direction from the inlet to the outlet of the reactor where each cell is assumed to contain three phases, each well mixed within itself and axial distance ( $\Delta z$ ) of each cell is assumed to be equal to the diameter of the catalyst particle (=0.254 cm). Input data on flow velocities, feedstock

and catalyst properties, temperature and pressure were specified for the first cell. Concentration of hydrogen in the VGO feed at the entrance of the reactor is assumed to be zero ( $C_{H_2}^L=0$ ). The outputs of the 1<sup>st</sup> cell were estimated; the outputs of the 1<sup>st</sup> cell were the inputs to 2<sup>nd</sup> cell and so on. Figure 4.12 presents computational flow sheet of the calculation procedure.

Table 4.2: Experimental data on hydrotreating of VGO on pilot plant scale.  
Experimental data taken from Mederos and Ancheyta [36]

<u>Feedstock</u>	<u>Value</u>
API gravity	22
Molecular weight	441.9
Mean average boiling point ( $^{\circ}C$ )	476
Sulfur (wt %)	2.009
<u>Operation conditions</u>	<u>Value</u>
Gas superficial velocity (cm/s)	0.28
Oil superficial velocity (cm/s)	$1.75 \times 10^{-2}$
Catalytic bed length (cm)	31.58
Internal diameter (cm)	2.54
Temperature ( $^{\circ}C$ )	380
Pressure (MPa)	5.3
Gas composition (mol%)	
H <sub>2</sub>	100
H <sub>2</sub> S	0
Light hydrocarbons	0
<u>Catalyst</u>	<u>Value</u>
Equivalent diameter (mm)	2.54
Specific surface area (m <sup>2</sup> /g)	175

Pore volume (cm <sup>3</sup> /g)	0.56
Mean pore diameter (Å)	127
Molybdenum content (wt %)	10.7
Nickel content (wt %)	2.9
Bulk density (g/cm <sup>3</sup> )	0.8163

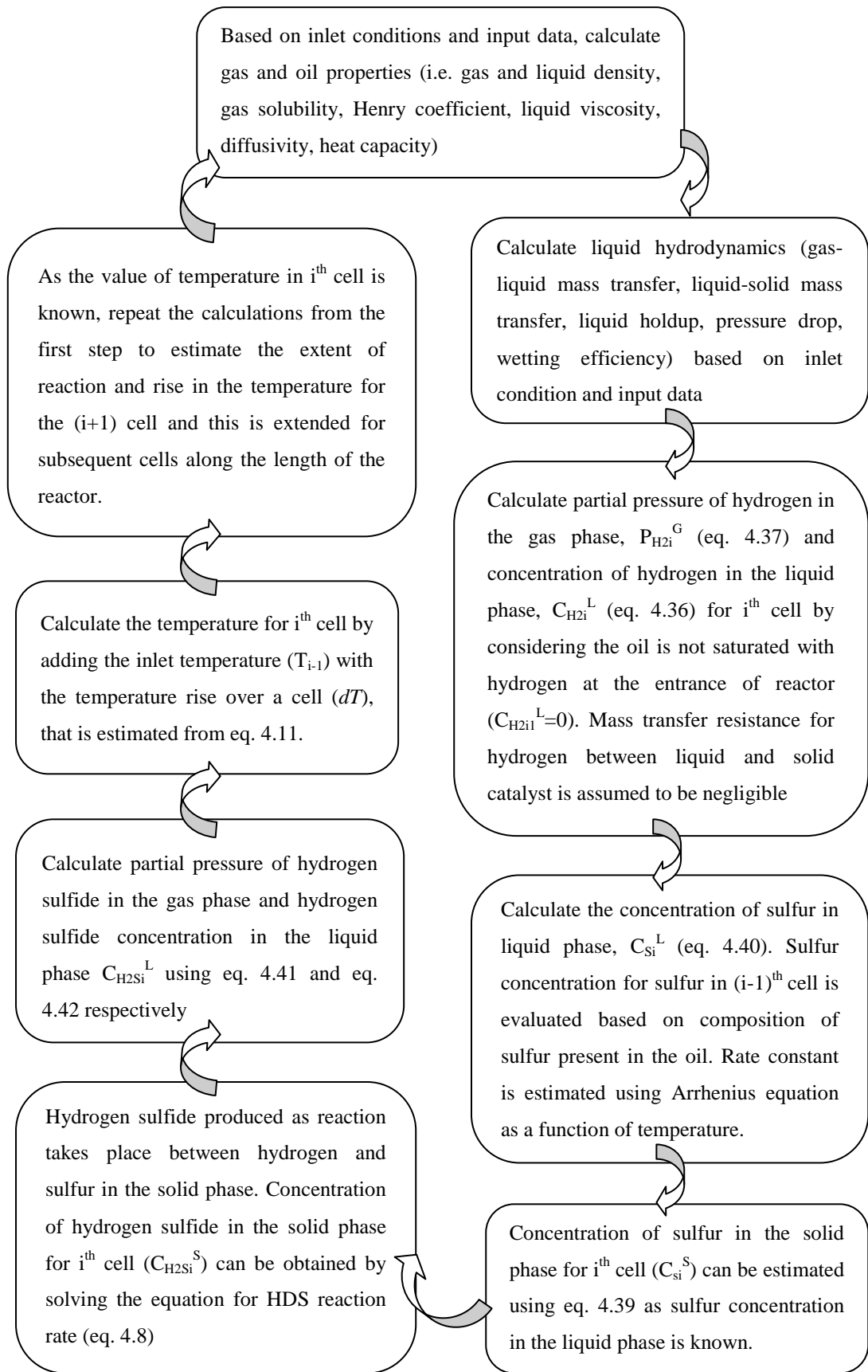


Figure 4.12: Computational flow sheet of the calculation procedure

#### 4.6.1 Results of the Simulation for the Pilot Plant

Hydrogen profiles along the reactor in the gas, liquid and solid phases are shown in Figure 4.13. It is observed that hydrogen partial pressure in the gas phase (Figure 4.13a) decreases rapidly as it increases in the liquid phase (Figure 4.13b) due to the high gas-liquid mass transfer in the entry zone. Further down in the reactor, mass transfer rate decreases as hydrogen concentration in the liquid phase increases to near saturation.

In the liquid phase, concentration of hydrogen (Figure 4.13b) increases rapidly until a certain point due to high hydrogen mass transfer. Beyond this point, liquid phase is nearly saturated with hydrogen due to the availability of excess hydrogen in the gas phase. It should be noted that the shape of hydrogen partial pressures in the gas phase and concentration profiles of hydrogen in the liquid phase are determined by the mass transfer and reaction rate ( $H_2$  consumption) in the catalyst phase. Estimates for hydrogen concentration in the gas and liquid phase from the present model are compared with the simulation results of Mederos and Ancheyta [36] and they are in reasonable agreement.

Concentration of hydrogen in solid phase increases rapidly as hydrogen in liquid phase diffuses out into the solid phase (Figure 4.15c). It can be seen that hydrogen concentrations in the liquid and solid phases are very close. Mass transfer resistance between liquid and solid phases can be negligible.

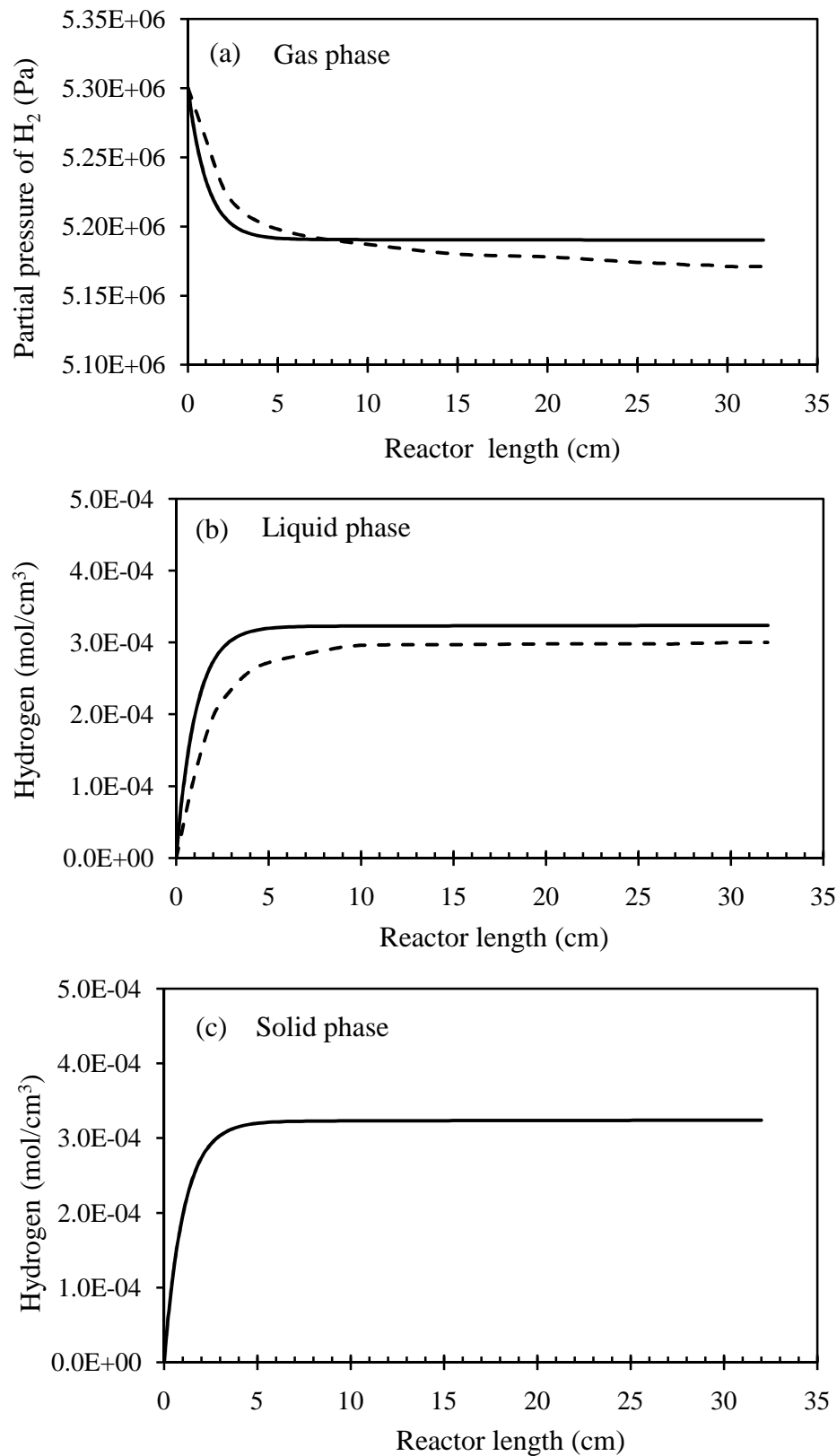


Figure 4.13: Hydrogen profiles along the reactor length in (a) gas phase, (b) liquid phase and (c) solid phase; (—) present model, (----) simulation data of Mederos and Ancheyta [36] ( $T=380^{\circ}\text{C}$ ,  $P=5.3\text{MPa}$ ,  $u_{oL}=0.0175\text{cm/s}$ )

Dissolved hydrogen and sulfur in the liquid phase diffuse into the solid catalyst phase for the conversion of sulfur and hydrogen to hydrogen sulfide. As a result, sulfur concentration in the liquid phase decreases along the reactor length as illustrated in Figure 4.14a. The hydrodesulfurization process reduces the sulfur concentration in the liquid phase of  $3.471 \times 10^{-5} \text{ mol/cm}^3$  to  $9.566 \times 10^{-6} \text{ mol/cm}^3$  with 72% sulfur removal. Prediction for sulfur concentration in the liquid phase at the exit of the reactor by the model compares well with the experimental observations. In the solid phase, sulfur concentration increases initially as it diffuses from the liquid phase to the solid phase, and then decreases as hydrodesulfurization reaction occurs (Figure 4.14b). Sulfur concentrations in the liquid and solid phases are very close. Mass transfer resistance between liquid and solid phases can be negligible.

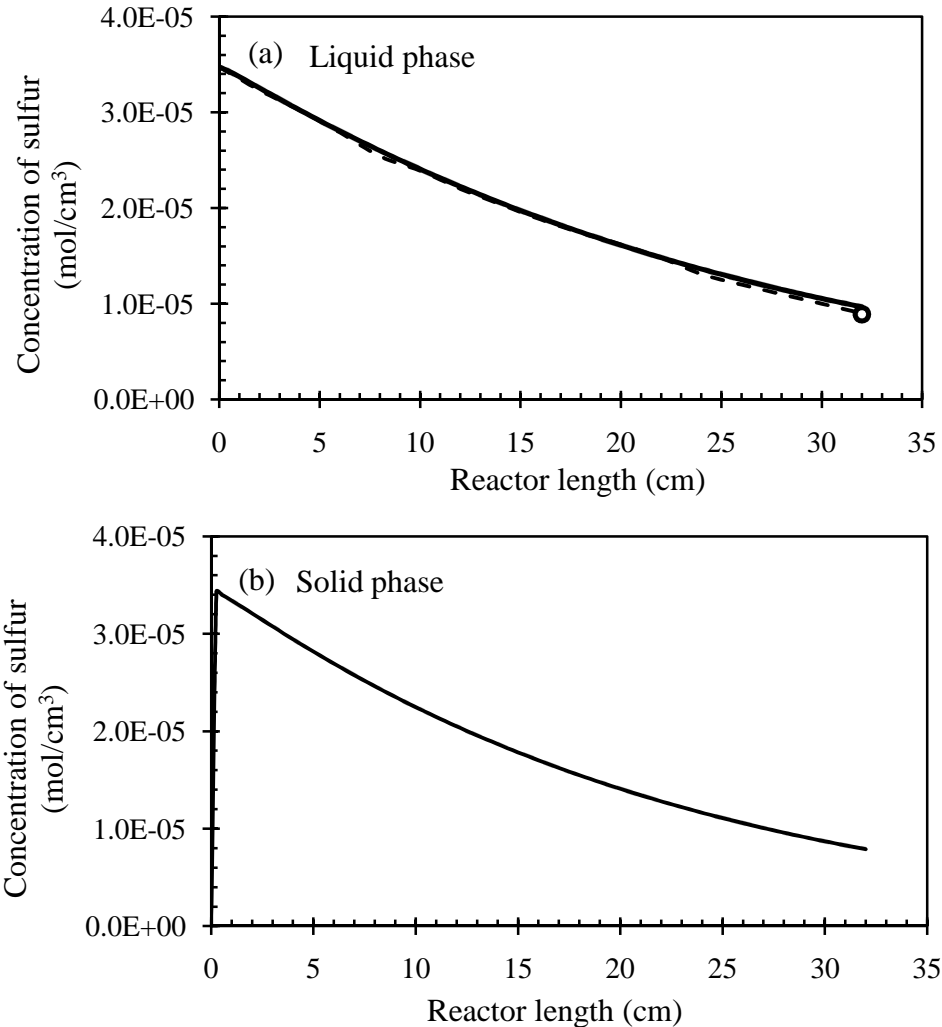


Figure 4.14: Sulfur concentrations profile in (a) liquid phase, (b) solid phase; (—) present model, (----) simulation data of Mederos and Ancheyta [36], (o) experimental value (T=380°C, P=5.3MPa,  $u_{oL}=0.0175\text{cm/s}$ )

Hydrogen sulfide produced in the catalyst phase by reaction of hydrogen with sulfur compounds diffuses into the liquid phase and eventually into the gas phase. It can be seen that the concentration of hydrogen sulfide in solid phase first increases rapidly in the initial part of the catalyst bed due to the high reaction rate and then it decreases as reactants are consumed along the bed length (Figure 4.15a). Catalyst to liquid phase mass transfer coefficient has to be high to reduce the hydrogen sulfide concentration in the catalyst phase. Otherwise, it can have detrimental effect on the catalytic conversion due to inhibition effect of hydrogen sulfide.

Hydrogen sulfide in solid phase diffuses out into the liquid phase (Figure 4.15b) and the trend for hydrogen sulfide concentration in liquid phase along the bed length is same as in solid phase due to high liquid-solid mass transfer. Hydrogen sulfide in liquid phase eventually diffuses out into gas phase along the reactor length and concentration of hydrogen sulfide in the gas phase increases gradually along the reactor length (Figure 4.15c). Competition between reaction rate, solid-liquid mass transfer rate and liquid-gas mass transfer rate determines the overall shape of hydrogen sulfide in liquid phase and gas phase. The trend for hydrogen sulfide concentration in gas phase compare reasonably well with results reported by Mederos and Ancheyta [36] as shown in Figure 4.15c. However there is some discrepancy between the estimates of the present model on liquid phase hydrogen sulfide concentration profile along the bed length compared to the results reported by Mederos and Ancheyta [36]. This could be due to the differences in the values of mass transfer coefficients between the various phases used in the two different models.

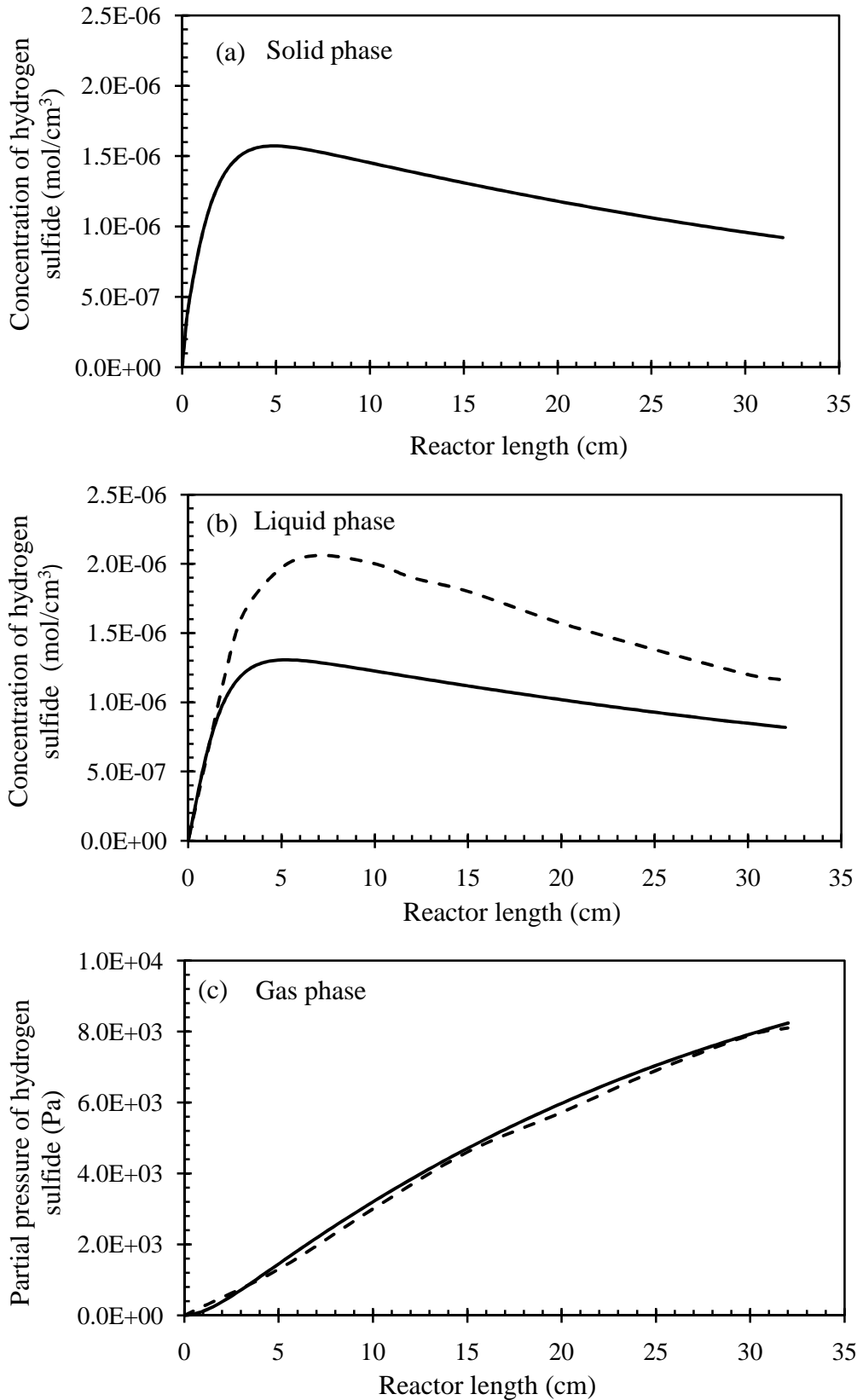


Figure 4.15: Hydrogen sulfide profiles along the reactor length in (a) solid phase, (b) liquid phase, (c) gas phase; (—) present model, (----) simulation data of Mederos and Ancheyta [36] ( $T=380^{\circ}\text{C}$ ,  $P=5.3\text{MPa}$ ,  $u_{oL}=0.0175\text{cm/s}$ )

Figure 4.16 presents bed temperature profile along the reactor. Since the hydrodesulfurization reaction is exothermic, bed temperature rises as sulfur gets converted along the length of the reactor. The temperature increases from 653K to 658K. However, the temperature rise through the reactor was little as sulfur content in VGO feed is considered very low. For oils with higher sulfur content, the temperature rise can be much higher and may necessitate cooling by cold injection of hydrogen. An increase in bed temperature would increase reaction rate and hence accelerates the heat production due to exothermic reaction.

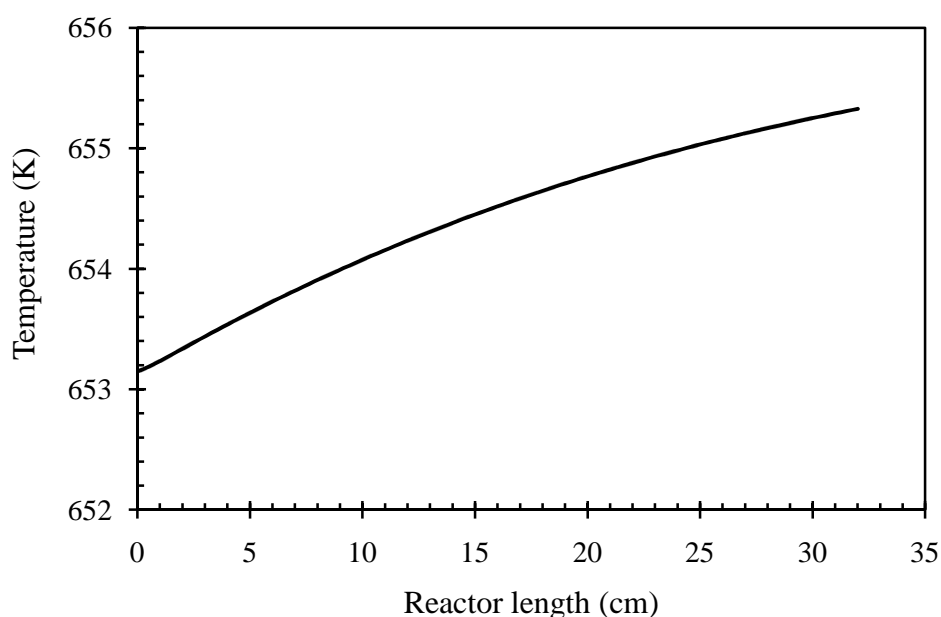


Figure 4.16: Bed temperature profile ( $P=5.3\text{MPa}$ ,  $u_{oL}=0.0175\text{cm/s}$ )

#### 4.6.2 Simulation Study to Explore the Performance of the Pilot Plant

In order to meet sulfur specifications, the validated 1-D reactor model is employed to investigate several parameters affecting reactor performance. Experimental data on pilot plant reactor were used for reactor performance analysis. The effect of reactor length, reactor inlet temperature, operating pressure and liquid velocity on sulfur removal were simulated with the other parameters being kept the same as the base operating conditions.

#### 4.6.2.1 Effect of Reactor Length

Figure 4.17 presents the effect of reactor length on sulfur concentration at the exit of reactor. It shows that sulfur removal increases as reactor length increases, due to the residence time for the reaction increases. Sulfur content in the VGO can be reduced to 10ppm as reactor length increases up to 165cm.

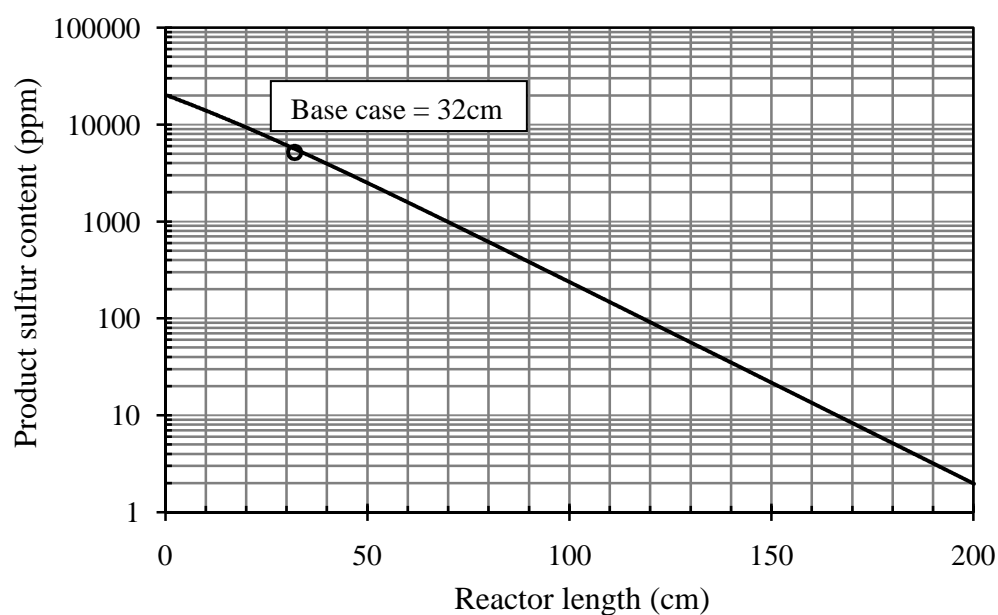


Figure 4.17: Effect of reactor length on product sulfur content, (o) experimental, (—) present model ( $T = 380^{\circ}\text{C}$ ,  $P = 5.3\text{MPa}$ ,  $u_{oL} = 0.00175\text{cm/s}$ )

#### 4.6.2.2 Effect of Liquid Velocity

A lower liquid velocity leads to longer residence time, which corresponds to the higher sulfur removal. The product sulfur content decreases with decreasing liquid velocity. The effect of liquid velocity on product sulfur content is shown in Figure 4.18. It shows that sulfur content in the VGO can be reduced to 10 ppm in a reactor length of 32 cm at operating temperature of  $380^{\circ}\text{C}$  and pressure of 5.3MPa (base case) as liquid velocity decreases to  $1.5 \times 10^{-3}\text{cm/s}$ .

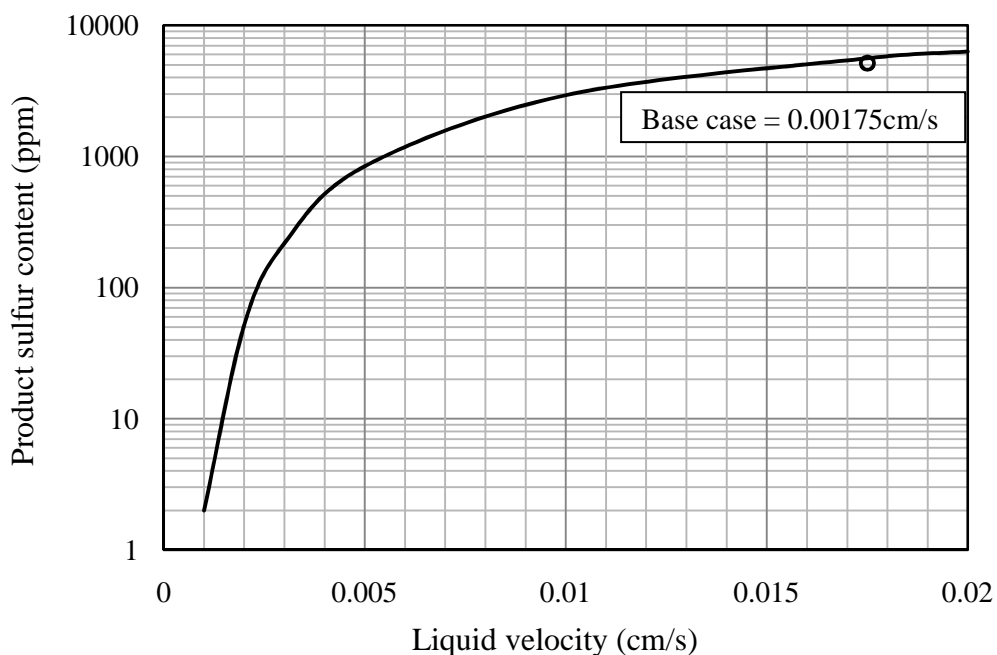


Figure 4.18: Effect of liquid velocity on product sulfur content, (o) experimental, (—) present model ( $T = 380^{\circ}\text{C}$ ,  $P = 5.3\text{MPa}$ ,  $Z = 32\text{cm}$ )

#### 4.6.2.3 Effect of Feed Inlet Temperature

Feed inlet temperature can have prominent effect on mass transfer rate of hydrogen and reaction rate. It would enhance the amount of dissolved hydrogen and rate constant which in turn improves the conversion of sulfur into hydrogen sulfide. As shown in Figure 4.19, by increasing feed inlet temperature, the hydrodesulfurization reaction significantly enhanced. Sulfur content in the VGO can be reduced to 10 ppm in a reactor length of 32 cm (base case) at an operating temperature of  $430^{\circ}\text{C}$ . At these temperatures hydrocracking can take place. It will be interesting to carry out desulfurization in the hydrocracker itself.

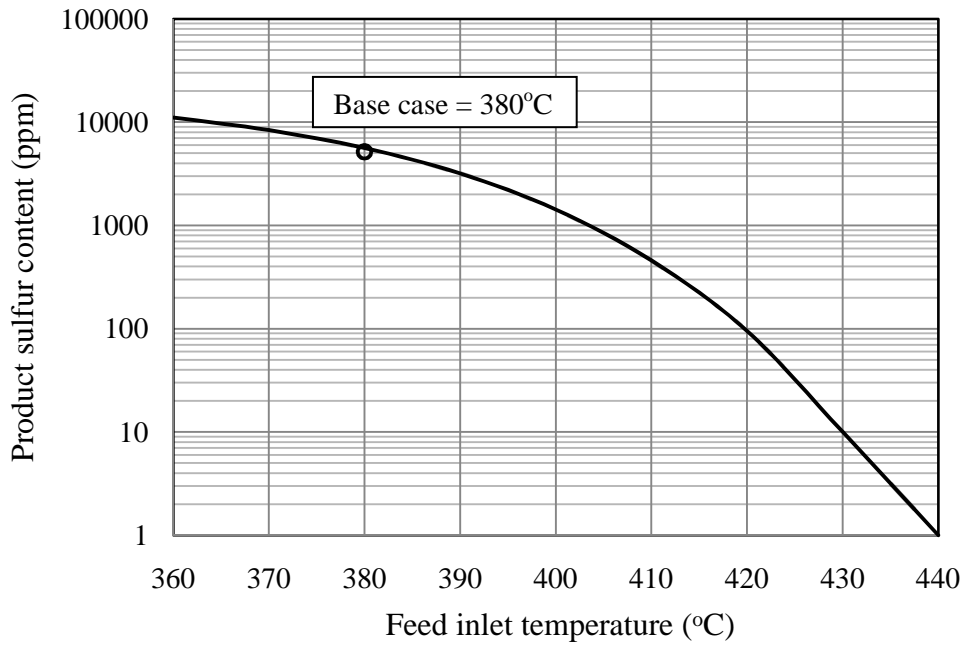


Figure 4.19: Effect of feed inlet temperature on product sulfur content, (o) experimental, (—) present model ( $P = 5.3\text{MPa}$ ,  $u_{oL} = 0.00175\text{cm/s}$ ,  $Z = 32\text{cm}$ )

#### 4.6.2.4 Effect of Reactor Pressure

Higher operating pressure can increase solubility of hydrogen in the liquid phase and hence higher hydrogen concentration in the liquid phase for HDS reaction. Figure 4.20 presents the variation of product sulfur content with the reactor pressure. As observed, the product sulfur content decreases with increasing operating pressure. However, effect of pressure is not significant compared to the effect of feed inlet temperature.

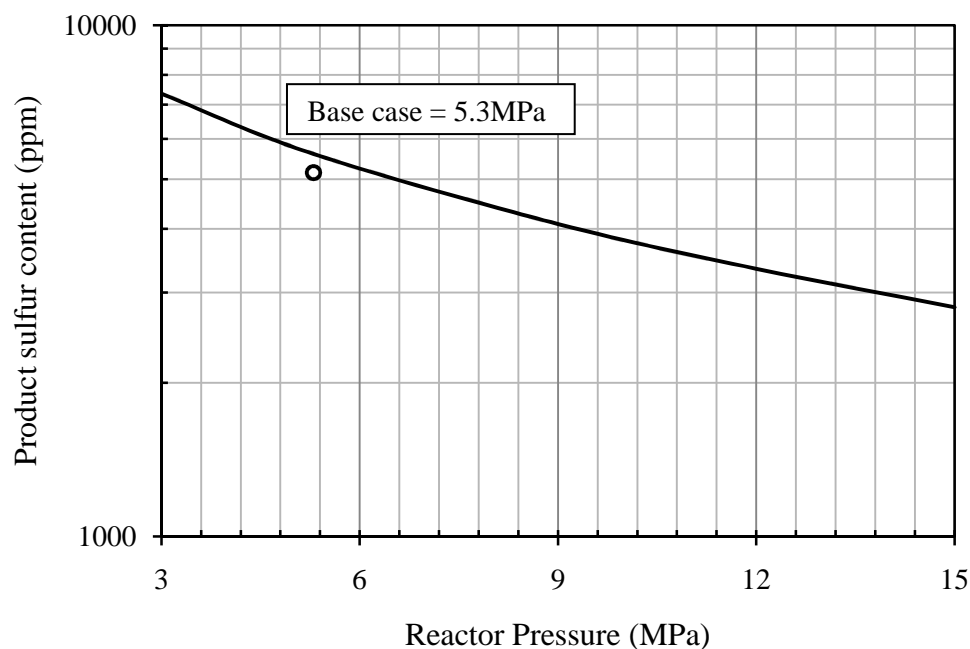


Figure 4.20: Effect of operating pressure on product sulfur content, (o) experimental, (—) present model ( $T = 380^{\circ}\text{C}$ ,  $u_{oL} = 0.00175\text{cm/s}$ ,  $Z = 32\text{cm}$ )

#### 4.7 Simulation of HDS Commercial Unit

Sulfur in the oil fractions need to be reduced to a very low level to meet the stringent sulfur requirements being imposed. Replacing the existing commercial reactor or increasing the reactor length is a costly option. Other possibilities should be considered for improving the reactor performances. The 1-D cell in series model developed in the preceding sections is able to explain the essential features of hydrodesulfurization process and it can be used to simulate other possibilities.

In the present section, the model is used to simulate the performance of a commercial size hydrotreating reactor for the possibility of

- reducing hydrogen sulfide in the feed gas,
- increasing the feed temperature,
- increasing reactor pressure and
- decreasing liquid velocity

to meet the limit on sulfur in the product. Properties of the feedstock, catalysts, operating variables and reactor dimensions are summarized in Table 4.3.

Table 4.3: Data on hydrotreating of VGO on commercial scale. Data taken from Mederos and Ancheyta [36]

<u>Feedstock</u>	<u>Value</u>
API gravity	22
Molecular weight	441.9
Mean average boiling point ( $^{\circ}\text{C}$ )	476
Sulfur (wt %)	2.009
Total nitrogen (wppm)	1284
Basic nitrogen (wppm)	518
Total aromatics (wt %)	41.9
<u>Catalyst</u>	<u>Value</u>
Equivalent diameter (mm)	2.54
Specific surface area ( $\text{m}^2/\text{g}$ )	175
Pore volume ( $\text{cm}^3/\text{g}$ )	0.56
Mean pore diameter ( $\text{\AA}$ )	127
Molybdenum content (wt %)	10.7
Nickel content (wt %)	2.9
Bulk density ( $\text{g}/\text{cm}^3$ )	0.8163
<u>Operation conditions</u>	<u>Value</u>
Gas superficial velocity (cm/s)	10.63
Liquid superficial velocity (cm/s)	0.63
Catalytic bed length (cm)	853.44
Internal diameter (cm)	304.8
Temperature ( $^{\circ}\text{C}$ )	380
Pressure (MPa)	5.3
Feed composition (mol %)	
$\text{H}_2$	81.63
$\text{H}_2\text{S}$	3.06
Light hydrocarbons	15.31

#### 4.7.1 Effect of Presence of Hydrogen Sulfide (H<sub>2</sub>S) in the Feed Hydrogen

Presence of high concentration of hydrogen sulfide in the hydrogen gas feed stream (3.06% mol) can have adverse effect on the hydrodesulfurization process. In the presence of high concentration of hydrogen sulfide in the feed gas, concentration profiles of hydrogen sulfide in the gas and liquid phases are illustrated in Figures 4.21 and 4.22 respectively. It can be clearly seen that partial pressure of hydrogen sulfide in the gas phase decreases initially as hydrogen sulfide in the feed gas (3.06% mol) rapidly dissolve in the liquid phase until reaches its saturation point, due to the mass transfer of hydrogen sulfide from the gas phase to the liquid phase. Then, the hydrogen sulfide partial pressure increases as hydrogen sulfide produced by the hydrodesulfurization in the catalyst phase diffuses to the liquid phase and eventually to the gas phase (Figure 4.21).

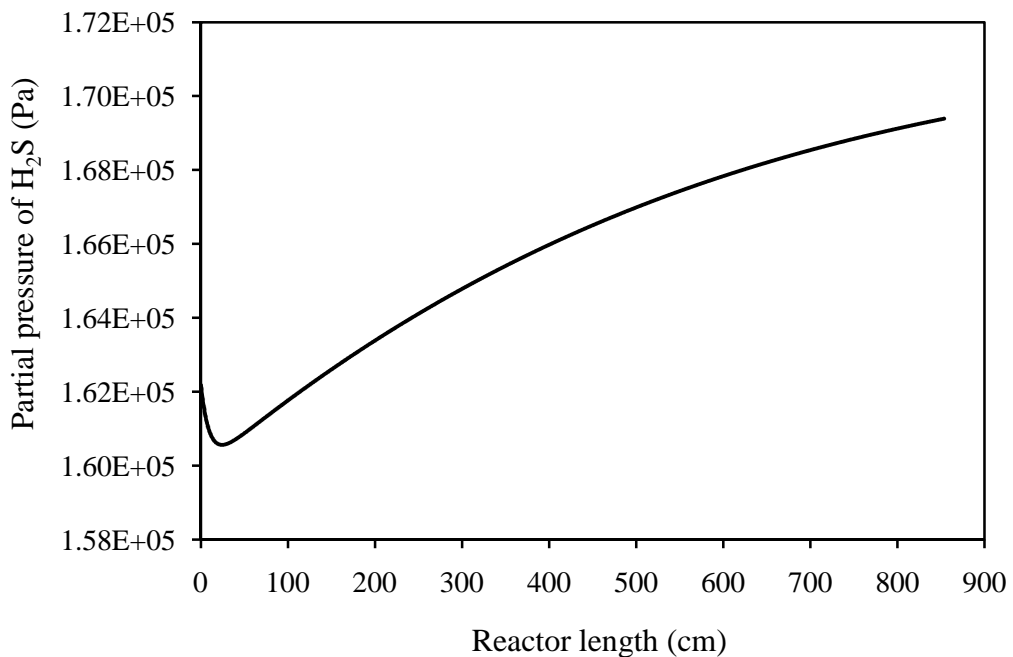


Figure 4.21: Partial pressure profiles of hydrogen sulfide in gas phase for commercial reactor

On the other hand, hydrogen sulfide concentration in the liquid phase increases rapidly in the reactor entry zone due to mass transfer from the gas phase (Figure 4.22). Further down in the reactor, concentration of hydrogen sulfide in the liquid phase decreases as it diffuses out to the gas phase at a faster rate than the hydrogen sulfide arriving from the solid phase due to the hydrodesulfurization reaction.

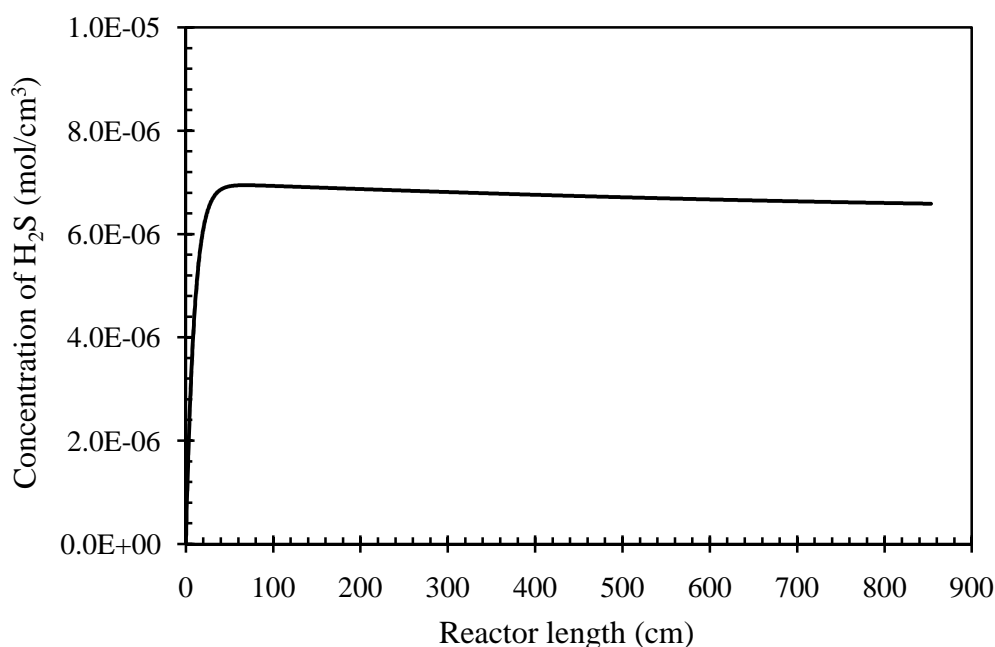


Figure 4.22: Concentration profile of hydrogen sulfide in liquid phase for commercial reactor

Presence of hydrogen sulfide in the feed hydrogen (3.06% mol) has a strong effect on sulfur removal rate, as it decrease the solubility of hydrogen in the liquid phase and hence reduces the amount of hydrogen in the solid catalyst for sulfur conversion. Also, hydrodesulfurization reaction kinetics is retarded with higher hydrogen sulfide concentration. Concentration of sulfur compound in the liquid phase along the commercial reactor with reactor length of 853.5cm is presented in Figure 4.23. In presence of hydrogen sulfide in the feed gas, sulfur concentration of 20092ppm has reduced to 3829 ppm with sulfur removal of 81%. Hydrogen sulfide in the gas stream can be decreased by incorporating an amine scrubber. Considering the hydrogen sulfide content in the gas feed reduces from 3.06% mol to 0% mol, it was found that the conversion of sulfur increases up to 97% with outlet sulfur concentration of 594ppm.

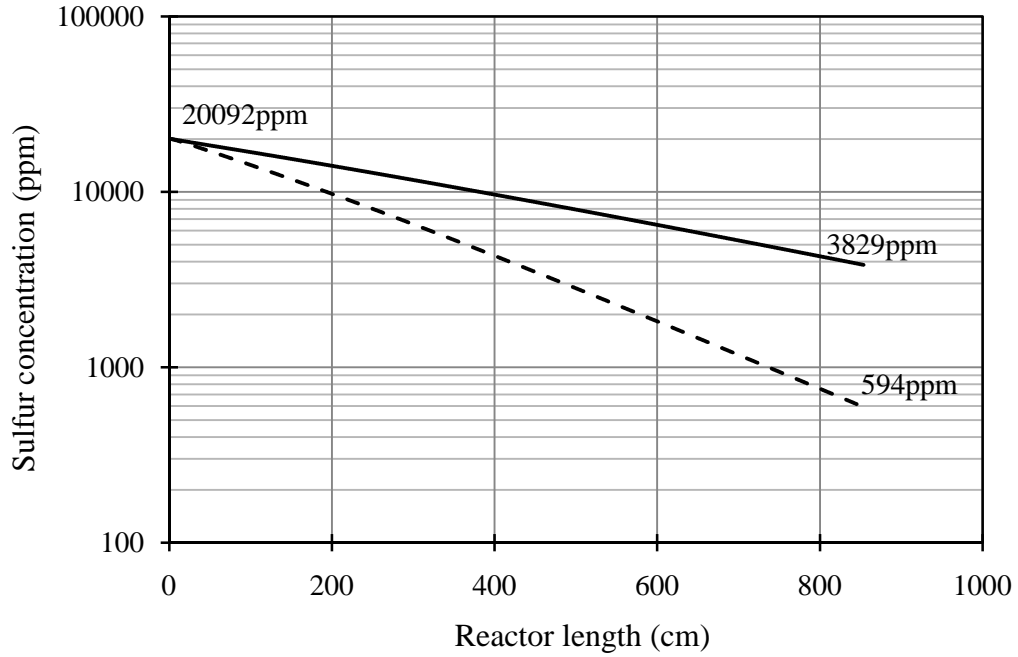


Figure 4.23: Sulfur concentration profiles in liquid phase for commercial reactor, (—) with 3.06% mol H<sub>2</sub>S content, (----) without H<sub>2</sub>S content

#### 4.7.2 Effect of Feed Inlet Temperature

The effect of feed temperature on product sulfur content is shown in Figure 4.24. By increasing feed inlet temperature, sulfur removal significantly improved. Higher temperature would enhance the amount of dissolved hydrogen and rate constant which in turn improves the sulfur conversion. Sulfur content in the VGO for commercial reactor can be reduced to 10 ppm as feed temperature inlet increases up to 416°C.

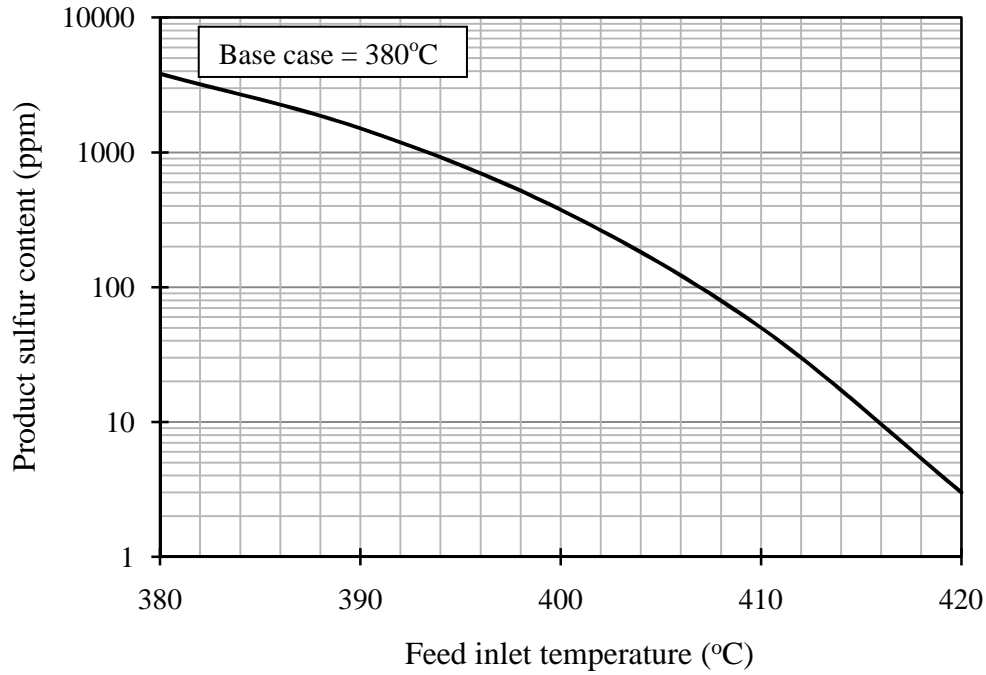


Figure 4.24: Effect of feed inlet temperature on product sulfur content  
(P = 5.3MPa,  $u_{oL} = 0.63\text{cm/s}$ )

### 4.7.3 Effect of Reactor Pressure

The effect of reactor pressure on sulfur removal is presented in Figure 4.25. Higher reactor pressure would increase solubility of hydrogen in the liquid phase and hence lead to higher sulfur conversion. However, the effect of reactor pressure on sulfur conversion is insignificant and this is not a viable option.

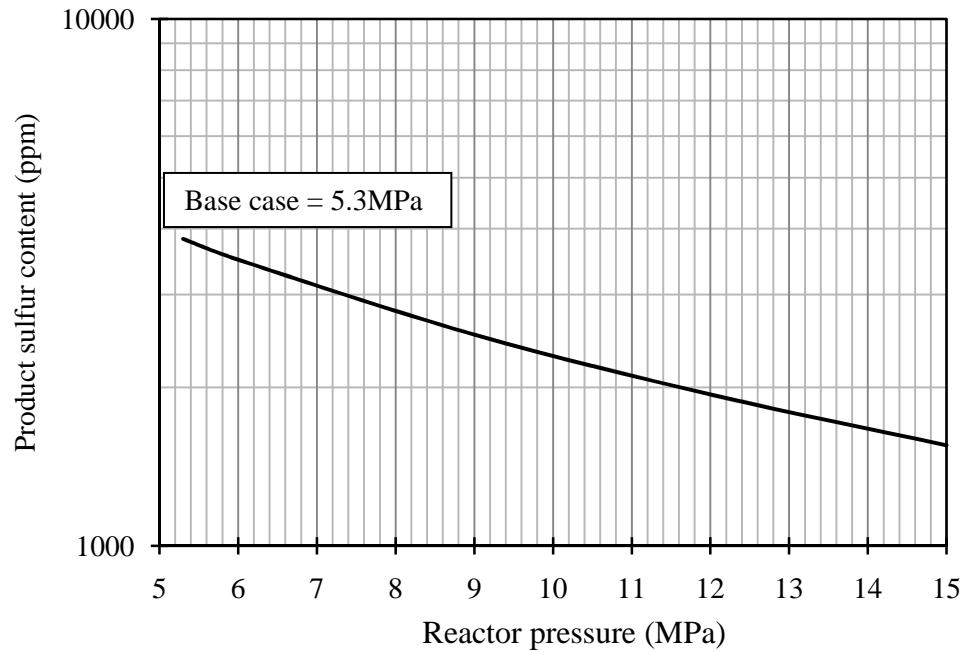


Figure 4.25: Effect of reactor pressure on product sulfur content ( $T = 380^{\circ}\text{C}$ ,  
 $u_{oL} = 0.63\text{cm/s}$ )

#### 4.7.4 Effect of Liquid Velocity

A lower in liquid velocity leads to higher sulfur removal due to longer liquid residence time. The effect of liquid velocity on sulfur removal is presented in Figure 4.26. Sulfur removal increases with decreasing liquid velocity. It is observed that sulfur content in VGO for commercial reactor can be reduced to 10ppm by decreasing liquid velocity of 0.63cm/s to 0.14cm/s. This reduces the throughput drastically and hence is not a viable option.

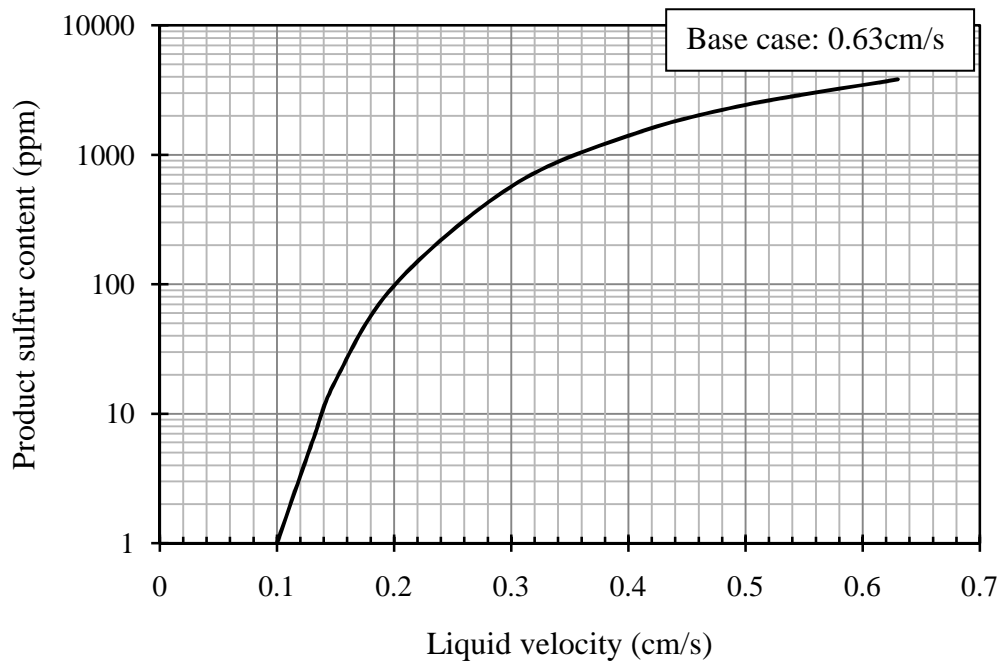


Figure 4.26: Effect of liquid velocity on product sulfur content  
(T = 380°C, P = 5.3MPa)

## 4.8 Conclusions

- i. A steady state one-dimensional cells-in-series model was developed to predict the behavior of a trickle bed hydrodesulfurization reactor. The reactor model was established based on mass and energy balances, reaction rate based on Langmuir-Hinshelwood kinetics for HDS reaction and integrated with reactor hydrodynamics.
- ii. The model was validated with the literature experimental data on a pilot reactor for sulfur concentration at the exit of reactor.
- iii. The model was used to simulate HDS in a commercial unit to explore the possibility of reducing sulfur content to meet the stringent sulfur requirements being imposed. This can be achieved using the existing reactor units by increasing the feed temperature and reducing hydrogen sulfide in the feed gas.

## Notation

$a_{GL}$	Gas-liquid interfacial area per unit volume ( $\text{cm}^2/\text{cm}^3$ )
$a_{LS}$	Liquid-solid interfacial area per unit volume ( $\text{cm}^2/\text{cm}^3$ )
$C_i^j$	Molar concentration of component in $j$ phase at $i$ cell ( $\text{mol}/\text{cm}^3$ )
$c_P^j$	Heat capacity of $j$ phase ( $\text{J}/\text{g} \cdot \text{K}$ )
$D_i^L$	Molecular diffusivity of compound $i$ in liquid phase viscosity ( $\text{cm}^2\text{s}^{-1}$ )
$d_p$	Particle diameter ( $\text{cm}$ )
$d_{15.6}$	Specific gravity at $15.6^\circ\text{C}$
$\Delta H_{HDS}$	Heat of reaction ( $\text{J}/\text{mol}$ )
$H_i$	Henry law constant for compound I ( $\text{Pa} \cdot \text{m}^3/\text{mol}$ )
$h_{GL}$	Gas-liquid heat transfer coefficient ( $\text{Js}^{-1}\text{cm}^{-2}\text{K}^{-1}$ )
$h_{LS}$	Liquid-solid heat transfer coefficient ( $\text{Js}^{-1}\text{cm}^{-2}\text{K}^{-1}$ )
$k_{GL}$	Gas-liquid mass transfer coefficient ( $\text{cm}/\text{s}$ )
$k_{LS}$	Liquid-solid mass transfer coefficient ( $\text{cm}/\text{s}$ )
$k_o$	Frequency factor
$k_{HDS}$	Rate constant for hydrodesulfurization reaction ( $\text{cm}^3\text{g}^{-1}\text{s}^{-1}$ )
$K_{H_2S}$	Adsorption equilibrium constant for $\text{H}_2\text{S}$ ( $\text{cm}^3 \text{mol}^{-1}$ )
$p_{ai}$	Partial pressure of gas component at $i$ cell ( $\text{Pa}$ )
$P$	Reactor pressure (psia)
$r_{HDS}$	Reaction rate of hydrodesulfurization ( $\text{mol} \cdot \text{g}^{-3}\text{s}^{-1}$ )
$R$	Gas constants, 8.314
$\text{Re}_L$	Reynolds number
$Ga_L$	Galileo number
$T_i$	Temperature at $i$ cell ( $\text{K}$ )
$T_{MeABP}$	Mean average boiling point ( $^\circ\text{R}$ )
$u_{oG}$	Gas superficial velocity ( $\text{cm}/\text{s}$ )
$u_{oL}$	Liquid superficial velocity ( $\text{cm}/\text{s}$ )

$v_i$	Molar volume of solute at its normal boiling temperature ( $\text{cm}^3 \text{mol}^{-1}$ )
$v_L$	Molar volume of liquid solvent at its normal boiling temperature ( $\text{cm}^3 \text{mol}^{-1}$ )
$v_c$	Critical specific volume ( $\text{cm}^3/\text{mol}$ )
$z$	Axial coordinate (cm)

*Greek letters*

$\varepsilon_p$	Particle volume fraction
$\eta$	Effectiveness factor
$\lambda_i$	Solubility coefficient of the compound $i$ ( $\text{NI kg}^{-1} \text{MPa}^{-1}$ )
$\mu_L$	Liquid viscosity (mPa.s)
$\rho_p$	Catalyst density ( $\text{g/cm}^3$ )
$\rho_B$	Catalyst bulk density ( $\text{g/cm}^3$ )
$\rho_G$	Gas density ( $\text{g/cm}^3$ )
$\rho_L$	Liquid density ( $\text{g/cm}^3$ )
$\rho_{20}$	Liquid density at $20^\circ\text{C}$ ( $\text{g/cm}^3$ )
$\rho_o$	Liquid density at standard conditions ( $15.5^\circ\text{C}$ and $103.3\text{kPa}$ ), ( $\text{lb}_m/\text{ft}^3$ )
$\Delta\rho_T$	Temperature correction of liquid density, ( $\text{lb}_m/\text{ft}^3$ )
$\Delta\rho_p$	Pressure dependence of liquid density, ( $\text{lb}_m/\text{ft}^3$ )

*Subscripts and superscripts*

$i$	cell
$H_2$	Hydrogen
$HC$	Hydrocarbon
$H_2S$	Hydrogen sulfide
$G$	Gas
$L$	Liquid
$S$	Solid

## CHAPTER 5

### SUMMARY, CONCLUSIONS AND RECOMMENDATIONS

#### 5.1 Summary

As good quality crudes are depleting fast, there is a greater need to process sour crudes. At the same time, the regulated sulfur limits in the products are becoming more stringent. Trickle bed reactors are widely used to reduce sulfur content in vacuum gas oil (VGO) by hydrodesulfurization reaction with hydrogen. There is a great need to explore the possibility to improve the hydrodesulfurization process in the trickle bed reactors to meet the future regulations. Modeling to understand the phenomena occurring in the reactor can be a great help in establishing the options for better reactor performance.

Performance of trickle bed reactors is influenced by the residence time of the reactants (sulfur compounds in VGO), inter-phase mass transfer and reaction kinetics. Residence time in the reactor depends on the liquid flow rate and liquid holdup. A Submerged Particle Model was developed to estimate liquid holdup and pressure drop in trickle bed reactor considering gas to flow around particles enveloped by trickling liquid. Experimental data available in the literature on liquid holdup for various gas-liquid systems were used for the evaluation of the model developed. The model equation explained the experimental observations for liquid holdup reasonably well, and the results were discussed in terms of varying parameters such as gas and liquid velocities, liquid viscosity, particle sizes, operating pressure and temperature. Liquid holdup increases with increasing liquid velocity and liquid viscosity. On the other hand, liquid holdup decreases with increasing gas velocity, particle size, pressure and temperature.

Ergun's equation for pressure drop in packed beds was adopted to estimate pressure drop for gas flow in trickle beds. Liquid holdup reduces the cross sectional

area for gas flow and increases the tortuosity of gas flow path. Tortuosity of gas flow was proposed to be a function of gas phase volume fraction. The model predictions for two phase pressure drop compared well with the experimental observations reported in the literature. Pressure drop increases with increasing gas and liquid velocities as well as operating pressure. On the other hand, pressure drop decreases with increasing temperature and catalyst particle size.

A steady state one-dimensional multiphase cells-in-series model was developed to describe the behavior of hydrodesulfurization process in a trickle bed reactor. The model includes mass and energy balances equations for gas, liquid and solid phases. The reactor model equations for each cell were formulated based on mass and energy balances incorporating transport and kinetic parameters. Reaction kinetics reported in the literature for the hydrodesulfurization reaction based on Langmuir Hinshelwood mechanism was assumed. Trickle bed hydrodynamics and transport parameters were estimated using selected correlations taken from literature. Liquid holdup and pressure drop in trickle bed reactor were estimated from the validated submerged particle model. The reactor model was validated using experimental data on hydrotreating of vacuum gas oil (VGO) on a pilot reactor reported by Mederos and Ancheyta [41]. The trends for hydrogen and hydrogen sulfide concentrations in the gas and liquid phases as well as sulfur concentration in the liquid phase along the reactor length were in line with the literature data. Bed temperature rises along the reactor length due to the exothermic reaction of hydrodesulfurization.

The validated 1-D cell-in-series model then was used to simulate the hydrodesulfurization reaction in a commercial unit to investigate possibility of reducing sulfur content in the VGO to meet the stringent sulfur requirements. The effect of hydrogen sulfide in the hydrogen feed gas, inlet feed temperature, reactor pressure and liquid velocity were simulated. It was found that sulfur removal could be improved by increasing feed inlet temperature, increasing reactor pressure, decreasing hydrogen sulfide in the gas streams and decreasing liquid velocity. Increasing feed temperature and reducing hydrogen sulfide in the feed gas are the two viable options to improve the reactor performance. Effect of reactor pressure on sulfur removal is insignificant while reducing liquid velocity significantly reduced the throughput.

## **5.2 Conclusions**

- 1) Equations to estimate liquid holdup and pressure drop in trickle beds are developed considering that gas flows through tortuous flow paths in a bed of wetted particles. The equations are validated with literature data covering a wide range of operating conditions.
- 2) A one-dimensional cells-in-series model has been developed to describe hydrodesulfurization (HDS) process in a trickle bed reactor. The model is validated with literature data.
- 3) Based on the model simulations, the required desulfurization of VGO can be achieved in the existing reactors by increasing the feed temperature.

## **5.3 Recommendation**

Increasing the temperature of feed can enhance hydrodesulfurization, but this can also promote hydro cracking as well. Hence, it is necessary to develop catalysts for hydrocracking and hydrodesulfurization which can tolerate sulfur. Also, the model should be extended to include both hydrocracking and hydrodesulfurization.

## REFERENCES

- [1] J. G. Speight, "Feedstock composition," in *The Desulfurization of Heavy Oils and Residua*, 2nd ed. New York: Marcel Dekker, 2000, pp. 83–104.
- [2] G. H. Gary and G. E. Handwerk, "Hydrotreating," in *Petroleum Refining-Technology and Economics*, 4th ed. New York: Marcel Dekker, 2001, pp. 175–180.
- [3] J. G. Speight, "Hydrotreating and Desulfurization," in *The Chemistry & Technology of Petroleum*, 4th ed. New York: Marcel Dekker Inc, 1999.
- [4] "Oil Market Report," International Energy Agency, Sept 2010, pp. 1–59. Available: <http://omrpublic.iea.org/currentissues/full.pdf>
- [5] H. Alboudwarej, J. Felix, S. Taylor, R. Badry, C. Bremner, C. Skeates, A. Baker, D. Palmer, K. Pattison, M. Beshry, G. Brown and R. Calvo, J. A. C. Triana, R. Hathcock, K. Koerner, T. Hughes, D. Kundu, J. L. Cardenas and C. West, "Highlighting heavy oil," *Oilfield Review*, vol.18, pp. 34–53, 2006.
- [6] Country Analysis Brief. (2010, Dec.) *Malaysia Energy Data, Statistics and Analysis-Oil, Gas, Electricity, Coal*. [online]. Available: <http://www.eia.doe.gov/EMEU/cabs/Malaysia/pdf.pdf>
- [7] P. Singh. (2009). *Pollution, Degradation and Contamination*. Issue 3. [online]. Available: <http://www.doe.gov.my/files/Publication/Impak/Impak09bil%203.pdf>
- [8] A. E. Saez and Carbonell, "Hydrodynamics parameters for gas-liquid concurrent flow in packed beds," *AIChE J.*, vol. 31, pp. 52–62, 1985.
- [9] R. A. Holub, M. P. Dudukovic and P. A. Ramachandran, "A phenomenological model of pressure drop, liquid holdup and flow regime transition in gas-liquid trickle flow," *Chem. Eng. Sci.*, vol. 47, pp. 2343–2348, 1992.

- [10] A. Attou, C. Boyer and G. Ferschneider, "Modeling of the hydrodynamics of the concurrent gas-liquid trickle flow through a trickle bed reactor," *Chem. Eng. Sci.*, vol. 54, pp. 785-802, 1999.
- [11] R. G. Carbonell, "Multiphase flow models in packed beds," *Oil Gas Sci. Technol-Rev. IFP.*, vol. 55, pp. 417-425, 2000.
- [12] M. Bhaskar, G. Valavarasu, B. Sairam, K. S. Balaraman and K. Balu, "Three phase reactor model to simulate the performance of pilot-plant and industrial trickle bed reactors sustaining hydrotreating reactions," *Ind. Eng. Chem. Res.*, vol. 43, pp. 6654-6669, 2004.
- [13] M. A. Rodriguez and J. Ancheyta, "Modeling of hydrodesulphurization (HDS), hydrodenitrogenation (HDN), and the hydrogenation of aromatics (HDA) in a vacuum gas oil hydrotreater," *Energy Fuel*, vol. 18, pp. 789-794, 2004.
- [14] C. Murali, R. K. Voolapalli, N. Ravichander, D. T. Gokak and N. V. Choudary, "Trickle bed reactor model to simulate the performance of commercial diesel hydrotreating unit," *Fuel*, vol. 86, pp. 1176-1184, 2007.
- [15] F. S. Mederos, J. Ancheyta and J. Chen, "Review on criteria to ensure ideal behaviors in trickle-bed reactors," *Appl. Catal. A: Gen.*, vol. 355, pp. 1-19, 2009.
- [16] J. G. Speight and B. Ozum, "Hydrotreating" in *Petroleum Refining Processes*, 1st ed. New York: Marcel Dekker, pp. 439-484, 2002.
- [17] M. R. Riazi, "Characteristic and Properties of Petroleum Fraction", 1st ed. ASTM International Standards Worldwide, 2005.
- [18] S. Parkash, "Distillate Hydrotreating," in *Refining Processes Handbook*, 1st ed. Elsevier, pp. 29-48, 2003.
- [19] J. P. Wauquier, "Fractionation and elemental analysis of crude oils and petroleum cuts," in *Petroleum Refining (Crude oil, Petroleum products, Process flowsheets)*, Edition Technips, pp. 17-34, 1995.
- [20] G. Biardia and G. Baldi, "Three phase catalytic reactors," *Catal. Today*, vol. 52, pp. 223-234, 1999.
- [21] G. F. Froment, "Modeling in the development of hydrotreatment processes," *Catal. Today*, vol. 98, pp. 43-54, 2004.

- [22] V. G. Baldovino-Medrano, S. A. Giraldo and A. Centeno, "Reactivity of dibenzothiophene type molecules over Pd catalysts," *J. Mol. Catal. A: Chem.*, vol. 301, pp. 127–133, 2009.
- [23] M. Xiaoliang, S. Kinya and M. Isao, "Hydrodesulfurization reactivities of various sulfur compounds in vacuum gas oil," *Ind. Eng. Chem. Res.*, vol. 32, pp. 2487–2494, 1996.
- [24] A. Alvarez and J. Ancheyta, "Simulation and analysis of different quenching alternatives for an industrial vacuum gasoil hydrotreater," *Chem. Eng. Sci.*, vol. 63, pp. 662–673, 2008.
- [25] K. Sertic-Bionda, Z. Gomzi and T. Saric, "Testing of hydrodesulfurization process in small trickle bed reactor," *Chem. Eng. J.*, vol. 106, pp. 105–110, 2005.
- [26] Z. Liu, Y. Zheng, W. Wang, Q. Zhang and L. Jia. "Simulation of hydrotreating of light cycle oil with a system dynamics model," *Appl. Catal. A Gen.*, vol. 339, pp. 209–220, 2008.
- [27] F. Jimenez, V. Kafarov and M. Nunez, "Modeling of industrial reactor for hydrotreating of vacuum gas oils. Simultaneous hydrodesulfurization, hydrodenitrogenation and hydrodearomatization reactions," *Chem. Eng. J.*, vol. 134, pp. 200–208, 2007.
- [28] M. Gray, *Upgrading of Petroleum Residues and Heavy oils*, 1st ed. New York: Marcel Dekker, pp. 10–25, 1994.
- [29] M. J. Macias and J. Ancheyta, "Simulation of an isothermal hydrodesulfurization small reactor with different catalyst particle shapes," *Catal. Today*, vol. 98, pp. 243–252, 2004.
- [30] C. Botchwey, "Syntheses, characterization and kinetics of nickel-tungsten nitride catalysts for hydrotreating of gas oil," Ph.D. dissertation, Dept. Chem. Eng., Saskatchewan Univ. Saskatoon, 2010.
- [31] A. de Bruijn, I. Naka and J. E. M. Sonnemans, "Effect of the noncylindrical shape of extrudates on the hydrodesulfurization of oil fractions," *Ind. Eng. Chem. Proc. Des. Dev.* vol. 20, pp. 40–45, 1981.
- [32] D. Nemeč, and J. Levec. "Flow through packed bed reactors: Single phase flow," *Chem. Eng. Sci.*, vol. 60, pp. 6947–6957, 2005.

- [33] B. H. Cooper, B. B. L. Donnis and B. Moyses, "Hydroprocessing conditions affect catalyst shape selection," *Oil Gas J.*, pp. 39–44, 1986.
- [34] J. Ancheyta, J. A. D. Munoz and M. J. Macías, "Experimental and theoretical determination of the particle size of hydrotreating catalysts of different shapes." *Catal. Today*, vol. 109, pp. 120–127, 2005.
- [35] M. E. Trivizadakis, D. Giakoumakis and A. J. Karabelas, "A study of particle shape and size effects on hydrodynamic parameters of trickle beds," *Chem. Eng. Sci.*, vol. 61, pp. 5534–5543, 2006.
- [36] F. S. Mederos and J. Ancheyta, "Mathematical modeling and simulation of hydrotreating reactor: Cocurrent versus countercurrent operation," *Appl. Catal. Gen.*, vol. 332, pp. 8–21, 2007.
- [37] M. H. Al-Dahhan, F. Larachi, M. P. Dudukovic and A. Laurent, "High pressure trickle bed reactors: A review," *Ind. Eng. Chem. Res.*, vol. 36, pp. 3292–3314, 1997.
- [38] K. D. P. Nigam and F. Larachi, "Process intensification in trickle-bed reactors," *Chem. Eng. Sci.*, vol. 60, pp. 5880–5894, 2005.
- [39] Z. M. Cheng, X. C. Fang, R. H. Zeng, B. P. Han, L. Huang and W. K. Yuan, "Deep removal of sulfur and aromatics from diesel through two-stage concurrently and countercurrently operated fixed bed reactors," *Chem. Eng. Sci.*, vol. 59, pp. 5465–5472, 2004.
- [40] B. W. van Hasselt, P. J. M. Lebens, H. P. A. Calis, F. Kapteijn, S. T. Sie, J. A. Moulijn and C. M. van den Bleek, "A numerical comparison of alternative three-phase reactors with a conventional trickle bed reactor. The advantages of countercurrent flow for hydrodesulfurization," *Chem. Eng. Sci.*, vol. 54, pp. 4791–4799, 1999.
- [41] R. Maiti, R. Khanna, and K. D. P. Nigam, "Hysteresis in trickle-bed reactors: A review," *Ind. Eng. Chem. Res.*, vol. 45, pp. 5185–5198, 2006.
- [42] B. Aydin and F. Larachi, "Trickle bed hydrodynamics and flow regime transitions at elevated temperature for a newtonian and a non newtonian", *Chem. Eng. Sci.*, vol. 60, pp. 6687–6701, 2005.
- [43] M. H. Al-Dahhan and M. P. Dudukovic, "Pressure drop and liquid holdup in high pressure trickle bed reactors," *Chem. Eng. Sci.*, vol. 49, pp. 5681–5698, 1994.

- [44] M. J. Ellman, N. Midoux, A. Laurent and J. C. A. Charpentier, "New improved pressure drop correlation for trickle-bed reactors," *Chem. Eng. Sci.*, vol.43, pp. 2201–2206, 1988.
- [45] M. J. Ellman, N. Midoux, G. Wild, A. Laurent and J. C. A. Charpentier, "New improved liquid holdup correlation for trickle-bed reactors," *Chem. Eng. Sci.*, vol. 45, pp. 1677–1684, 1990.
- [46] F. Larachi, A. Laurent, N. Midoux and G. Wild, "Experimental study of a trickle bed reactors operating at high pressure: Two-phase pressure drop and liquid saturation," *Chem. Eng. Sci.*, vol. 46, pp. 1233–1246. 1991a.
- [47] A. Lakota, J. Levec and R. G. Carbonell, "Hydrodynamics of trickling flow in packed beds: Relative permeability concept," *AIChE J.*, vol. 48, pp. 731–738, 2002.
- [48] D. Nemeč, G. Bercic, and J. Levec. "The hydrodynamics of trickling flow in packed beds operating at high pressures. The relative permeability concept," *Chem. Eng. Sci.*, vol. 56, pp. 5955–5962, 2001.
- [49] D. Nemeč and J. Levec, "Two-phase concurrent flow," *Chem. Eng. Sci.*, vol. 60, pp. 6958–6970, 2005.
- [50] R. A. Holub, M. P. Duduković and P. A. Ramachandran, "Pressure drop, liquid holdup and flow regime transition in trickle flow," *AIChE J.*, vol. 39, pp. 302-321, 1993.
- [51] M. H. Al-Dahhan, M. R. Khadilkar, Y. Wu and M. P. Duduković, "Prediction of pressure drop and liquid holdup in high pressure trickle bed reactors," *Ind. Eng. Chem. Res.*, vol. 37, pp. 793–798, 1998.
- [52] I. Iliuta and F. Larachi, "The generalized slit model: Pressure gradient, liquid holdup and wetting efficiency in gas-liquid trickle flow," *Chem. Eng. Sci.*, vol. 54, pp. 5039–5045, 1999.
- [53] I. Iliuta, F. Larachi and M. H. Al-Dahhan, "Double-slit model for partially wetted trickle flow hydrodynamics," *AIChE J.*, vol. 46, pp. 597–609, 2000.
- [54] P. R. Gunjal, V. V. Ranade, and R. V. Chaudhari, "Liquid distribution and RTD in trickle bed reactors: Experiments and CFD simulations," *Can. J. Chem. Eng.*, vol. 81, pp. 821–830, 2003.

- [55] P. R. Gunjal, M. N. Kashid, V. V. Ranade and R. V. Chaundhari, "Hydrodynamics of trickle bed reactors: Experiments and CFD modeling," *Ind. Eng. Chem. Res.*, vol. 44, pp. 6278–6294, 2005.
- [56] A. Atta, S. Roy and K. D. P. Nigam, "Prediction of pressure drop and liquid holdup in trickle bed reactor using relative permeability concept in CFD," *Chem. Eng. Sci.*, vol. 62, pp. 5870–5879, 2007.
- [57] J. C. Charpentier and M. Favier, "Some liquid holdup experimental data in trickle bed reactors for foaming and nonfoaming hydrocarbons," *AIChE J.*, vol. 21, pp. 1213–1218, 1975.
- [58] J. G. Boelhouwer, "Non-steady operation of trickle bed reactors: hydrodynamics, mass and heat transfer," Ph.D. dissertation, Dept. Chem. Eng., Technische Univ., Eindhoven, 2001.
- [59] S. Ergun, "Fluid flow through packed columns," *Chem. Eng. Progress*, vol. 48, pp. 89–94, 1952.
- [60] I. F. Macdonald, M. S. El-Sayed, K. Mow and F. A. L. Dullien, "Flow through porous media. The Ergun equation revisited," *Ind. Eng. Chem. Fundam.*, vol. 18, pp. 199–208, 1978.
- [61] K. Grosser, R. G. Carbonell and S. Sundaresan, "Onset of pulsing in two-phase cocurrent downflow through a packed bed," *AIChE J.*, vol. 34, pp. 1850–1860, 1988.
- [62] A. Kundu, K. D. P. Nigam and R. P. Verma, "Catalyst wetting characteristics in trickle bed reactors," *AIChE J.*, vol. 49, pp. 2253–2263, 2003.
- [63] E. Ozahi, M. Y. Gundogdu and M. O. Carpinlioglu, "A modification on Ergun's correlation for use in cylindrical packed beds with non-spherical particles," *Adv. Powder Technol.*, vol. 19, pp. 369–38, 2008.
- [64] I. Iliuta, F. Larachi, B. P. A. Grandjean, "Pressure drop and liquid holdup in trickle flow reactors: Improved Ergun constants and slip correlations for the slit model," *Ind. Eng. Chem. Res.*, vol. 37, pp. 4542–4550, 1998.
- [65] A. K. Saroha and R. Khera, "Hydrodynamic study of fixed beds with concurrent upflow and downflow," *Chem. Eng. Process*, vol. 45, pp. 455–460, 2006.

- [66] J. Guo and M. H. Al-Dahhan, "Liquid holdup and pressure drop in the gas-liquid co-current downflow packed bed reactor under elevated pressures," *Chem. Eng. Sci.*, vol. 59, pp. 5387–5393, 2004.
- [67] P. Harriott, *Chemical Reactor Design*, 1st ed. New York: Marcel Dekker, 2003, pp. 83–104.
- [68] B. Aydin and F. Larachi, "Trickle bed hydrodynamics for (non)-newtonian foaming liquids in non-ambient conditions," *Chem. Eng. J.*, vol. 143, pp. 236–243, 2008.
- [69] R. P. Larkins, P. R. White and D. W. Jeffrey, "Two phase concurrent flow in packed beds," *AIChE J.*, vol. 7, pp. 231–239, 1961.
- [70] J. L. Turpin and R. L. Huntington, "Prediction of pressure drop for two-phase, two component concurrent flow in packed beds," *AIChE J.*, vol. 13, pp. 1196–1202, 1967.
- [71] G. J. Kramer, "Static liquid hold-up and capillary rise in packed beds," *Chem. Eng. Sci.*, vol. 53, pp. 2985–2992, 1998.
- [72] M. S. Fu and C. S. Tan, "Liquid holdup and axial dispersion in trickle bed reactors," *Chem. Eng. Sci.*, vol. 51, pp. 5357–5361, 1996.
- [73] V. Specchia and G. Baldi, "Pressure drop and liquid holdup for two phase concurrent flow in packed beds," *Chem. Eng. Sci.*, vol. 32, pp. 515–523, 1977.
- [74] C. Boyer, C. Volpi and G. Ferschneider, "Hydrodynamics of trickle bed reactors at high pressure: Two-phase flow model for pressure drop and liquid holdup, formulation and experimental validation," *Chem. Eng. Sci.*, vol. 62, pp. 7026–7032, 2007.
- [75] Q. Xiao, A. M. Anter, Z. M. Cheng and W. K. Yuan, "Correlations for dynamic liquid holdup under pulsing flow in a trickle bed reactor", *Chem. Eng. J.*, vol. 78, pp. 125–129, 2000.
- [76] M. A. Ayude, O. M. Martinez and M. C. Cassanello, "Modulation of liquid holdup along a trickle bed reactor with periodic operation," *Chem. Eng. Sci.*, vol. 62, pp. 6002–6014, 2007.
- [77] R. Sidi-Boumedine and L. Raynal, "Influence of the viscosity on the liquid holdup in trickle bed reactors with structured packings," *Catal. Today*, vol. 105, pp. 673–679, 2005.

- [78] J. C. Charpentier, C. Prost and P. Goff, "Chute de pression pour des écoulements à co-courant dans les colonnes a garnissage arrosé: Comparaison avec le garnissage noyé," *Chem. Eng. Sci.*, vol. 24, pp. 1777–1794, 1969.
- [79] J. F. Davidson, "The holdup and liquid film coefficient of packed towers, Part II: Statistical models of random packings," *Trans. Instn Chem. Eng.*, vol. 37, pp. 131–136, 1959.
- [80] W. J. A. Wammes, J. Middlekamp, W. J. Huisman and C. M. deBaas, "Hydrodynamics in a concurrent gas-liquid trickle bed at elevated pressures," *AIChE J.*, vol. 37, pp. 1849–1862, 1991.
- [81] Y. Jiang, M. R. Khadilkar, M. H. Al-Dahhan and M. P. Dudukovic, "CFD modeling of multiphase in packed bed reactors: Results and applications," *AIChE J.*, vol. 48, pp. 716–730, 2002.
- [82] A. Souadnia and M. A. Latifi, "Analysis of two-phase flow distribution in trickle bed reactors," *Chem. Eng. Sci.*, vol. 56, pp. 5977–5985, 2001.
- [83] C. S. L. Narasimhan, R. P. Verma, A. Kundu and K. D. P. Nigam, "Modeling hydrodynamics of trickle bed reactors at high pressure," *AIChE J.*, vol. 48, pp. 2459–2474, 2002.
- [84] X. Ma, K. Sakanishi and I. Mochida, "Hydrodesulfurization reactivities of various sulfur compounds in diesel fuel," *Ind. Eng. Chem. Res.*, vol. 33, pp. 218–222, 1994.
- [85] S. K. Shabina, I. R. Choudhury, A. P Pulikotti, S. Singh, U. Manna and R. P. Verma, "Novel kinetic model for production of ULSD," in *Proc. Petrotech.*, New Delhi: India, Jan 2003.
- [86] J. Ancheyta, M. J. Angeles, M. J. Macias, G. Marroquin, and R. Morales, "Changes in apparent reaction order and activation energy in the hydrodesulfurization of real feedstocks," *Energy Fuels*, vol. 16, pp. 189–193, 2002.
- [87] H. S. Fogler, *Elements of Chemical Reaction Engineering*, 4th ed. New York: Prentice Hall, 2006, pp. 645–687.
- [88] D. H. Broderick and B. C. Gates, "Hydrogenolysis and hydrogenation of dibenzothiophene catalyzed by sulfided CoO-MoO<sub>3</sub>/γ-Al<sub>2</sub>O<sub>3</sub>: The reaction kinetics," *AIChE J.*, vol. 27, pp. 663–673, 1981.

- [89] H. Korsten, and U. Hoffmann, “Three phase reactor model for hydrotreating in pilot trickle bed reactors,” *AIChE J.*, vol. 42, pp. 1350–1360, 1996.
- [90] M. J. Girgis and B. C. Gates, “Reactivities, reaction networks and kinetics in high pressure catalytic hydroprocessing,” *Ind. Eng. Chem. Res.*, vol. 30, pp. 2021–2058, 2001.
- [91] D. Tsamatsoulis and N. Papayannakos, “Investigation of intrinsic HDS kinetics of a VGO in a trickle bed reactor with backmixing effects,” *Chem. Eng. Sci.*, vol. 53, pp. 3449–3458, 1998.
- [92] J. Chen, and Z. Ring, “Modeling and simulation of a fixed bed pilot plant hydrotreater,” *Ind. Eng. Chem. Res.*, vol. 40, pp. 3294–3300, 2001.
- [93] R. Cotta, M. Wolf-Maciel and R. Maciel Filho, “A case of HDT industrial reactor for middle distillates”, *Comput. Chem. Eng.*, vol. 24, pp. 1731–1735, 2000.
- [94] F. S. Mederos, M. A. Rodríguez, J. Ancheyta and E. Arce, “Dynamic modeling and simulation of catalytic hydrotreating reactors”, *Energy Fuels*, vol. 20, pp. 936–945, 2006.
- [95] V. G. Rao and A. A. H. Drinkenburg, “Pressure drop and hydrodynamic properties of pulses in two phase gas–liquid downflow through packed columns,” *Can. J. Chem. Eng.*, vol. 61, pp. 158–167, 1983.
- [96] M. J. Szady and S. Sundaresan, “Effect on boundaries on trickle bed hydrodynamics,” *AIChE J.*, vol 37, pp. 1237–1241, 1991.
- [97] I. Iliuta, F. C. Thyron and O. Muntean, “Hydrodynamics characteristics of two-phase flow through fixed beds: air/Newtonian and non-Newtonian liquids,” *Chem. Eng. Sci.*, vol. 51, pp. 4987–4995, 1996.
- [98] M. Mota, J. Teixeira, A. Yelshin, “Analysis of packed beds of spherical particles of different sizes,” *Separ. Purif. Tech.*, vol. 15, pp. 59–68, 1999.
- [99] F.A.L. Dullien, “Single phase flow through porous media and pore structure,” *Chem. Eng. J.*, vol. 10, pp. 1–34, 1975.
- [100] T. Ahmed, *Reservoir Engineering Handbook*, 2nd ed. Houston, TX: Gulf Publishing, 2000, pp. 74–126.
- [101] B. E. Poling, J. M. Prausnitz and J. P. O’Connell, “Properties of gases and liquid,” 5th ed. New York: Mc-Graw Hill, 2000.

- [102] M. H. Al-Dahhan and M. P. Dudukovic, "Catalyst wetting efficiency in trickle-bed reactors at high pressure," *Chem. Eng. Sci.*, vol. 50, pp. 2377–2389, 1995.
- [103] C. J. Geankoplis, "Principle of Mass Transfer," in *Transport Processes and Separation Process Principles*, 4th ed. New Jersey: Prentice Hall, 2003, pp. 410–457.

## APPENDIX A

### SUBMERGED PARTICLE MODEL SAMPLE CALCULATIONS

This chapter presents sample calculations of submerged particle model to estimate liquid holdup and pressure drop in trickle beds. Experimental data of Trivizadakis et al. [35] as listed in Table A.1 were used for sample model calculation.

Table A.1: Experimental data of Trivizadakis et al. [35]

<i>Water-air system</i>	
Temperature	25°C
Pressure	1 atm
Gas mass velocity (kg/m <sup>2</sup> .s)	0.12-0.37
Liquid mass velocity (kg/m <sup>2</sup> .s)	2.4
Catalyst shape	cylinder
Catalyst diameter (mm)	1.5
Average length (mm)	3.11
Bed voidage, $\varepsilon$	0.40

Liquid holdup in trickle beds is evaluated using eq. (3.12)

$$\varepsilon_{Ld} = \left[ \left( \frac{\varepsilon_p u_{oL}^2}{d_p g} \right) \cdot \frac{\rho_L}{\rho_L - \rho_G} \cdot \left( \frac{180 \mu_L \varepsilon_p}{d_p \rho_L u_{oL}} + 1.8 \right) \right]^{1/3} \left( \frac{1}{\left\{ 1 \pm \left[ \frac{\rho_L (\varepsilon_p + \varepsilon_{Ld})}{(\rho_L - \rho_G) \varepsilon_{Ld}} \right] \frac{(P_1 - P_2)_{TP}}{Z \rho_L g} \right\}} \right)^{1/3}$$

Viscosity of water (25°C, 1 atm) =  $8.9 \times 10^{-4}$  kg/m.s

Viscosity of air (25°C, 1 atm) =  $1.8 \times 10^{-5}$  kg/m.s

Water density (25°C, 1 atm) =  $997$  kg/m<sup>3</sup>

Air density (25°C, 1 atm) =  $1.2$  kg/m<sup>3</sup>

Liquid velocity can be estimated as

$$u_{oL} = \frac{\text{liquid mass velocity}}{\text{liquid density}}$$
$$u_{oL} = \frac{2.4 \frac{\text{kg}}{\text{m}^2 \cdot \text{s}}}{997 \frac{\text{kg}}{\text{m}^3}} = 2.41 \times 10^{-3} \frac{\text{m}}{\text{s}}$$

Gas velocity can be estimated as

$$u_{oG} = \frac{\text{gas mass velocity}}{\text{gas density}}$$
$$u_{oG} = \frac{0.125 \frac{\text{kg}}{\text{m}^2 \cdot \text{s}}}{1.2 \frac{\text{kg}}{\text{m}^3}} = 0.104 \frac{\text{m}}{\text{s}}$$

Since catalyst particles are not spherical, equivalent surface volume mean diameter ( $d_e$ ) need to be determined instead of particle diameter. The equivalent surface volume mean diameter  $d_e$  was evaluated using eq. 3.11.

$$\frac{6}{d_e} = \frac{S_p}{V_p}$$
$$= \frac{2\pi \frac{d_p^2}{4} + \pi d_p h}{\frac{\pi d_p^2 h}{4}}$$
$$= \frac{2}{h} + \frac{4}{d_p}$$
$$= \frac{2}{3.31 \text{ mm}} + \frac{4}{1.5 \text{ mm}}$$

$$d_e = 1.81 \text{ mm}$$

The sum of the volume fraction of the gas and liquid adds up to the bed porosity,

$$\varepsilon_G + \varepsilon_L = \varepsilon$$

$$\begin{aligned}\varepsilon_G &= \varepsilon - \varepsilon_L \\ &= 0.4 - \varepsilon_L\end{aligned}$$

Particle holdup,  $\varepsilon_p$  is estimated as

$$\begin{aligned}\varepsilon_p &= 1 - \varepsilon \\ &= 1 - 0.4 \\ &= 0.6\end{aligned}$$

Substituted these values, dynamic liquid holdup can be estimated as

$$\varepsilon_{Ld} = \left[ \left( \frac{(0.00241)^2 \frac{\text{m}^2}{\text{s}^2}}{0.00181 \text{ m} \times 9.81 \frac{\text{m}}{\text{s}^2}} \right) \cdot \frac{997 \frac{\text{kg}}{\text{m}^3}}{(997 - 1.2) \frac{\text{kg}}{\text{m}^3}} \right]^{1/3} \cdot \left[ \frac{180 \times \left( 8.9 \times 10^{-4} \frac{\text{kg}}{\text{m.s}} \right) \times 0.6}{0.00181 \text{ m} \times \left( 997 \frac{\text{kg}}{\text{m}^3} \right) \times \left( 0.00241 \frac{\text{m}}{\text{s}} \right)} + 1.8 \right]$$

$$\left( \frac{0.6}{\left\{ 1 \pm \left[ \frac{997 \frac{\text{kg}}{\text{m}^3} (0.6 + \varepsilon_{Ld})}{(997 - 1.2) \frac{\text{kg}}{\text{m}^3} \varepsilon_{Ld}} \right] \frac{(P_1 - P_2)_{TP}}{Z} \right\} \left( 997 \frac{\text{kg}}{\text{m}^3} \right) \cdot 9.81 \frac{\text{m}}{\text{s}^2}} \right)^{1/3}$$

The term of pressure drop  $\frac{(P_1 - P_2)_{TP}}{Z}$  in liquid holdup equation is estimated using eq.

3.25.

$$\frac{(P_1 - P_2)_{TP}}{Z} = \left[ \frac{72}{\varepsilon_G^{1.5}} \frac{\mu_G (\varepsilon_p + \varepsilon_{Ld})^{2/3} \varepsilon_p^{1/3}}{d_p u_{oG} \rho_G} + \frac{0.455}{\varepsilon_G^{2.25}} \right] \left[ \frac{\rho_G u_{oG}^2 \varepsilon_p^{1/3} (\varepsilon_p + \varepsilon_{Ld})^{2/3}}{\varepsilon_G^3 d_p} \right]$$

$$\frac{(P_1 - P_2)_{TP}}{Z} = \left[ \frac{72}{(0.4 - \varepsilon_{Ld})^{1.5}} \cdot \frac{\left(1.8 \times 10^{-5} \frac{\text{kg}}{\text{m.s}}\right) (0.6 + \varepsilon_{Ld})^{2/3} (0.6)^{1/3}}{(0.00181 \text{ m}) \cdot \left(0.104 \frac{\text{m}}{\text{s}}\right) \cdot \left(1.2 \frac{\text{kg}}{\text{m}^3}\right)} + \frac{0.455}{(0.4 - \varepsilon_{Ld})^{2.25}} \right] \times$$

$$\left[ \frac{\left(1.2 \frac{\text{kg}}{\text{m}^3}\right) \cdot \left(0.104 \frac{\text{m}}{\text{s}}\right)^2 (0.6)^{1/3} (0.6 + \varepsilon_{Ld})^{2/3}}{(0.4 - \varepsilon_{Ld})^3 (0.00181 \text{ m})} \right]$$

Equations for dynamic liquid holdup and pressure drop were solved simultaneously to obtain prediction values of liquid holdup and pressure gradient in trickle beds. Prediction of dynamic liquid holdup can be obtained by iteration procedure. From the simulations, the values of dynamic liquid holdup and pressure drop obtained were

$$\varepsilon_{Ld} = 0.147$$

$$\frac{(P_1 - P_2)_{TP}}{Z} = 9467.477 \text{ Pa}$$

For some investigators that present their experimental data in term of total liquid holdup, it is noted that the total liquid holdup can be estimated by adding the value of dynamic liquid holdup with static liquid holdup. Static liquid holdup can be estimated using the correlation of Saez and Carbonell [8].

$$\varepsilon_{Ls} = \frac{1}{20 + 0.9E_o}$$

with

$$E_o = \frac{\rho_L g [d_p (1 - \varepsilon)]^2}{\sigma}$$

Table A.2: Simulation results predicted by Submerged Particle Model for data of Trivizadakis et al. [35]

$G(\text{kg/m}^2 \cdot \text{s})$	$\rho_G(\text{kg/m}^3)$	$u_{oG}(\text{m/s})$	$\mu_G(\text{kg / m.s})$	$L(\text{kg/m}^2 \cdot \text{s})$	$u_{oL}(\text{m/s})$	$\rho_L(\text{kg/m}^3)$	$\mu_L(\text{kg / m.s})$	$d_e(\text{m})$	$\varepsilon_p$	$\varepsilon$	$g(\text{m/s}^2)$
0.125	1.2	0.104167	1.80E-05	2.4	0.00241	997	8.90E-04	1.81E-03	0.6	0.4	9.81
0.152	1.2	0.126667	1.80E-05	2.4	0.00241	997	8.90E-04	1.81E-03	0.6	0.4	9.81
0.18	1.2	0.15	1.80E-05	2.4	0.00241	997	8.90E-04	1.81E-03	0.6	0.4	9.81
0.205	1.2	0.170833	1.80E-05	2.4	0.00241	997	8.90E-04	1.81E-03	0.6	0.4	9.81
0.235	1.2	0.195833	1.80E-05	2.4	0.00241	997	8.90E-04	1.81E-03	0.6	0.4	9.81
0.262	1.2	0.218333	1.80E-05	2.4	0.00241	997	8.90E-04	1.81E-03	0.6	0.4	9.81
0.29	1.2	0.241667	1.80E-05	2.4	0.00241	997	8.90E-04	1.81E-03	0.6	0.4	9.81

Liquid		Gas									
$E_1$	$E_2$	$\varepsilon_{Ld}$ (assume)	$\varepsilon_{Ld}$ (model)	$\varepsilon_{Ld}$ (exp)	Deviation (%)	$E_1$	$E_2$	$\varepsilon_G$	$\Delta P/h$	$\Delta P/h(\text{exp})$	Deviation (%)
180	1.8	0.147	0.147	0.152	3.289	436.638	6.795	0.253	9467.477	8000	-18.343
180	1.8	0.141	0.141	0.150	6.00	425.523	6.537	0.259	10930.276	11000	0.633
180	1.8	0.137	0.137	0.158	13.29	416.036	6.320	0.263	12430.020	12050	-3.154
180	1.8	0.133	0.133	0.152	12.5	408.840	6.157	0.267	13766.389	14550	5.386
180	1.8	0.129	0.129	0.150	14.0	401.398	5.989	0.271	15376.883	16700	7.923
180	1.8	0.126	0.126	0.149	15.4	395.569	5.859	0.274	16839.172	18600	9.467
180	1.8	0.123	0.123	0.148	20.3	390.215	5.741	0.277	18373.268	20650	11.025

## APPENDIX B

### PROPERTIES AND HYDRODYNAMICS (1-D CELL IN SERIES MODEL)

This chapter presents sample calculation to estimate properties and hydrodynamics of hydrodesulfurization reaction. These parameters would be integrated with reaction, mass and energy balances for the evaluation of reactor behavior and performance. Experimental data of Mederos and Ancheyta [36] on hydrotreating of vacuum gas oil (VGO) on pilot plant scale were used for sample calculations of trickle bed properties and hydrodynamic.

Table B.1: Input Data for Hydrodesulfurization Reaction [36]

<u>Feedstock</u>	<u>Value</u>
API gravity	22
Molecular weight	441.9
Mean average boiling point ( $^{\circ}\text{C}$ )	476
Sulfur (wt %)	2.009
<u>Operation conditions</u>	<u>Value</u>
Gas superficial velocity (cm/s)	0.28
Oil superficial velocity (cm/s)	$1.75 \times 10^{-2}$
Catalytic bed length (cm)	31.58
Internal diameter (cm)	2.54
Temperature ( $^{\circ}\text{C}$ )	380
Pressure (MPa)	5.3
Gas composition (mol %)	
H <sub>2</sub>	100
H <sub>2</sub> S	0
Light hydrocarbons	0

## B.1 Oil Density

Oil density at process conditions was evaluated from eq. 4.15.

$$\rho_L(P, T) = \rho_0 + \Delta\rho_P - \Delta\rho_T$$

where  $\rho_0$  ( $\text{lb}_m/\text{ft}^3$ ) is liquid density at standard condition,  $P$  is reactor pressure (psia) and  $T$  is reactor temperature in Rankine ( $^\circ\text{R}$ ).

### B.1.1 Density of Oil at Standard Condition

API gravity = 22

$$\text{SG (at } 60^\circ\text{F)} = \frac{141.5}{131.5 + 22} = 0.922$$

Thus, the density of VGO at standard condition ( $60^\circ\text{F}$  and 1 atm) is  $0.922 \text{ g/cm}^3$

$$\begin{aligned}\rho_o &= 0.922 \frac{\text{g}}{\text{cm}^3} \times \frac{1 \text{ lb}_m}{453.594 \text{ g}} \times \frac{28.317 \text{ cm}^3}{1 \text{ ft}^3} \\ &= 57.559 \frac{\text{lb}_m}{\text{ft}^3}\end{aligned}$$

### B.1.2 Correction of Oil Density for High Pressure ( $\Delta\rho_P$ )

As shown in Table B.1, hydrodesulfurization reaction is operated at high pressure. Correction of oil density for high pressure ( $\Delta\rho_P$ ) can be estimated using eq. 4.16.

Feed inlet temperature =  $380^\circ\text{C}$  @  $1175.67^\circ\text{R}$

Reactor pressure =  $3.5 \text{ MPa}$  @  $768.703 \text{ psia}$

$$\begin{aligned}\Delta\rho_P &= \left[ 0.167 + 16.181 \times 10^{-0.0425\rho_0} \right] \left( \frac{P}{1000} \right) - 0.01 \left[ 0.299 + 263 \times 10^{-0.0603\rho_0} \right] \left( \frac{P}{1000} \right)^2 \\ &= \left[ 0.167 + 16.181 \times 10^{-0.0425(57.559)} \right] \left( \frac{768.703}{1000} \right) - 0.01 \left[ 0.299 + 263 \times 10^{-0.0603(57.559)} \right] \left( \frac{768.703}{1000} \right)^2 \\ &= 0.1706 \text{ lb}_m/\text{ft}^3\end{aligned}$$

### B.1.3 Correction of Oil Density for High Temperature ( $\Delta\rho_T$ )

Correction of oil density for high pressure ( $\Delta\rho_p$ ) is evaluated from eq. 4.17.

$$\Delta\rho_T = \left( 0.0133 + 152.4 [\rho_0 + \Delta\rho_p]^{-2.45} \right) (T_L - 520) - \left( 8.1 \times 10^{-6} - 0.0622 \times 10^{-0.764[\rho_0 + \Delta\rho_p]} \right) (T - 520)^2$$

$$\Delta\rho_T = \left[ \begin{array}{l} \left( 0.0133 + 152.4 [57.559 + 0.1706]^{-2.45} \right) (1175.67 - 520) - \\ \left( 8.1 \times 10^{-6} - 0.0622 \times 10^{-0.764[57.559 + 0.1706]} \right) (1175.67 - 520)^2 \end{array} \right]$$

$$\Delta\rho_T = 10.0715 \text{Ib}_m/\text{ft}^3$$

### B.1.4 Oil Density at Process Conditions

$$\begin{aligned} \rho_L(P,T) &= \rho_0 + \Delta\rho_p - \Delta\rho_T \\ &= 57.559 \frac{\text{Ib}_m}{\text{ft}^3} + 0.1706 \frac{\text{Ib}_m}{\text{ft}^3} - 10.0715 \frac{\text{Ib}_m}{\text{ft}^3} = 47.6581 \frac{\text{Ib}_m}{\text{ft}^3} \\ &= 47.6581 \frac{\text{Ib}_m}{\text{ft}^3} \times \frac{453.594 \text{ g}}{1 \text{ Ib}_m} \times \frac{1 \text{ ft}^3}{28.317 \text{ cm}^3} \\ &= 0.7634 \frac{\text{g}}{\text{cm}^3} \end{aligned}$$

## B.2 Gas Solubilities

### B.2.2 Solubility of Hydrogen

Solubility of hydrogen  $\lambda_{H_2}$  (NI/ MPa kg oil) is estimated using eq. 4.18, where  $T_L$  is liquid temperature in degree Celsius ( $^{\circ}\text{C}$ ),  $\rho_{20}$  is liquid density at  $20^{\circ}\text{C}$  ( $\text{g}/\text{cm}^3$ ).

$$\begin{aligned} \rho_{20} &= 57.309 \text{Ib}_m/\text{ft}^3 \text{ (ASTM)} \\ &= 0.918 \text{g}/\text{cm}^3 \end{aligned}$$

$$\lambda_{H_2} = -0.559729 - 0.42947 \times 10^{-3} T_L + 3.07539 \times 10^{-3} \left( \frac{T_L}{\rho_{20}} \right) + 1.94593 \times 10^{-6} T_L^2 + \frac{0.835783}{\rho_{20}^2}$$

$$\lambda_{H_2} = -0.559729 - 0.42947 \times 10^{-3} (380) + 3.07539 \times 10^{-3} \left( \frac{380}{0.918} \right) + 1.94593 \times 10^{-6} (380)^2 + \frac{0.835783}{(0.918)^2}$$

$$= 1.8229 \text{ NIH}_2 / \text{MPa kg oil}$$

## B.2.2 Solubility of Hydrogen Sulfide

Solubility of hydrogen sulfide  $\lambda_{H_2S}$  was estimated as described in eq. 4.19.

$$\lambda_{H_2S} = \exp [3.367 - 0.00847 T_L]$$

$$= \exp [3.367 - 0.00847 (380)]$$

$$= 1.160 \text{ NI H}_2\text{S} / \text{MPa kg oil}$$

## B.3 Henry Coefficients

Henry coefficients of gases was estimated from eq. 4.20

$$H_i = \frac{v_N}{\lambda_i \rho_L}$$

where  $H_i$  is Henry coefficient ( $\text{Pa} \cdot \text{m}^3 / \text{mol}$ ),  $v_N$  is molar gas volume at standard condition,  $\rho_L$  is liquid density at process conditions.

$$H_{H_2} = \frac{22.4 \frac{\text{L}}{\text{mol}}}{1.8229 \frac{\text{L}}{\text{MPa kg}} \times 763.4 \frac{\text{kg}}{\text{m}^3}}$$

$$= 1.610 \times 10^4 \text{ Pa m}^3 / \text{mol}$$

$$= 1.610 \times 10^{10} \text{ Pa cm}^3 / \text{mol}$$

$$\begin{aligned}
H_{H_2S} &= \frac{22.4 \frac{\text{L}}{\text{mol}}}{1.160 \frac{\text{L}}{\text{MPa kg}} \times 763.4 \frac{\text{kg}}{\text{m}^3}} \\
&= 2.530 \times 10^4 \text{ Pa m}^3/\text{mol} \\
&= 2.530 \times 10^{10} \text{ Pa cm}^3/\text{mol}
\end{aligned}$$

#### B.4 Dynamic Liquid Viscosity

Dynamic liquid viscosity was evaluated from eq. 4.21, where  $\mu_L$  is dynamic liquid viscosity in (mPa.s), T is temperature in Rankine ( $^{\circ}\text{R}$ ) and API is the oil gravity.

$$\begin{aligned}
a &= 10.313 [\log_{10}(T - 460)] - 36.447 \\
&= 10.313 [\log_{10}(1175.67 - 460)] - 36.447 \\
&= -7.006
\end{aligned}$$

$$\begin{aligned}
\mu_L &= 3.141 \times 10^{10} (T - 460)^{-3.444} [\log_{10}(API)^a] \\
&= 3.141 \times 10^{10} (1175.67 - 460)^{-3.444} [\log_{10}(22)^{-7.006}] \\
&= 0.58803 \text{ mPa.s}
\end{aligned}$$

#### B.5 Diffusivity

Diffusion coefficient of solute in the liquid  $D_i^L$  was calculated from eq. 4.23.

$$D_i^L = 8.93 \times 10^{-8} \left( \frac{v_L^{0.267}}{v_i^{0.433}} \right) \left( \frac{T}{\mu_L} \right)$$

where unit of  $D_i^L$  is ( $\text{cm}^2/\text{s}$ ), T is liquid temperature in Kelvin,  $\mu_L$  is dynamic viscosity (mPa.s),  $v_i$  and  $v_L$  are molar volumes of solute and liquid solvent respectively at its normal boiling point ( $\text{cm}^3/\text{mol}$ ).

Mean average boiling point,  $T_{MeABP} = 476^{\circ}\text{C} = 1348.47^{\circ}\text{R}$

Specific gravity at  $15.6^{\circ}\text{C}$ ,  $d_{15.6} = 0.922$

Molar volume of liquid was evaluated as defined in eq. 4.24

$$\begin{aligned}v_c^m &= 7.5214 \times 10^{-3} T_{MeABP}^{0.2896} d_{15.6}^{-0.7666} \\ &= 7.5214 \times 10^{-3} (1348.47)^{0.2896} (0.922)^{-0.7666} \\ &= 0.06453 \text{ft}^3/\text{lb}_m\end{aligned}$$

$$\begin{aligned}v_c &= 0.06453 \frac{\text{ft}^3}{\text{lb}_m} \times 441.9 \frac{\text{g}}{\text{mol}} \times \frac{1 \text{lb}_m}{453.59 \text{g}} \times \frac{28.317 \text{cm}^3}{1 \text{ft}^3} \\ &= 1780.106 \text{cm}^3/\text{mol}\end{aligned}$$

$$\begin{aligned}v_i &= 0.285 v_c^{1.048} \\ &= 0.285 (1780.106)^{1.048} \\ &= 726.628 \text{cm}^3/\text{mol}\end{aligned}$$

Molar volumes of solute (i.e.  $\text{H}_2$ ,  $\text{H}_2\text{S}$  and sulfur) at its normal boiling point are obtained from Geankoplis [103].

$$v_{\text{H}_2} = 14.3 \text{cm}^3/\text{mol}$$

$$v_{\text{H}_2\text{S}} = 32.9 \text{cm}^3/\text{mol}$$

$$v_{\text{S}} = 25.6 \text{cm}^3/\text{mol}$$

$$\begin{aligned}D_{\text{H}_2}^L &= 8.93 \times 10^{-8} \left( \frac{726.628^{0.267}}{14.3^{0.433}} \right) \left( \frac{653.15}{0.58803} \right) \\ &= 1.8204 \times 10^{-4} \text{cm}^2/\text{s}\end{aligned}$$

$$\begin{aligned}D_{\text{H}_2\text{S}}^L &= 8.93 \times 10^{-8} \left( \frac{726.628^{0.267}}{32.9^{0.433}} \right) \left( \frac{653.15}{0.58803} \right) \\ &= 1.2691 \times 10^{-4} \text{cm}^2/\text{s}\end{aligned}$$

$$\begin{aligned}D_{\text{S}}^L &= 8.93 \times 10^{-8} \left( \frac{726.628^{0.267}}{25.6^{0.433}} \right) \left( \frac{653.15}{0.58803} \right) \\ &= 1.4147 \times 10^{-4} \text{cm}^2/\text{s}\end{aligned}$$

## B.6 Mass Transfer Coefficients

Estimation of gas-liquid mass transfer and the liquid-solid mass transfer are obtained from eqs. 4.26 and 4.27 respectively.

### B.6.1 Gas-Liquid Mass Transfer Coefficient

$$\frac{k_{GL_i} a_{GL}}{D_i^L} = 7 \left( \frac{\rho_L u_L}{\mu_L} \right)^{0.4} \left( \frac{\mu_L}{\rho_L D_i^L} \right)^{0.5}$$

#### B.6.1.1 Hydrogen

$$\begin{aligned} k_{GL(H_2)} a_{GL} &= 7 \left( \frac{0.7634 \times 1.75 \times 10^{-2}}{0.58803} \right)^{0.4} \left( \frac{0.58803}{0.7634 \times 1.8204 \times 10^{-4}} \right)^{0.5} (1.8204 \times 10^{-4}) \\ &= 0.01824 \text{ s}^{-1} \end{aligned}$$

#### B.6.1.2 Hydrogen Sulfide

$$\begin{aligned} k_{GL(H_2S)} a_{GL} &= 7 \left( \frac{0.7634 \times 1.75 \times 10^{-2}}{0.58803} \right)^{0.4} \left( \frac{0.58803}{0.7634 \times 1.2691 \times 10^{-4}} \right)^{0.5} (1.2691 \times 10^{-4}) \\ &= 0.01523 \text{ s}^{-1} \end{aligned}$$

### B.6.2 Liquid-Solid Mass Transfer Coefficient

$$\frac{k_{LS_i}}{D_i^L a_{LS}} = 1.8 \left( \frac{\rho_L u_L}{a_{LS} \mu_L} \right)^{0.5} \left( \frac{\mu_L}{\rho_L D_i^L} \right)^{0.333}$$

$$a_{LS} = \frac{6(1-\varepsilon)}{d_p}$$

$$= \frac{6(1-0.4)}{0.254} = 14.173 \frac{\text{cm}^2}{\text{cm}^3}$$

### B.6.2.1 Sulfur

$$k_{LS(s)} = 1.8 \left( \frac{0.7634 \frac{\text{g}}{\text{cm}^3} \times 1.75 \times 10^{-2} \frac{\text{cm}}{\text{s}}}{14.173 \frac{\text{cm}^2}{\text{cm}^3} \times 0.58803 \times 10^{-2} \frac{\text{g}}{\text{cm.s}}} \right)^{0.5} \left( \frac{0.58803 \times 10^{-2} \frac{\text{g}}{\text{cm.s}}}{0.7634 \frac{\text{g}}{\text{cm}^3} \times 1.4147 \times 10^{-4} \frac{\text{cm}^2}{\text{s}}} \right)^{0.333}$$
$$\times 1.4147 \times 10^{-4} \frac{\text{cm}^2}{\text{s}} 14.173 \frac{\text{cm}^2}{\text{cm}^3}$$
$$= 5.4768 \times 10^{-3} \text{ cm/s}$$

$$k_{LS(s)} a_{LS} = 5.4768 \times 10^{-3} \frac{\text{cm}}{\text{s}} \times 14.173 \frac{\text{cm}^2}{\text{cm}^3}$$
$$= 0.07762 \text{ s}^{-1}$$

### B.6.2.2 Hydrogen sulfide

$$k_{LS(H_2S)} = 1.8 \left( \frac{0.7634 \frac{\text{g}}{\text{cm}^3} \times 1.75 \times 10^{-2} \frac{\text{cm}}{\text{s}}}{14.173 \frac{\text{cm}^2}{\text{cm}^3} \times 0.58803 \times 10^{-2} \frac{\text{g}}{\text{cm.s}}} \right)^{0.5} \left( \frac{0.58803 \times 10^{-2} \frac{\text{g}}{\text{cm.s}}}{0.7634 \frac{\text{g}}{\text{cm}^3} \times 1.2691 \times 10^{-4} \frac{\text{cm}^2}{\text{s}}} \right)^{0.333}$$
$$\times 1.2691 \times 10^{-4} \frac{\text{cm}^2}{\text{s}} 14.173 \frac{\text{cm}^2}{\text{cm}^3}$$
$$= 5.0942 \times 10^{-3} \text{ cm/s}$$

$$k_{LS(H_2S)} a_{LS} = 5.0942 \times 10^{-3} \frac{\text{cm}}{\text{s}} \times 14.173 \frac{\text{cm}^2}{\text{cm}^3}$$
$$= 0.0722 \text{ s}^{-1}$$

## B.7 Heat Capacity

Heat capacities of gas and liquid are estimated from eqs. 4.28 and 4.33 respectively.

### B.7.1 Heat Capacity of Liquid

Heat capacity of liquid,  $c_p^L$  (kJ/kg.K) can be estimated as follows, where  $K_w$  is the Watson characterization factor,  $T_b$  is normal boiling point (K).

$$c_p^L = A_1 + A_2T + A_3T^2$$

$$K_w = \frac{(1.8T_b)^{1/3}}{SG}$$
$$= \frac{(1.8 \times 749.15)^{1/3}}{0.922} = 11.985$$

$$A_1 = -4.90383 + [0.099319 + 0.104281 SG]K_w + \left( \frac{4.81407 - 0.194833 K_w}{SG} \right)$$
$$= -4.90383 + [0.099319 + 0.104281 (0.922)][11.985] + \left( \frac{4.81407 - 0.194833 (11.985)}{0.922} \right)$$
$$= 0.1279$$

$$A_2 = [7.53624 + 6.214610K_w] \times \left( 1.12172 - \frac{0.27634}{SG} \right) \times 10^{-4}$$
$$= [7.53624 + 6.214610(11.985)] \times \left( 1.12172 - \frac{0.27634}{0.922} \right) \times 10^{-4}$$
$$= 0.00674$$

$$A_3 = -[1.35652 + 1.11863K_w] \times \left( 2.9027 - \frac{0.70958}{SG} \right) \times 10^{-7}$$
$$= -[1.35652 + 1.11863(11.985)] \times \left( 2.9027 - \frac{0.70958}{0.922} \right) \times 10^{-7}$$
$$= -3.149 \times 10^{-6}$$

$$c_p^L = A_1 + A_2T + A_3T^2$$
$$= 0.1279 + 0.00674 (653.15) - 3.149 \times 10^{-6} (653.15^2)$$
$$= 3.188 \text{ J/g.K}$$

## B.7.2 Heat Capacity of Gas

Molar heat capacity of gas  $c_p^G$ , can be estimated as follows, where  $R$  is the gas constant,  $c_p^G$  is the molar heat capacity and  $T$  is temperature in Kelvin.

$$\frac{c_p^G}{R} = A + BT + CT^2 + DT^3 + ET^4$$

### B.7.2.1 Heat Capacity of Hydrogen

$$c_p^G = \left[ 3.24631 + 0.00143467 (653.15) + (-2.894 \times 10^{-6})(653.15)^2 + 2.58 \times 10^{-9} (653.15)^3 \right] \\ + (-7.391 \times 10^{-13})(653.15)^4 \\ \times (8.314)$$

$$= 29.3757 \text{ J/mol.K}$$

$$c_p^G = \frac{29.3757 \frac{\text{J}}{\text{mol.K}}}{2.016 \frac{\text{g}}{\text{mol}}} = 14.571 \frac{\text{J}}{\text{g.K}}$$

## APPENDIX C

### REACTOR BEHAVIOR (1-D CELL-IN-SERIES MODEL)

This chapter presents sample calculation of 1-D cell-in-series model to estimate species concentrations (hydrogen, sulfur and hydrogen sulfide) and temperature profile along the reactor axis. The model equations are solved by incorporating properties of materials, hydrodynamics and reaction kinetics parameters.

#### C.1 Hydrogen Concentrations in Gas and Liquid Phases

As hydrogen is the only gas present in the gas phase, hydrogen partial pressure at the inlet of reactor is assumed to be equivalent to reactor pressure. Partial pressure of hydrogen in the gas phase for  $i^{\text{th}}$  cell and concentration of hydrogen in the liquid phase for  $i^{\text{th}}$  cell can be calculated using eqs. 4.36 and 4.35 respectively.

Reactor pressure = 5.3MPa

$$p_{i-1(H_2)}^G = 5.3\text{MPa}$$

$$C_{i-1(H_2)}^L = 0$$

##### C.1.1 Hydrogen Partial Pressure in Gas Phase

Partial pressure of hydrogen in the gas phase for  $i^{\text{th}}$  cell can be evaluated as

$$p_{i(H_2)}^G = \frac{\left( u_{oG} p_{i-1(H_2)}^G + \frac{u_{oL} C_{i-1(H_2)}^L k_{GL_{H_2}} a_{GL} \Delta z RT}{u_{oL} + k_{GL_{H_2}} a_{GL} \Delta z} \right)}{\left( \frac{u_{oG} H_{i(H_2)} + k_{GL_{H_2}} a_{GL} \Delta z RT}{H_{i(H_2)}} - \frac{(k_{GL_{H_2}} a_{GL} \Delta z)^2 RT}{H_{i(H_2)} (u_{oL} + k_{GL_{H_2}} a_{GL} \Delta z)} \right)}$$

$$P_{i(H_2)}^G = \frac{0.28(5.3 \times 10^6) + \frac{1.75 \times 10^{-2}(0)(0.01824)(0.254)(8.314 \times 10^6)(653.15)}{1.75 \times 10^{-2} + (0.01824)(0.254)}}{\left[ \left( \frac{0.28(1.61 \times 10^{10}) + (0.01824)(0.254)(8.314 \times 10^6)(653.15)}{1.61 \times 10^{10}} \right) \right]}$$

$$= 5.2767 \times 10^6 \text{ Pa}$$

### C.1.1 Hydrogen Concentration in Liquid Phase

Concentration of hydrogen in the liquid phase for  $i^{\text{th}}$  cell can be estimated as

$$C_{i(H_2)}^L = \frac{u_{oL} C_{i-1(H_2)}^L + \frac{P_{i(H_2)}^G}{H_{i(H_2)}} k_{GL(H_2)} a_{GL} \Delta z}{u_{oL} + k_{GL(H_2)} a_{GL} \Delta z}$$

$$C_{i(H_2)}^L = \frac{1.75 \times 10^{-2} \frac{\text{cm}}{\text{s}} (0) + \frac{5.2767 \times 10^6 \text{ Pa}}{1.61 \times 10^{10}} (0.01824 \text{ s}^{-1})(0.254 \text{ cm})}{1.75 \times 10^{-2} \frac{\text{cm}}{\text{s}} + 0.01824 \text{ s}^{-1} (0.254 \text{ cm})}$$

$$= 6.8624 \times 10^{-5} \frac{\text{mol}}{\text{cm}^3}$$

The concentrations of hydrogen in liquid and solid phases are very close as mass transfer resistance of hydrogen between liquid and solid catalyst is assumed to be negligible.

## C.2 Sulfur Concentrations in Liquid and Solid Phases

### C.2.1 Inlet Sulfur Concentration

Area of reactor

$$\frac{\pi d_p^2}{4} = \frac{\pi (2.54^2)}{4} = 5.067 \text{ cm}^2$$

*Volumetric flow rate of oil*

= area of reactor × liquid superficial velocity

$$= 5.067 \text{ cm}^2 \times 1.75 \times 10^{-2} \text{ cm/s}$$

$$= 0.08867 \text{ cm}^3/\text{s}$$

*Oil mass flow rate*

= volumetric flow rate of oil × oil density

$$= 0.08867 \frac{\text{cm}^3}{\text{s}} \times 0.7634 \frac{\text{g}}{\text{cm}^3}$$

$$= 0.06769 \text{ g/s}$$

It is noted that sulfur content in the VGO is 2.009% mol

*Mass flow rate of sulfur*

$$= \frac{2.009}{100} \times 0.06769 \frac{\text{g}}{\text{s}} = 1.3599 \times 10^{-3} \frac{\text{g}}{\text{s}}$$

*Concentration of sulfur in VGO feed*

$$C_{i-(s)}^L = \frac{1.3599 \times 10^{-3} \frac{\text{g}}{\text{s}}}{441.9 \frac{\text{g}}{\text{mol}} \times 0.08867 \frac{\text{cm}^3}{\text{s}}} = 3.471 \times 10^{-5} \frac{\text{mol}}{\text{cm}^3}$$

### **C.2.2 Sulfur Concentration in Liquid Phase**

From kinetic data reported by Korsten and Hoffman [88], rate constant for hydrodesulfurization reaction and adsorption equilibrium constant for hydrogen sulfide were evaluated as

$$k_{HDS} = 4.266 \times 10^9 \frac{\text{cm}^3}{\text{g}\cdot\text{s}} \cdot e^{\left[ \frac{131993 \text{ J/mol}}{8.314 \frac{\text{J}}{\text{mol}\cdot\text{K}} (653.15 \text{ K})} \right]}$$
$$= 0.1185 \frac{\text{cm}^3}{\text{g}\cdot\text{s}}$$

$$K_{H_2S} = 41769.84 \frac{\text{cm}^3}{\text{mol}} \exp \frac{2761 \text{ J/mol}}{8.314 \frac{\text{J}}{\text{mol.K}} (653.15 \text{ K})}$$

$$= 69451.1 \frac{\text{cm}^3}{\text{mol}}$$

Concentration of sulfur in liquid phase for  $i^{\text{th}}$  cell was estimated from eq. 4.39

$$C_{i(s)}^L = \frac{u_{oL} C_{i-1(s)}^L}{u_{oL} + k_{LS(s)} a_{LS} \Delta z \left( 1 - \frac{k_{LS(s)} a_{LS}}{k_{LS(s)} a_{LS} + \eta \rho_B k_{HDS} \frac{(C_{H_2}^s)^{0.45}}{(1 + K_{H_2S}^s C_{H_2S}^s)^2}} \right)}$$

$$C_{i(s)}^L = \frac{1.75 \times 10^{-2} \frac{\text{cm}}{\text{s}} \cdot (3.471 \times 10^{-5} \frac{\text{mol}}{\text{cm}^3})}{1.75 \times 10^{-2} \frac{\text{cm}}{\text{s}} + 0.07762 \text{ s}^{-1} \cdot (0.254 \text{ cm})}$$

$$\left( 1 - \frac{0.07762 \text{ s}^{-1}}{0.07762 \text{ s}^{-1} + (0.3108) \cdot 0.8163 \frac{\text{g}}{\text{cm}^3} \cdot 0.1185 \frac{\text{cm}^3}{\text{g.s}} \cdot \frac{(6.8624 \times 10^{-5})^{0.45}}{(1 + 69451.1(0))^2}} \right)$$

$$= 3.451 \times 10^{-5} \frac{\text{mol}}{\text{cm}^3}$$

## C.2.2 Sulfur Concentration in Solid Phase

Concentration of sulfur in solid phase for  $i^{\text{th}}$  cell was calculated using eq. 4.38.

$$C_{i(s)}^S = \frac{k_{LS(s)} a_{LS} C_{i(s)}^L}{k_{LS(s)} a_{LS} + \eta \rho_B k_{HDS} \frac{(C_{H_2}^s)^{0.45}}{(1 + K_{H_2S}^s C_{H_2S}^s)^2}}$$

$$C_{i(s)}^S = \frac{0.07762s^{-1} \cdot \left(3.451 \times 10^{-5} \frac{\text{mol}}{\text{cm}^3}\right)}{0.07762s^{-1} + (0.3108) \cdot \left(0.8163 \frac{\text{g}}{\text{cm}^3}\right) \cdot 0.1185 \frac{\text{cm}^3}{\text{g}\cdot\text{s}} \cdot \left(\frac{(6.8624 \times 10^{-5})^{0.45}}{(1 + 69451.1(0))^2}\right)}$$

$$= 3.433 \times 10^{-5} \frac{\text{mol}}{\text{cm}^3}$$

### C.3 Hydrogen Sulfide Concentration

#### C.3.1 Hydrogen Sulfide Concentration in Solid Phase

Hydrogen sulfide generated in the solid phase is due to reaction between hydrogen and sulfur compounds at the surface of the catalyst. Hydrogen sulfide concentration in the solid phase can be estimated from eq. 4.8.

$$k_{LS(s)} a_{LS} (C_{i(H_2S)}^S - C_{i(H_2S)}^L) \Delta z = \eta \rho_B \Delta z r_{HDS}$$

$$C_{i(H_2S)}^S = \frac{\eta \rho_B \Delta z k_{HDS} \frac{(C_{H_2}^S)^{0.45}}{(1 + K_{H_2S}^S C_{H_2S}^S)^2}}{k_{LS(s)} a_{LS} \Delta z} + C_{i(H_2S)}^L$$

$$= \frac{(0.3108) \cdot 0.8163 \frac{\text{g}}{\text{cm}^3} \cdot 0.1185 \frac{\text{cm}^3}{\text{g}\cdot\text{s}} \cdot \frac{(6.8624 \times 10^{-5})^{0.45}}{(1 + 69451.1(0))^2}}{(0.07762s^{-1}) \cdot (0.254 \text{ cm})} + 1.6424 \times 10^{-7} \frac{\text{mol}}{\text{cm}^3}$$

$$= 3.555 \times 10^{-7} \frac{\text{mol}}{\text{cm}^3}$$

#### C.3.1 Hydrogen Sulfide Concentration in Liquid Phase

Concentration of hydrogen sulfide in the liquid phase can be estimated from eq. 4.41

$$C_{i(H_2S)}^L = \frac{u_{oL} C_{i-1(H_2S)}^L + \eta \rho_B k_{HDS} \frac{(C_{H_2}^s)^{0.45}}{(1 + K_{H_2S}^s C_{H_2S}^s)^2} \Delta z + \frac{u_{oG} P_{i-1(H_2S)}^G k_{GL(H_2S)} a_{GL} \Delta z}{u_{oG} H_i + k_{GL(H_2S)} a_{GL} \Delta z RT}}{u_{oL} + k_{GL(H_2S)} a_{GL} \Delta z \left[ 1 - \frac{k_{GL(H_2S)} a_{GL} \Delta z RT}{u_{oG} H_i + k_{GL(H_2S)} a_{GL} \Delta z RT} \right]}$$

$$C_{i(H_2S)}^L = \frac{\left[ 1.75 \times 10^{-2} \frac{\text{cm}}{\text{s}} \cdot \left( 0 \frac{\text{mol}}{\text{cm}^3} \right) + (0.3108) \cdot 0.8163 \frac{\text{g}}{\text{cm}^3} \cdot \left( 0.1185 \frac{\text{cm}^3}{\text{g} \cdot \text{s}} \right) \cdot \frac{(6.8624 \times 10^{-5})^{0.45}}{(1 + 69451.1(0))^2} \cdot (0.254 \text{ cm}) \right.}{\left. + \frac{\left( 0.28 \frac{\text{cm}}{\text{s}} (0 \text{ Pa}) (0.07762 \text{ s}^{-1}) (0.254 \text{ cm}) \right)}{\left( 0.28 \frac{\text{cm}}{\text{s}} \cdot \left( 2.53 \times 10^{10} \frac{\text{Pa cm}^3}{\text{mol}} \right) + (0.07762 \text{ s}^{-1}) \cdot (0.254 \text{ cm}) \cdot \left( 8.314 \frac{\text{J}}{\text{mol} \cdot \text{K}} \right) \cdot (653.15 \text{ K}) \right)} \right]}{\left[ 1.75 \times 10^{-2} \frac{\text{cm}}{\text{s}} + (0.07762 \text{ s}^{-1}) \cdot (0.254 \text{ cm}) \times \right.}{\left. 1 - \frac{\left( (0.07762 \text{ s}^{-1}) \cdot (0.254 \text{ cm}) \cdot \left( 8.314 \frac{\text{J}}{\text{mol} \cdot \text{K}} \right) \cdot (653.15 \text{ K}) \right)}{\left( 0.28 \frac{\text{cm}}{\text{s}} \cdot \left( 2.53 \times 10^{10} \frac{\text{Pa cm}^3}{\text{mol}} \right) + (0.07762 \text{ s}^{-1}) \cdot (0.254 \text{ cm}) \cdot \left( 8.314 \frac{\text{J}}{\text{mol} \cdot \text{K}} \right) \cdot (653.15 \text{ K}) \right)} \right]}$$

$$= 1.6424 \times 10^{-7} \frac{\text{mol}}{\text{cm}^3}$$

### C.3.1 Partial Pressure of Hydrogen Sulfide in Gas Phase

Partial pressure of hydrogen sulfide in the gas phase can be estimated by rearranging eq. 4.40

$$P_{i-1(H_2S)}^G = \frac{H_{i(H_2S)} \left( u_{oG} P_{i-1(H_2S)}^G + k_{GL(H_2S)} a_{GL} C_{i(H_2S)}^L \Delta z RT \right)}{u_{oG} H_{i(H_2S)} + k_{GL(H_2S)} a_{GL} \Delta z RT}$$

$$= \frac{2.53 \times 10^{10} \frac{\text{Pa}}{\text{cm}^3 \cdot \text{mol}} \left( 0.28 \frac{\text{cm}}{\text{s}} \cdot \left( 0 \frac{\text{mol}}{\text{cm}^3} \right) + \left( (0.07762 \text{ s}^{-1}) \cdot \left( 1.6424 \times 10^{-7} \frac{\text{mol}}{\text{cm}^3} \right) \cdot (0.254 \text{ cm}) \cdot \left( 8.314 \frac{\text{J}}{\text{mol} \cdot \text{K}} \right) \cdot (653.15 \text{ K}) \right) \right)}{\left( 0.28 \frac{\text{cm}}{\text{s}} \right) \cdot \left( 2.53 \times 10^{10} \frac{\text{Pa cm}^3}{\text{mol}} \right) + (0.07762 \text{ s}^{-1}) \cdot (0.254 \text{ cm}) \cdot \left( 8.314 \frac{\text{J}}{\text{mol} \cdot \text{K}} \right) \cdot (653.15 \text{ K})}$$

$$= 12.286 \text{ Pa}$$

## C.4 Bed Temperature

The gas and liquid phases have the same inlet temperature. Under a steady state operating condition, it is assumed that the heat transfer inside the particle is fast enough. The temperature gradient among the gas, liquid and catalyst at any particular axial position of the reactor is negligible ( $T_{Gi} = T_{Li} = T_{Si} = T_i$ ). Bed temperature can be evaluated using eq. 4.12.

$$(u_{oG}\rho_G c_P^G + u_{oL}\rho_L c_P^L)(T_i - T_{(i-1)}) = \Delta z \rho_B \eta_j r_{HDS} (-\Delta H_{HDS})$$

$$\Delta T = \frac{\Delta z \rho_B \eta_j r_{HDS} (-\Delta H_{HDS})}{(u_{oG}\rho_G c_P^G + u_{oL}\rho_L c_P^L)}$$

$$= \frac{\left[ 0.254 \text{cm} \cdot \left( 0.8163 \frac{\text{g}}{\text{cm}^3} \right) \cdot (0.3108) \cdot \left( 0.1185 \frac{\text{cm}^3}{\text{g}\cdot\text{s}} \right) \cdot \frac{(6.8624 \times 10^{-5})^{0.45} \cdot 3.451 \times 10^{-5} \frac{\text{mol}}{\text{cm}^3}}{[1 + 69451.1(0)]^2} \right]}{\left[ \left( 25000 \frac{\text{J}}{\text{mol}} \right) \right]}$$

$$= \frac{\left[ 0.28 \frac{\text{cm}}{\text{s}} \cdot \left( 1.96613 \frac{\text{g}}{\text{cm}^3} \right) \cdot \left( 14.571 \frac{\text{J}}{\text{g}\cdot\text{K}} \right) + 1.75 \times 10^{-2} \cdot 0.8163 \frac{\text{g}}{\text{cm}^3} \cdot 3.188 \frac{\text{J}}{\text{g}\cdot\text{K}} \right]}{}$$

$$= 0.017 \text{ K}$$

$$T_i = T_{i-1} + \Delta T$$

$$= 653.15 + 0.017$$

$$= 653.167$$

The algebraic equation of concentrations and temperature over the 1<sup>st</sup> cell was solved for based on inlet condition. The parameters for 2<sup>nd</sup> cell can be solved by considering the 1<sup>st</sup> cell was the input for the 2<sup>nd</sup> cell. This was extended for subsequent cells to estimate extent of reaction and rise in temperature along the reactor length. The simulation results for hydrodesulfurization of VGO on pilot plant scale including reactor hydrodynamic, properties as well as concentrations and temperature along the reactor length are presented in Table C.1.

Table C.1: Simulation results of hydrodesulfurization of VGO on pilot plant scale estimated by 1-D cell-in series-model

cell	Z(cm)	$u_{oG}$ (cm/s)	$\rho_G$ (kg/m <sup>3</sup> )	$\rho_P$ (lb/ft <sup>3</sup> )	$\rho_T$ (lb/ft <sup>3</sup> )	$P$ (psia)	$\rho_L$ (g/cm <sup>3</sup> )	$d_p$ (cm)	$\lambda$ (H <sub>2</sub> )	$H_{(H_2)}$ (Pacm <sup>3</sup> /mol)	$D_{H_2}^L$ (cm <sup>2</sup> /s)
0	0	0.28	1.9661	0.1706	10.0715	768.7027	0.7634	0.2540	1.8229	1.6097E+04	1.8204E-04
1	0.254	0.28	1.9574	0.1706	10.0718	765.3247	0.7634	0.2540	1.8230	1.6096E+04	1.8206E-04
2	0.508	0.28	1.9506	0.1706	10.0722	762.6652	0.7634	0.2540	1.8230	1.6095E+04	1.8209E-04
3	0.762	0.28	1.9451	0.1706	10.0726	760.5715	0.7634	0.2540	1.8232	1.6095E+04	1.8212E-04
4	1.016	0.28	1.9409	0.1706	10.0731	758.9230	0.7634	0.2540	1.8233	1.6094E+04	1.8215E-04
5	1.27	0.28	1.9382	0.1706	10.0735	757.6252	0.7634	0.2540	1.8234	1.6093E+04	1.8218E-04
6	1.524	0.28	1.9348	0.1706	10.0740	756.6033	0.7634	0.2540	1.8235	1.6092E+04	1.8222E-04
7	1.778	0.28	1.9326	0.1706	10.0745	755.7987	0.7634	0.2540	1.8236	1.6091E+04	1.8225E-04
8	2.032	0.28	1.9309	0.1706	10.0749	755.1651	0.7633	0.2540	1.8237	1.6090E+04	1.8228E-04
9	2.286	0.28	1.9296	0.1706	10.0754	754.6662	0.7633	0.2540	1.8238	1.6090E+04	1.8231E-04
10	2.54	0.28	1.9285	0.1706	10.0759	754.2733	0.7633	0.2540	1.8239	1.6089E+04	1.8235E-04
11	2.794	0.28	1.9276	0.1706	10.0763	753.9639	0.7633	0.2540	1.8241	1.6088E+04	1.8238E-04
12	3.048	0.28	1.9269	0.1706	10.0768	753.7201	0.7633	0.2540	1.8242	1.6087E+04	1.8241E-04
13	3.302	0.28	1.9264	0.1706	10.0773	753.5281	0.7633	0.2540	1.8243	1.6086E+04	1.8244E-04
14	3.556	0.28	1.9259	0.1706	10.0777	753.3768	0.7633	0.2540	1.8244	1.6085E+04	1.8247E-04
15	3.81	0.28	1.9255	0.1706	10.0782	753.2575	0.7633	0.2540	1.8245	1.6085E+04	1.8251E-04
16	4.064	0.28	1.9252	0.1706	10.0786	753.1634	0.7633	0.2540	1.8246	1.6084E+04	1.8254E-04
17	4.318	0.28	1.9250	0.1706	10.0791	753.0892	0.7633	0.2540	1.8247	1.6083E+04	1.8257E-04
18	4.572	0.28	1.9247	0.1706	10.0795	753.0307	0.7633	0.2540	1.8248	1.6082E+04	1.8260E-04
19	4.826	0.28	1.9245	0.1706	10.0800	752.9844	0.7633	0.2540	1.8249	1.6081E+04	1.8263E-04
⋮	⋮	⋮	⋮	⋮	⋮	⋮	⋮	⋮	⋮	⋮	⋮
125	31.75	0.28	1.9190	0.1706	10.1106	752.7603	0.7628	0.2540	1.8324	1.6026E+04	1.8477E-04
126	32.004	0.28	1.9189	0.1706	10.1108	752.7600	0.7628	0.2540	1.8325	1.6025E+04	1.8478E-04

(cont)

Cell	Z(cm)	$u_{oL}$ (cm/s)	$\varepsilon_p$	$\varepsilon_L$	$k_{GL} a_{GL}$ ( $s^{-1}$ )	$\eta$	$p_{i-1(H_2)}^G$ (Pa)	$p_{i(H_2)}^G$ (Pa)	$C_{i-1(H_2)}^L$ (mol/cm <sup>3</sup> )	$C_{i(H_2)}^L$ (mol/cm <sup>3</sup> )	$C_{i-1(s)}^L$ (mol/cm <sup>3</sup> )	$C_{i(s)}^L$ (mol/cm <sup>3</sup> )
0	0	1.75E-02	0.6	0.05127	0.01824	0.31082	5.3000E+06	5.2767E+06	0	6.8624E-05	3.471E-05	3.4510E-05
1	0.254	1.75E-02	0.6	0.05127	0.01824	0.31082	5.2767E+06	5.2584E+06	6.8624E-05	1.2265E-04	3.451E-05	3.4264E-05
2	0.508	1.75E-02	0.6	0.05127	0.01824	0.31083	5.2584E+06	5.2439E+06	1.2265E-04	1.6518E-04	3.426E-05	3.3992E-05
3	0.762	1.75E-02	0.6	0.05127	0.01825	0.31083	5.2439E+06	5.2326E+06	1.6518E-04	1.9867E-04	3.399E-05	3.3707E-05
4	1.016	1.75E-02	0.6	0.05126	0.01825	0.31084	5.2326E+06	5.2236E+06	1.9867E-04	2.2503E-04	3.371E-05	3.3414E-05
5	1.27	1.75E-02	0.6	0.05126	0.01825	0.31084	5.2236E+06	5.2166E+06	2.2503E-04	2.4578E-04	3.341E-05	3.3117E-05
6	1.524	1.75E-02	0.6	0.05126	0.01825	0.31084	5.2166E+06	5.2110E+06	2.4578E-04	2.6213E-04	3.312E-05	3.2818E-05
7	1.778	1.75E-02	0.6	0.05126	0.01825	0.31085	5.2110E+06	5.2067E+06	2.6213E-04	2.7499E-04	3.282E-05	3.2518E-05
8	2.032	1.75E-02	0.6	0.05125	0.01825	0.31085	5.2067E+06	5.2032E+06	2.7499E-04	2.8513E-04	3.252E-05	3.2219E-05
9	2.286	1.75E-02	0.6	0.05125	0.01825	0.31086	5.2032E+06	5.2005E+06	2.8513E-04	2.9310E-04	3.222E-05	3.1921E-05
10	2.54	1.75E-02	0.6	0.05125	0.01825	0.31086	5.2005E+06	5.1984E+06	2.9310E-04	2.9939E-04	3.192E-05	3.1624E-05
11	2.794	1.75E-02	0.6	0.05125	0.01826	0.31087	5.1984E+06	5.1967E+06	2.9939E-04	3.0434E-04	3.162E-05	3.1329E-05
12	3.048	1.75E-02	0.6	0.05125	0.01826	0.31087	5.1967E+06	5.1954E+06	3.0434E-04	3.0824E-04	3.133E-05	3.1036E-05
13	3.302	1.75E-02	0.6	0.05124	0.01826	0.31088	5.1954E+06	5.1943E+06	3.0824E-04	3.1131E-04	3.104E-05	3.0745E-05
14	3.556	1.75E-02	0.6	0.05124	0.01826	0.31088	5.1943E+06	5.1935E+06	3.1131E-04	3.1373E-04	3.075E-05	3.0456E-05
15	3.81	1.75E-02	0.6	0.05124	0.01826	0.31088	5.1935E+06	5.1929E+06	3.1373E-04	3.1564E-04	3.046E-05	3.0170E-05
16	4.064	1.75E-02	0.6	0.05124	0.01826	0.31089	5.1929E+06	5.1923E+06	3.1564E-04	3.1715E-04	3.017E-05	2.9885E-05
17	4.318	1.75E-02	0.6	0.05123	0.01826	0.31089	5.1923E+06	5.1919E+06	3.1715E-04	3.1834E-04	2.989E-05	2.9603E-05
18	4.572	1.75E-02	0.6	0.05123	0.01827	0.31090	5.1919E+06	5.1916E+06	3.1834E-04	3.1928E-04	2.960E-05	2.9322E-05
19	4.826	1.75E-02	0.6	0.05123	0.01827	0.31090	5.1916E+06	5.1914E+06	3.1928E-04	3.2002E-04	2.932E-05	2.9044E-05
⋮	⋮	⋮	⋮	⋮	⋮	⋮	⋮	⋮	⋮	⋮	⋮	⋮
125	31.75	1.75E-02	0.6	0.05109	0.01836	0.31119	5.1901E+06	5.1901E+06	3.2382E-04	3.2383E-04	9.780E-06	9.6726E-06
126	32.004	1.75E-02	0.6	0.05109	0.01836	0.31119	5.1901E+06	5.1901E+06	3.2383E-04	3.2384E-04	9.673E-06	9.5660E-06

(cont)

Cell	Z(cm)	$k_{LS(s)}$ (cm/s)	$a_{LS}$ (cm <sup>-1</sup> )	$k_{LS(s)}a_{LS}$ (cm <sup>-1</sup> )	S (ppm)	$C_{i-1(s)}^S$ (mol/cm <sup>3</sup> )	$C_{i(s)}^S$ (mol/cm <sup>3</sup> )	$D_{H_2}^L$ (cm <sup>2</sup> /s)	$\Delta H_{HDS}$ (J/mol)	$k_{HDS}$ (cm <sup>3</sup> /g.s)
0	0	5.4768E-03	14.173	0.07762	20092	0.000E+00	3.433E-05	1.4147E-04	251000	1.185E-01
1	0.254	5.4773E-03	14.173	0.07763	19976	3.433E-05	3.405E-05	1.4149E-04	251000	1.186E-01
2	0.508	5.4780E-03	14.173	0.07764	19834	3.405E-05	3.375E-05	1.4151E-04	251000	1.187E-01
3	0.762	5.4787E-03	14.173	0.07765	19677	3.375E-05	3.345E-05	1.4153E-04	251000	1.188E-01
4	1.016	5.4794E-03	14.173	0.07766	19512	3.345E-05	3.315E-05	1.4156E-04	251000	1.189E-01
5	1.27	5.4802E-03	14.173	0.07767	19343	3.315E-05	3.285E-05	1.4158E-04	251000	1.190E-01
6	1.524	5.4809E-03	14.173	0.07768	19171	3.285E-05	3.255E-05	1.4161E-04	251000	1.191E-01
7	1.778	5.4817E-03	14.173	0.07769	18998	3.255E-05	3.225E-05	1.4163E-04	251000	1.192E-01
8	2.032	5.4825E-03	14.173	0.07770	18825	3.225E-05	3.195E-05	1.4166E-04	251000	1.193E-01
9	2.286	5.4832E-03	14.173	0.07772	18652	3.195E-05	3.166E-05	1.4168E-04	251000	1.195E-01
10	2.54	5.4840E-03	14.173	0.07773	18479	3.166E-05	3.136E-05	1.4171E-04	251000	1.196E-01
11	2.794	5.4848E-03	14.173	0.07774	18308	3.136E-05	3.107E-05	1.4173E-04	251000	1.197E-01
12	3.048	5.4855E-03	14.173	0.07775	18137	3.107E-05	3.078E-05	1.4176E-04	251000	1.198E-01
13	3.302	5.4863E-03	14.173	0.07776	17968	3.078E-05	3.049E-05	1.4178E-04	251000	1.199E-01
14	3.556	5.4871E-03	14.173	0.07777	17799	3.049E-05	3.020E-05	1.4181E-04	251000	1.200E-01
15	3.81	5.4878E-03	14.173	0.07778	17632	3.020E-05	2.992E-05	1.4183E-04	251000	1.201E-01
16	4.064	5.4885E-03	14.173	0.07779	17466	2.992E-05	2.963E-05	1.4186E-04	251000	1.203E-01
17	4.318	5.4893E-03	14.173	0.07780	17302	2.963E-05	2.935E-05	1.4188E-04	251000	1.204E-01
18	4.572	5.4900E-03	14.173	0.07781	17139	2.935E-05	2.907E-05	1.4190E-04	251000	1.205E-01
19	4.826	5.4907E-03	14.173	0.07782	16976	2.907E-05	2.880E-05	1.4193E-04	251000	1.206E-01
⋮	⋮	⋮	⋮	⋮	⋮	⋮	⋮	⋮	⋮	⋮
↓	↓	↓	↓	↓	↓	↓	↓	↓	↓	↓
126	31.75	5.5413E-03	14.173	0.07854	5666	9.685E-06	9.578E-06	1.4359E-04	251000	1.284E-01
127	32.004	5.5416E-03	14.173	0.07854	5604	9.578E-06	9.472E-06	1.4360E-04	251000	1.285E-01

(cont)

Cell	Z(cm)	$D_{H_2S}^L$ (cm <sup>2</sup> /s)	$k_{LS(H_2S)}$ (cm/s)	$k_{LS(H_2S)}a_{LS}$ (cm <sup>-1</sup> )	$\lambda_{H_2S}$	$H_{H_2S}$ (Pacm <sup>3</sup> /mol)	$k_{GL(H_2S)}a_{GL}$ (cm <sup>-1</sup> )	$K_{H_2S}$ (cm <sup>3</sup> /g.s)	$(1 + K_{H_2S}C_{H_2S})^2$	$C_{i-1(H_2S)}^S$ (mol/cm <sup>3</sup> )
0	0	1.2691E-04	5.0942E-03	7.2201E-02	1.1600	2.5296E+10	1.5231E-02	69451.090	1.0000	0.0000E+00
1	0.254	1.2692E-04	5.0947E-03	7.2208E-02	1.1598	2.5300E+10	1.5232E-02	69450.150	1.0500	3.5550E-07
2	0.508	1.2694E-04	5.0953E-03	7.2217E-02	1.1596	2.5304E+10	1.5233E-02	69448.995	1.0809	5.7093E-07
3	0.762	1.2696E-04	5.0959E-03	7.2226E-02	1.1594	2.5310E+10	1.5234E-02	69447.722	1.1078	7.5651E-07
4	1.016	1.2698E-04	5.0966E-03	7.2235E-02	1.1591	2.5315E+10	1.5235E-02	69446.383	1.1310	9.1407E-07
5	1.27	1.2701E-04	5.0973E-03	7.2245E-02	1.1589	2.5321E+10	1.5236E-02	69445.006	1.1506	1.0465E-06
6	1.524	1.2703E-04	5.0980E-03	7.2256E-02	1.1586	2.5327E+10	1.5237E-02	69443.609	1.1671	1.1568E-06
7	1.778	1.2705E-04	5.0987E-03	7.2266E-02	1.1584	2.5332E+10	1.5238E-02	69442.203	1.1808	1.2477E-06
8	2.032	1.2707E-04	5.0995E-03	7.2276E-02	1.1581	2.5338E+10	1.5239E-02	69440.795	1.1920	1.3220E-06
9	2.286	1.2710E-04	5.1002E-03	7.2286E-02	1.1579	2.5344E+10	1.5240E-02	69439.388	1.2012	1.3822E-06
10	2.54	1.2712E-04	5.1009E-03	7.2296E-02	1.1576	2.5350E+10	1.5242E-02	69437.987	1.2085	1.4306E-06
11	2.794	1.2714E-04	5.1016E-03	7.2306E-02	1.1573	2.5356E+10	1.5243E-02	69436.593	1.2144	1.4690E-06
12	3.048	1.2716E-04	5.1023E-03	7.2316E-02	1.1571	2.5361E+10	1.5244E-02	69435.207	1.2190	1.4992E-06
13	3.302	1.2719E-04	5.1030E-03	7.2326E-02	1.1568	2.5367E+10	1.5245E-02	69433.830	1.2226	1.5224E-06
14	3.556	1.2721E-04	5.1037E-03	7.2336E-02	1.1566	2.5373E+10	1.5246E-02	69432.462	1.2253	1.5400E-06
15	3.81	1.2723E-04	5.1044E-03	7.2346E-02	1.1563	2.5379E+10	1.5247E-02	69431.105	1.2273	1.5529E-06
16	4.064	1.2725E-04	5.1051E-03	7.2356E-02	1.1561	2.5384E+10	1.5248E-02	69429.757	1.2287	1.5620E-06
17	4.318	1.2727E-04	5.1058E-03	7.2366E-02	1.1559	2.5390E+10	1.5250E-02	69428.420	1.2296	1.5679E-06
18	4.572	1.2730E-04	5.1065E-03	7.2375E-02	1.1556	2.5395E+10	1.5251E-02	69427.093	1.2301	1.5713E-06
19	4.826	1.2732E-04	5.1071E-03	7.2385E-02	1.1554	2.5401E+10	1.5252E-02	69425.777	1.2303	1.5725E-06
⋮	⋮	⋮	⋮	⋮	⋮	⋮	⋮	⋮	⋮	⋮
↓	↓	↓	↓	↓	↓	↓	↓	↓	↓	↓
125	31.75	1.2881E-04	5.1542E-03	7.3052E-02	1.1389	2.5786E+10	1.5328E-02	69334.319	1.1325	9.2853E-07
126	32.004	1.2882E-04	5.1545E-03	7.3055E-02	1.1388	2.5788E+10	1.5328E-02	69333.817	1.1318	9.2119E-07

Cell	Z(cm)	$C_{i(H_2S)}^S$ (mol/cm <sup>3</sup> )	$C_{i-1(H_2S)}^L$ (mol/cm <sup>3</sup> )	$C_{i(H_2S)}^L$ (mol/cm <sup>3</sup> )	$p_{i-1(H_2S)}^G$ (Pa)	$p_{i(H_2S)}^G$ (Pa)	$c_p^L$ (J/g. K)	$c_p^G$ (J/g. K)	$T_{Li-1}$ (K)	$dT$	$T_{Li}$ (K)
0	0	3.5550E-07	0.0000E+00	1.6424E-07	0.0000E+00	1.2286E+01	3.1888	14.57078	653.150	0.017	653.167
1	0.254	5.7093E-07	1.6424E-07	3.3622E-07	1.2286E+01	3.7403E+01	3.1889	14.57079	653.167	0.021	653.189
2	0.508	7.5651E-07	3.3622E-07	4.9788E-07	3.7403E+01	7.4543E+01	3.1890	14.57081	653.189	0.024	653.212
3	0.762	9.1407E-07	4.9788E-07	6.4209E-07	7.4543E+01	1.2237E+02	3.1891	14.57082	653.212	0.025	653.237
4	1.016	1.0465E-06	6.4209E-07	7.6706E-07	1.2237E+02	1.7941E+02	3.1892	14.57083	653.237	0.025	653.263
5	1.27	1.1568E-06	7.6706E-07	8.7331E-07	1.7941E+02	2.4424E+02	3.1893	14.57085	653.263	0.026	653.288
6	1.524	1.2477E-06	8.7331E-07	9.6240E-07	2.4424E+02	3.1556E+02	3.1893	14.57086	653.288	0.026	653.314
7	1.778	1.3220E-06	9.6240E-07	1.0363E-06	3.1556E+02	3.9220E+02	3.1894	14.57087	653.314	0.026	653.340
8	2.032	1.3822E-06	1.0363E-06	1.0970E-06	3.9220E+02	4.7318E+02	3.1895	14.57089	653.340	0.026	653.367
9	2.286	1.4306E-06	1.0970E-06	1.1464E-06	4.7318E+02	5.5762E+02	3.1896	14.5709	653.367	0.026	653.392
10	2.54	1.4690E-06	1.1464E-06	1.1863E-06	5.5762E+02	6.4481E+02	3.1897	14.57092	653.392	0.026	653.418
11	2.794	1.4992E-06	1.1863E-06	1.2181E-06	6.4481E+02	7.3414E+02	3.1898	14.57093	653.418	0.026	653.444
12	3.048	1.5224E-06	1.2181E-06	1.2433E-06	7.3414E+02	8.2510E+02	3.1899	14.57095	653.444	0.026	653.469
13	3.302	1.5400E-06	1.2433E-06	1.2628E-06	8.2510E+02	9.1726E+02	3.1900	14.57096	653.469	0.025	653.495
14	3.556	1.5529E-06	1.2628E-06	1.2778E-06	9.1726E+02	1.0103E+03	3.1901	14.57097	653.495	0.025	653.520
15	3.81	1.5620E-06	1.2778E-06	1.2889E-06	1.0103E+03	1.1039E+03	3.1902	14.57099	653.520	0.025	653.545
16	4.064	1.5679E-06	1.2889E-06	1.2969E-06	1.1039E+03	1.1978E+03	3.1903	14.571	653.545	0.025	653.570
17	4.318	1.5713E-06	1.2969E-06	1.3024E-06	1.1978E+03	1.2919E+03	3.1904	14.57101	653.570	0.025	653.594
18	4.572	1.5725E-06	1.3024E-06	1.3057E-06	1.2919E+03	1.3859E+03	3.1905	14.57103	653.594	0.024	653.619
19	4.826	1.5721E-06	1.3057E-06	1.3073E-06	1.3859E+03	1.4799E+03	3.1906	14.57104	653.619	0.024	653.643
⋮	⋮	⋮	⋮	⋮	⋮	⋮	⋮	⋮	⋮	⋮	⋮
↓	↓	↓	↓	↓	↓	↓	↓	↓	↓	↓	↓
125	31.75	9.2119E-07	8.2322E-07	8.1961E-07	8.1958E+03	8.2337E+03	3.1970	14.57198	655.319	0.009	655.328
126	32.004	9.1658E-07	8.1961E-07	8.1603E-07	8.2337E+03	8.2712E+03	3.1970	14.57198	655.328	0.009	655.337

